CHAPTER 1
OVERVIEW

1.1. INTRODUCTION

The magnetotelluric method provides the geophysicist with a frequency domain electromagnetic tool that is not hampered by the presence of conductive overburden or sampling frequencies that do not allow for deep penetration. Variations in the earth's natural magnetic field supply frequencies ranging from nearly DC to several kilohertz, thus giving one the ability to study the electric substructure of the earth to great depths. The final results of magnetotelluric soundings are log-log plots showing apparent resistivity as a function of depth calculated from large amounts of data collected during a sounding. One of the main problems affecting the quality of the results is the presence of artificial electromagnetic sources that are too close to satisfy the assumption that the electromagnetic energy consists of plane waves. Statistical reductions of the data aim to minimise the effect of this 'noise'. Unfortunately, most of the basic minimisation techniques assume noise with a Gaussian distribution. In reality this is not the case and this leads to poor quality results. The aim of this study is to compare two statistical minimisation techniques that try to take the actual distribution of the noise into consideration.

1.2. SUMMARY OF CONTENTS

Chapter 2 gives a brief description of various sources of natural electromagnetic energy. It is important to be aware of the different sources since this will indicate the optimal time to do magnetotelluric soundings. The distance of the sources means that the electromagnetic energy is in the form of plane waves. This is one of the fundamental assumptions made in the deduction of the magnetotelluric theory. Chapter 3 starts with this assumption and uses Maxwell's equations to derive wave equations that describe the propagation of plane electromagnetic waves through the earth. By applying the wave equations to various geological models, it is possible to arrive at the equations describing the relation between the electric and magnetic fields measured at a sounding

station. These fields are related via the impedance tensor and it is the noise in this tensor that needs to be minimised.

Data acquisitioning and basic processing techniques are described in Chapter 4. One of the final results in this chapter shows the relation between apparent resistivity and impedance.

Chapter 5 contains a discussion on various statistical methods used to minimise the effect of noise in data. It starts out with the L_1- and L_2 norms that make the assumption of normally distributed noise. Two methods that address this problem are the Robust M-estimation and adaptive L_p norm techniques. The robust M-estimation method uses a weight function to ignore outliers in the data. This effectively causes the actual distribution to approach a normal distribution. With the adaptive L_p norm technique the actual distribution of the noise is used to determine the value of p that will be used to minimise the error. These methods are applied to synthetic data with both normal and non-normal error distributions and the results are compared.

Statistical reduction methods discussed in Chapter 5 are applied to real data in Chapter 6. Data for the case study were collected between Sishen and Keimoes along a traverse that crosses a number of tectonic boundaries. The final model calculated is compared to a deep reflection seismic line that ran along the same traverse. Chapter 7 discusses the final results obtained with the various statistical techniques.

CHAPTER 2

NATURAL SOURCES OF ELECTROMAGNETIC ENERGY

2.1. GENERAL

Cagnaird (1953) based the theory of the magnetotelluric method on two important assumptions:

- The source is a natural electromagnetic plane wave propagating vertically downward into the Earth and
- The Earth has a one dimensional electrical substructure.

The naturally occurring electromagnetic plane wave originates from a variety of sources and may comprise a wide range of frequencies, depending on the origin. The higher frequency component mainly emanates from meteorological activities such as lightning. Variations in the Earth's magnetic field linked to solar activity are responsible for a low frequency field.

2.2. SOURCES RELATED TO SOLAR ACTIVITIES

It is well known that the geomagnetic field is composed of three parts - the main field that originates from an internal source, the external field originating outside the earth and local variations in the main field caused by magnetic material in the earth's crust (Telford et al., 1976). The variable nature of the external field is of particular interest to us since it induces currents in the ionosphere which act as sources of natural electromagnetic energy

Pulkkinen and Baker (1997) describe geomagnetic activity as 'the general term used to define variations in the Earth's surface magnetic field caused by sources external to the Earth.' They point out that these variations are caused by fluctuations in current systems within the ionosphere and magnetosphere controlled by the variable nature of the solar wind, the interplanetary magnetic field (IMF) or the geometrical relation of the sun and earth.

2.1.1. Solar wind

The close relationship between geomagnetic variations and solar activity warrants a quick look at the basic morphology of the sun. Frazier (1985) describes the sun as 'a series of concentric layers that interact continuously.' Figure 2.1 shows a schematic diagram depicting these concentric layers.

In the solar core at extreme temperatures of 15 000 000°C and pressure 200 billion times the pressure at the earth's surface, hydrogen atoms are fused together to form helium, releasing massive amounts of energy during this process. As the energy passes through the radiation zone, decreases in temperature and pressure and a change in wavelength transform the gamma rays into X-rays and from there into ultraviolet and visible light. The convection zone consists of a cooler, more opaque gas and here the energy is moved upward by convection cells into the photosphere. The energy finally reaches the photosphere from where it is emitted into space. Solar gases are confined by magnetic loops form the sun's atmosphere or corona. Holes in the corona allow the constant movement of gas particles into space thus forming what is known as the solar wind.

The particles emitted by the sun consist mainly of ionized hydrogen that forms a plasma of protons and electrons (Kaufman and Keller, 1981). Experiments with the Lunik space probes four decades ago revealed a flux of positive ions of approximately 2×10^8 particles cm^{-2} sec^{-1} beyond a distance of 39 earth radii (R_E) (Snyder *et al.*, 1963). During the end of 1962 and into the beginning of 1963 the space probe Mariner measured the velocity of the interplanetary plasma for the first time directly and determined an average velocity of 504 km/s during the experiment (Snyder et al., 1963).

2.1.2. Relation between solar wind and geomagnetic activity

The geomagnetic field presents a barrier to the solar wind stopping it at roughly 10 R_E and deflecting it away from and around the earth (Moore and Delcourt, 1995). The protons and electrons are often deflected in opposite

directions causing a magnetic field that cancels the earth's magnetic field where it occurs. The boundary thus formed is known as the magnetopause (Kaufman and Keller, 1981). In the process the solar wind modifies the shape of the geomagnetic field compressing it on the daylight side and causing it to be extended on the opposite side (figure 2.2).

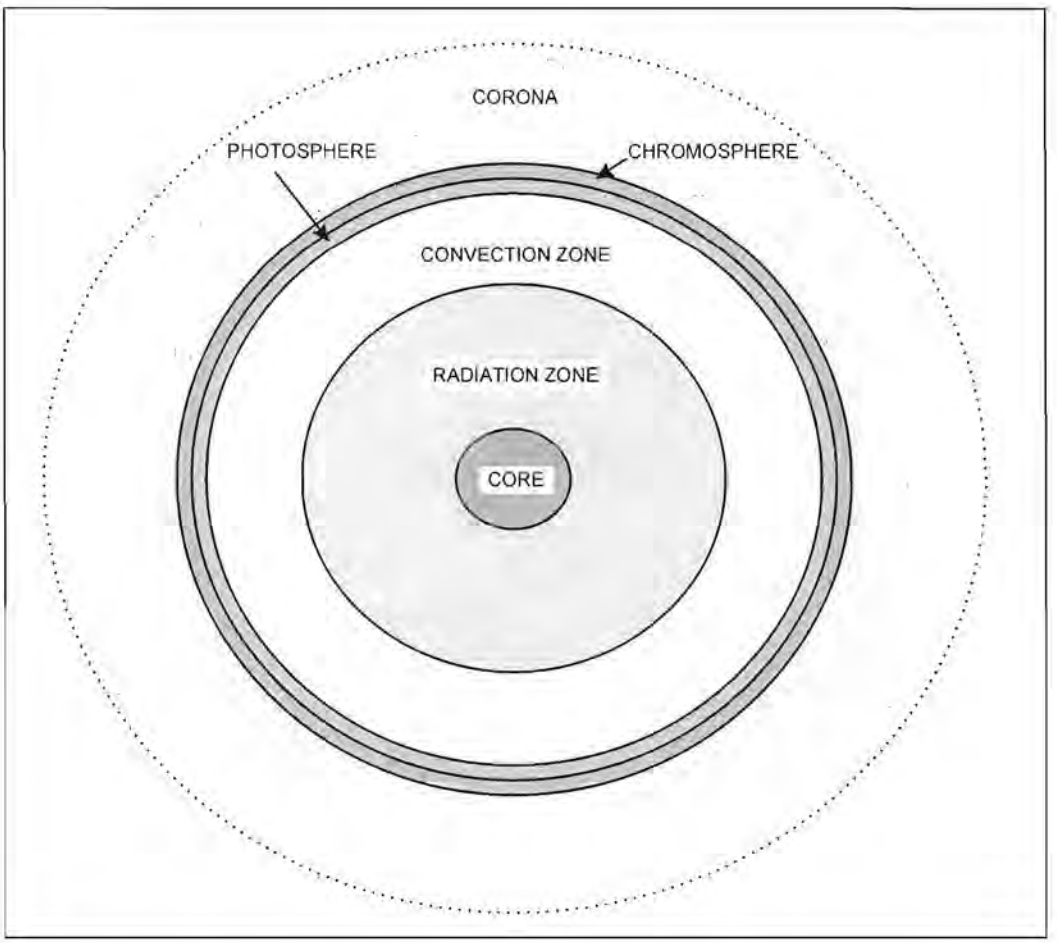

Figure 2.1. Simplified diagram depicting the morphology of the sun (adapted from Frazier, 1985).

The variable nature of the solar wind's strength and velocity cause the magnetopause to fluctuate. The size of the magnetosphere changes and new ionospheric currents form (Pulkkinen and Baker, 1997). When the solar wind is strongly enhanced, stronger magnetic effects known as magnetic storms occur.

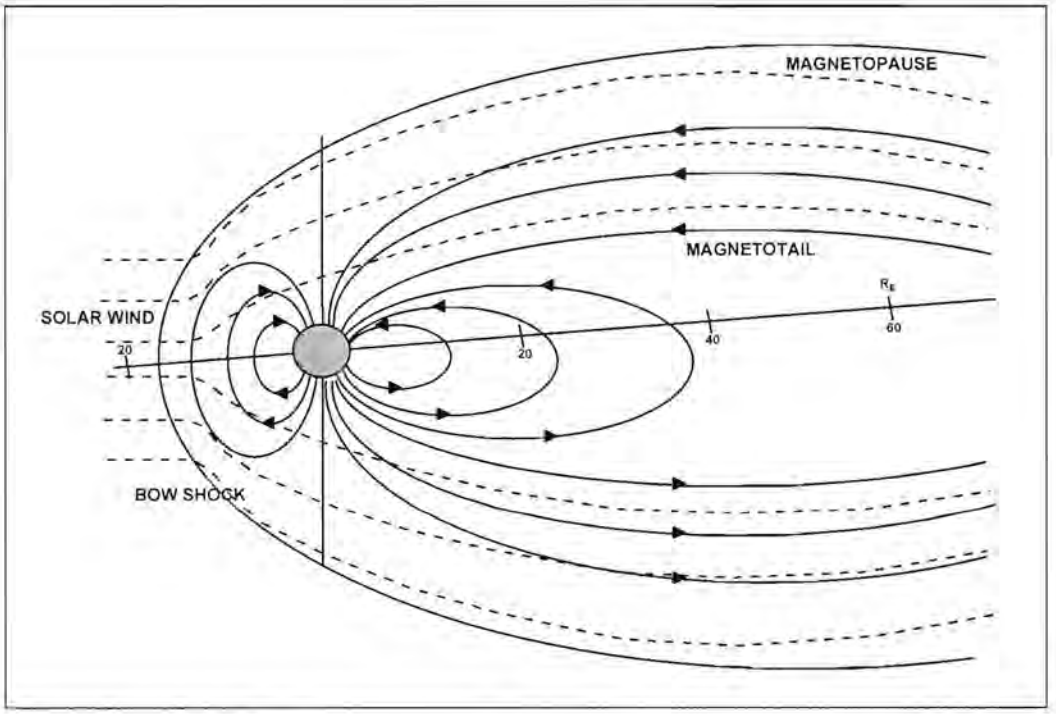

Figure 2.2. The Earth's magnetosphere (Moore, 1994).

2.1.3. Magnetic storms

Sunspots, areas of intense magnetic activity on the surface of the sun, release energy in the form of solar flares and other eruptions. Already in the previous century scientists observed that sunspots waxed and waned in cycles of nearly 11 years. These cycles correlate directly to times of increasing and decreasing geomagnetic activity. This and the fact that increased geomagnetic activity occurs at roughly 27 day intervals (period of the sun's rotation) led to the assumption that solar flares serve as the main instigators of large geomagnetic storms.

Solar flares were held responsible for solar energetic particle (SEP) events even when no flares were visible on the solar disk. These events were believed to result from flares on the back side of the sun. Several models were derived to explain the relatively long duration of most of these events compared with the short lifetime of a flare. One explanation for this

phenomenon was that the solar magnetic field extended through interplanetary space in the form of 'magnetic tubes.' Particles emitted by flares diffused through the solar atmosphere until they reached the tube of force that extended out to the earth at that time, slowly filling it and increasing the flux of particles measured on earth (figure 2.3). Rapid discharge of particles from the tube resulted in magnetic storms (Reid, 1964).

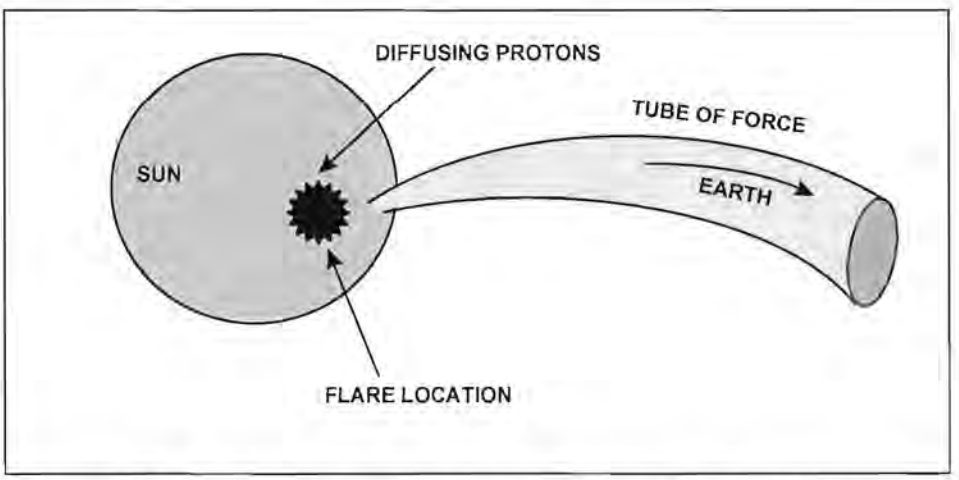

Figure 2.3. Reid's diffusive model for the initial phase of a solar proton event (Reid, 1964).

However, in recent years coronal mass ejections (CMEs) have gained prominence as presenting the crucial link between solar activity and transient interplanetary disturbances that cause large geomagnetic storms (Gosling et al., 1990). During coronal mass ejection events 10^{15} - 10^{16} gms of solar material are suddenly propelled outward into space at speeds ranging from less than 50 km/s to greater than 1200 km/s (Gosling et al., 1991). CMEs are not always observed in association with solar flares but when they are temporally related, CMEs usually begin to lift of from the sun before any substantial flaring activity has occurred (Gosling, 1993).

When CMEs have outward speeds exceeding that of the ambient solar wind a shock forms in front of the ejection and the slower moving plasma ahead is accelerated and deflected from its path (Sheeley et al., 1985). Gosling et al. (1990) show that a strong relation exists between these shock

disturbances, CMEs and large geomagnetic storms. Still, it is important to note that not all CMEs and shock disturbances cause geomagnetic storms. A prerequisite for the formation of major magnetic storms seems to be the presence of an intense, long-duration, southward-directed, interplanetary magnetic field (B_z) within the CME or shock (Tsurutani and Gonzalez, 1992; Lundstedt, 1996; Pulkinnen and Baker, 1997). The strong B_z may be a result of either compression of the ambient interplanetary magnetic field (IMF) by the shock, or of draping of the IMF about the fast CME or a combination of compression and draping (Gosling and McComas, 1987).

2.1.4. Geomagnetic activity as source for MT soundings

Variations in the geomagnetic field induce currents to flow in the ionized layers of the earth's atmosphere (at 80-160 km altitude). These currents in the ionosphere lead to a displacement of mass and together the magnetic and inertial forces give rise to magnetohydrodynamic waves (Kaufman and Keller, 1981). By the time the magnetic effects reach the earth's surface they are strongly modified and classified as micropulsations. These are divided into continuous (Pc) and irregular (Pi) pulsations. They in turn induce currents in conductive layers within the earth. Table 2.1 summarises further subdivisions of the two classes as discussed by Kaufman and Keller (1981).

2.3. SOURCES RELATED TO THUNDERSTORM ACTIVITY

Transient electromagnetic fields (also called atmospherics or sferics) associated with lightning provide the main natural energy at frequencies ranging from 3 Hz to 30 kHz. The electromagnetic field generated by a lightning stroke, shows high energy density at high frequencies when observed relatively nearby. As the energy propagates to greater distances through wave guide propagation, some lower frequencies are enhanced while the higher frequencies are attenuated (Kaufman and Keller, 1981). The measured field is a superposition of individual sferics originating from thunderstorms around the world (Zhang and Paulson, 1997).

Table 2.1. Summary of micropulsation's characteristics.

Classification			Appearance	Time of occurrence	Cause
Pc		Pc-1	Discrete signal with gradually increasing frequency (pearls)	Middle and low latitudes: nights and mornings High latitudes: noon and afternoon	Kinetic instabilities in magnetospheric plasma
		Pc-2	Two maxima on amplitude spectrum	Midday	Disturbance in geomagnetic field
		Pc-3	Two maxima on amplitude spectrum	Midday	Oscillations produced outside magnetosphere
		Pc-4	Two maxima on amplitude spectrum	Mid latitudes: middays High latitudes: night	Generated during onset of magnetic storms
		Pc-5	One maximum on amplitude spectrum	High latitudes: mornings and evenings	Interaction of solar wind with magnetopause
		Pc-6			
Pi	**Pi-1**	PiB	Groups of irregular variations with periods less than 15s	Occur with explosive phase of substorm (22:00-05:00)	Transverse vibration of magnetosphere boundary
		PiC	Irregular variations with dominant period of 5 to 10s	Occur in both explosive and quasi-stable phase of substorm	
		IPDP	Decrease in period during course of occurrence	16:00-01:00	Excited in auroral zone
	Pi-2		Decaying sequence of	Associated with	Related to force lines of

			oscillations with periods of 60-100s and duration of 5-10min	explosive phase of substorm	geomagnetic field along which auroral activity proceeds
	Pi-3		Periods>150s	Night time	Development of Kelvin-Helmholtz instability at boundary of magnetosphere

CHAPTER 3

BASIC THEORY OF THE MAGNETOTELLURIC METHOD

3.1 INTRODUCTION

Cagnaird and Tikhonov developed the theory underlying the magnetotelluric method independent of each other in the 1950's (Tikhonov, 1950; Cagnaird, 1953). They both observed that the electric and magnetic fields associated with telluric currents that flow in the Earth as a result of variations in the Earth's natural electromagnetic field, should relate to each other in a certain way depending on the electrical characteristics of the Earth. Since then tremendous advances have been made in the understanding, processing and interpretation of the data. However, the fundamental principles and assumptions have remained unchanged. This chapter presents the principles that form the basis of the magnetotelluric method.

3.2 MAXWELL'S EQUATIONS

The magnetotelluric method is a frequency domain electromagnetic technique. As with all electromagnetic methods the fundamental principles underlying the technique are summarised in Maxwell's equations given in differential form in equations (3.1) to (3.4) (Reitz et al. 1979).

$$\nabla \cdot \mathbf{B} = 0 \qquad \text{-------- (3.1)}$$

$$\nabla \cdot \mathbf{D} = q \qquad \text{-------- (3.2)}$$

$$\nabla \times \mathbf{E} = -\frac{\partial \mathbf{B}}{\partial t} \qquad \text{-------- (3.3)}$$

$$\nabla \times \mathbf{H} = \mathbf{J} + \frac{\partial \mathbf{D}}{\partial t} \qquad \text{-------- (3.4)}$$

The symbols are declared in the glossary.

It is important to have a clear understanding of these equations and therefore they will be discussed separately in more detail.

3.2.1. $\nabla \cdot \mathbf{B} = 0$

The divergence of a vector (**X**) is the limit of its surface integral per unit volume as the volume (V) enclosed by the surface goes to zero (Reitz, et al., 1979).

$$\nabla \cdot \mathbf{X} = \lim_{V \to 0} \frac{1}{V} \oint_S \mathbf{X} \cdot \mathbf{n} \, da \qquad \text{------- (3.5)}$$

In other words it describes the net flow through a surface enclosing the source of the flow. If $\nabla \cdot \mathbf{X} > 0$, there is a net outflow from the position of **X**. If $\nabla \cdot \mathbf{X} < 0$, there is a net inflow to the position of **X**. If $\nabla \cdot \mathbf{X} = 0$, there is no net inflow or outflow.

Therefore, $\nabla \cdot \mathbf{B} = 0$ indicates that for a closed surface surrounding the source of a magnetic field, the net result of the inflow and outflow per unit volume is zero as the volume goes to zero. This implies that the magnetic source has a negative and positive pole and that isolated magnetic poles do not exist. Figure 3.1 illustrates this point.

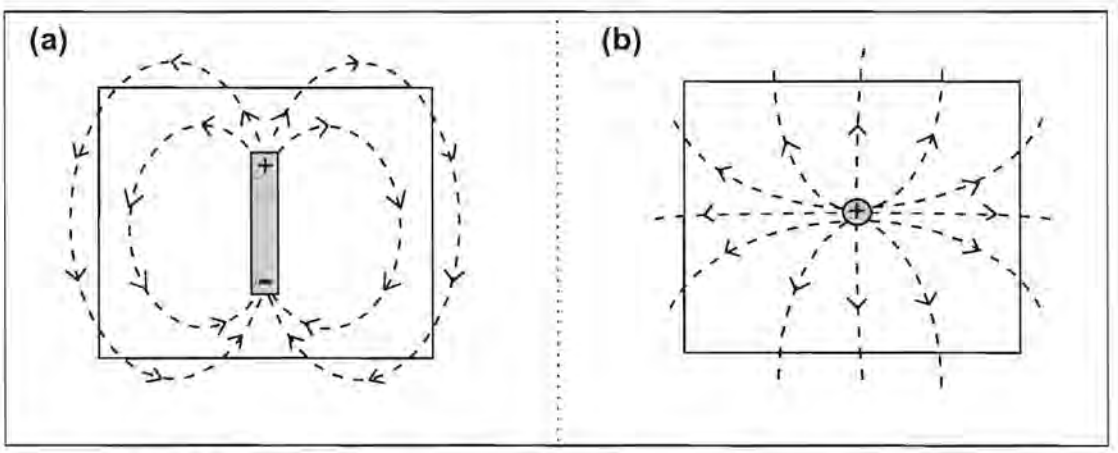

Figure 3.1 Maxwell's equation $\nabla \cdot \mathbf{B} = 0$ implies that the situation depicted in (a) prevails and that single magnetic poles as denoted in (b) cannot occur.

3.2.2. $\nabla \cdot \mathbf{D} = q$ (Gauss' law)

The electric flux across a closed surface is proportional to the net electric charge (q) enclosed by the surface.

$$\mathbf{D} = \varepsilon_0 \mathbf{E} + \mathbf{P} \qquad \text{------- (3.6)}$$

The electric displacement (**D**) includes the charge embedded in the dielectric medium ($\varepsilon_0\mathbf{E}$) as well as the polarisation charge (**P**). Reitz et al. (1979) defines polarisation as follows:

> *A small volume element of a dielectric medium which is electrically neutral has been polarised if a separation of the positive and negative charge has been effected. The volume element is then characterised by an electric dipole moment $\Delta\mathbf{p}$ that determines the electric field produced by the small volume Δv at distant points. **P** is the electric dipole moment per unit volume.*

3.2.3. $\nabla \times \mathbf{E} = -\frac{\partial \mathbf{B}}{\partial t}$ (Faraday's law)

Through experimentation it was found that an electromotive force (ξ) is associated with a change in magnetic flux (Φ) through a circuit.

$$\xi = -\frac{d\Phi}{dt} \qquad \text{------- (3.7)}$$

The EMF is independent of the way in which the flux changes. The minus sign indicates that the direction of the induced EMF is such as to oppose the change that produces it.

Define the EMF around an electric circuit as

$$\xi = \oint_c \mathbf{E} \cdot d\mathbf{l} \qquad \text{------- (3.8)}$$

and the magnetic flux as

$$\Phi = \int_S \mathbf{B} \cdot \mathbf{n}\, da \qquad \text{------- (3.9)}$$

where da is an infinitesimal area and **n** is the unit vector perpendicular to da. Equation (3.9) therefore gives the integral of the normal component of the magnetic field over a surface S.

Substituting (3.8) and (3.9) into (3.7) yield

$$\oint_c \mathbf{E}\cdot d\mathbf{l} = -\frac{d}{dt}\int_s \mathbf{B}\cdot\mathbf{n}\,da \qquad \text{------- (3.10)}$$

Stokes' theorem states that the line integral of a vector around a closed curve is equal to the integral of the normal component of its curl over any surface bounded by the curve ($\oint_c \mathbf{F}.d\mathbf{l} = \int_s \nabla\times\mathbf{F}\cdot\mathbf{n}\,da$). Therefore equation (3.10) can be written as

$$\int_s \nabla\times\mathbf{E}\cdot\mathbf{n}\,da = -\frac{d}{dt}\int_s \mathbf{B}\cdot\mathbf{n}\,da \qquad \text{------- (3.11)}$$

$$\int_s \nabla\times\mathbf{E}\cdot\mathbf{n}\,da = -\int_s \frac{\partial\mathbf{B}}{\partial t}\cdot\mathbf{n}\,da \qquad \text{------- (3.12)}$$

This holds true for all fixed surfaces, therefore

$$\nabla\times\mathbf{E} = -\frac{\partial\mathbf{B}}{\partial t} \qquad \text{------- (3.13)}$$

3.2.4. $\nabla\times\mathbf{H} = \mathbf{J} + \frac{\partial\mathbf{D}}{\partial t}$ (Ampere's law)

This law describes the magnetic field due to a current distribution. **J** is the transport current density that consists of the motion of free electrons or charged ions. The electric displacement **D** was defined in equation (3.6). $\frac{\partial\mathbf{D}}{\partial t}$ gives the variation of the electric displacement with time and is called the displacement current.

It is worthwhile to discuss the definition of the 'curl' and examine this in order to gain a better understanding of Ampere's and Faraday's laws. Reitz et al. (1979) define the curl of a vector as the limit of the ratio of the integral of the vector's cross product with the outward drawn normal over

a closed surface, to the volume enclosed by the surface as the volume goes to zero.

$$\nabla \times \mathbf{F} = \lim_{V \to 0} \frac{1}{V} \oint_S \mathbf{n} \times \mathbf{F} \, da \qquad \text{------- (3.14)}$$

The cross product of two vectors is the product of the magnitudes times the sine of the smallest angle between the two vectors, with the direction of the resultant vector perpendicular to the two vectors according to the right hand screw rule. The curl of a vector can therefore be interpreted as the tendency of a vector to rotate around an axis perpendicular to the vector and the normal (Ellis and Gulick, 1986). Figure 3.2 serves to illustrate this point.

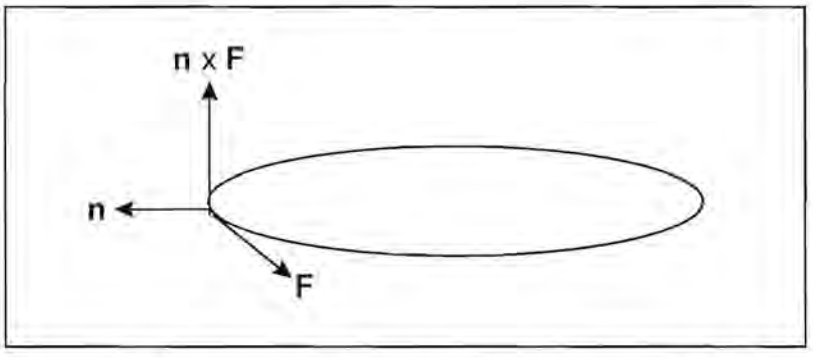

Figure 3.2. The curl of a vector (integration of **n** X **F** over the total closed surface divided by the enclosed volume V as V goes to zero)

3.3. WAVE EQUATIONS

A wave equation describes the wave propagation in a linear medium. To derive the wave equation for the magnetic field, one considers the curl of equation (3.4) (Reitz et al., 1979).

$$\nabla \times \nabla \times \mathbf{H} = \nabla \times \mathbf{J} + \nabla \times \frac{\partial \mathbf{D}}{\partial t} \qquad \text{------- (3.15)}$$

let $\mathbf{D} = \varepsilon \mathbf{E}$, $\mathbf{J} = \sigma \mathbf{E}$ and $\mathbf{B} = \mu_0 \mathbf{H}$ and use (3.3), then

$$\nabla \times \nabla \times \mathbf{H} = \sigma(\nabla \times \mathbf{E}) + \varepsilon \frac{\partial}{\partial t}(\nabla \times \mathbf{E})$$
$$= -\sigma\mu_0 \frac{\partial \mathbf{H}}{\partial t} - \varepsilon\mu_0 \frac{\partial^2 \mathbf{H}}{\partial t^2}$$

Using the identity $\nabla \times \nabla \times \mathbf{X} = \nabla\nabla \cdot \mathbf{X} - \nabla^2 \mathbf{X}$ and (3.1) lead to the wave equation for the magnetic field

$$\nabla^2 \mathbf{H} - \sigma\mu_0 \frac{\partial \mathbf{H}}{\partial t} - \varepsilon\mu_0 \frac{\partial^2 \mathbf{H}}{\partial t^2} = 0 \qquad \text{------- (3.16)}$$

The wave equation for the electric field can be derived similarly by taking the curl of (3.3). In a charge free medium where $\nabla \cdot \mathbf{D} = 0$ this results in

$$\nabla^2 \mathbf{E} - \sigma\mu_0 \frac{\partial \mathbf{E}}{\partial t} - \varepsilon\mu_0 \frac{\partial^2 \mathbf{E}}{\partial t^2} = 0 \qquad \text{------- (3.17)}$$

Equations (3.16) and (3.17) describe the electromagnetic field in a homogeneous, linear medium with no free charge density.

3.4. APPLICATION OF WAVE EQUATIONS IN THE MAGNETOTELLURIC METHOD

In the development of the theory for the magnetotelluric method, we make the following assumptions (Kaufman and Keller, 1981):

- The Earth consists of N horizontal layers, each with resistivity ρ_n and thickness h_n (Figure 3.3).
- A horizontal current sheet located above the surface of the Earth acts as a source for an electromagnetic field that depends only on the vertical (z) coordinate and the distribution of resistivities.

- The horizontal current sheet (j_x) in the source plane induces a uniform primary magnetic field (H_{0y}) that does not vary with z (z is positive downwards).

Temporal fluctuations of the primary magnetic field generate the primary horizontal electric field (E_{0x}). Variations in the primary electric field cause currents to flow in conductive layers in the Earth which in turn serve as source for the secondary electromagnetic field. Since we assume that the Earth consists of homogeneous layers, the current density does not change over the horizontal planes and the secondary electromagnetic field also consists of an electric field in the x-direction and a magnetic field in the y-direction.

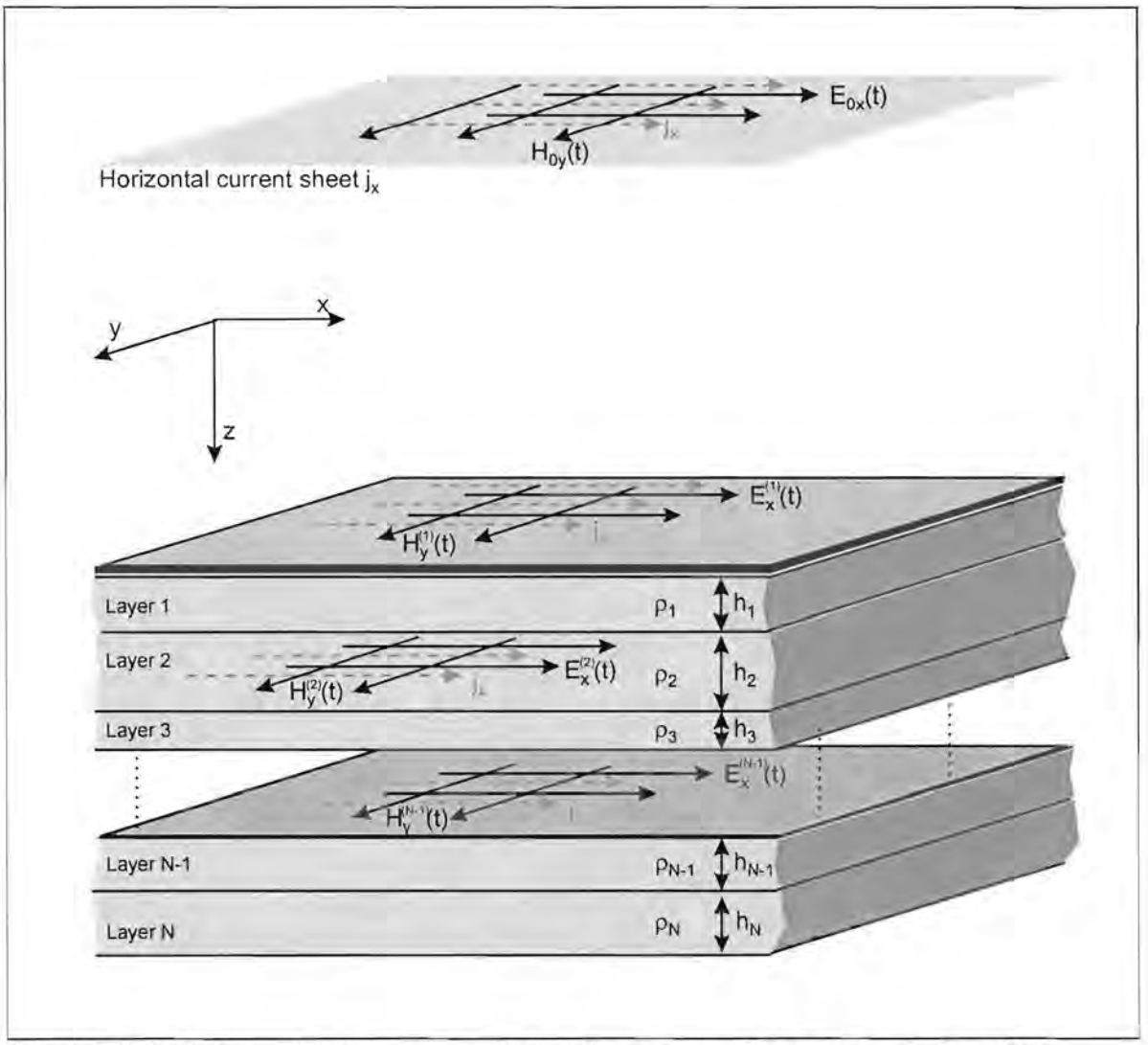

Figure 3.3 Schematic diagram depicting the assumptions made during the development of the MT theory

The total electromagnetic field is time dependant. Assume that the electric and magnetic components can be written as

$$\mathbf{E}(\mathbf{r},t) = E_x e^{-i\omega t} \qquad \text{------- (3.18)}$$

$$\mathbf{H}(\mathbf{r},t) = H_y e^{-i\omega t} \qquad \text{------- (3.19)}$$

In the above equations the time dependency $e^{-i\omega t}=\cos\omega t - i\sin\omega t$ implies an assumption that the fields are continuous harmonic oscillators.

Substitute (3.18) into (3.17) and remember that the electric field varies only in the z-direction. The wave equation for the electric field induced under the assumptions made at the beginning of the section therefore is

$$e^{-i\omega t}\left(\frac{\partial^2 E_x}{\partial z^2} + i\omega\mu\sigma E_x + \omega\mu D_x\right) = 0 \qquad \text{------- (3.20)}$$

According to Kaufman and Keller (1981) the displacement current can be neglected in the MT method. Equation (3.20) then becomes

$$e^{-i\omega t}\left(\frac{\partial^2 E_x}{\partial z^2} + i\omega\mu\sigma E_x\right) = 0 \qquad \text{------- (3.21)}$$

In order to satisfy (3.21) the electric field must have the following form in each layer (n)

$$E_x^{(n)} = e^{-iwt}\left(A_n e^{ik_n z} + B_n e^{-ik_n z}\right) \qquad \text{------- (3.22)}$$

where

$$k = \sqrt{i\omega\mu\sigma} \qquad \text{------- (3.23)}$$

is the wavenumber. Skindepth (δ) and wavenumber are related as follows

$$k = \frac{1+i}{\delta} \qquad \text{------- (3.24)}$$

Use (3.13) and (3.22) to determine the form of the magnetic field in each layer

$$H_y^{(n)} = e^{-iwt}\frac{k_n}{\omega\mu}\left(A_n e^{ik_n z} - B_n e^{-ik_n z}\right) \qquad \text{-------- (3.25)}$$

In (3.22) and (3.25) we assume that the tangential components of the electric and magnetic fields are continuous when passing through the interface between two layers. It is now possible to examine the behaviour of the electric and magnetic fields in different geological scenarios.

3.4.1. Uniform half-space

In a uniform half-space the electromagnetic energy must decrease with increasing depth since energy is transformed into heat. Since

$$e^{ikz} = e^{\frac{iz}{\delta}} e^{\frac{-z}{\delta}} \qquad \text{-------- (3.26)}$$

and

$$e^{-ikz} = e^{\frac{-iz}{\delta}} e^{\frac{z}{\delta}} \qquad \text{-------- (3.27)}$$

it is clear that in both (3.22) and (3.25) the first term between brackets represents the part of the field that decreases with increasing depth and the second term that part of the field that increases with increasing depth. For a uniform half-space, with the assumption that the field should approach 0 as z becomes very large, the electric and magnetic fields therefore reduce to

$$E_x = e^{-iwt}\left(Ae^{ikz}\right) \qquad \text{-------- (3.28)}$$

and

$$H_y = e^{-iwt}\frac{k}{\omega\mu}\left(Ae^{ikz}\right) \qquad \text{-------- (3.29)}$$

At the surface of the earth where z=0, (3.28) and (3.29) reduce to

$$E_x(0) = e^{-iwt}A \qquad \text{-------- (3.30)}$$

and

$$H_y(0) = e^{-iwt}\frac{k}{\omega\mu}A = E_x(0)\frac{k}{\omega\mu} \qquad \text{------- (3.31)}$$

The ratio of the electric field to the magnetic field is known as the impedance, Z.

$$Z_{xy} = \frac{E_x}{H_y} = \frac{\omega\mu}{k} \qquad \text{------- (3.32)}$$

If the electric field is orientated in the y direction, the impedance Z_{xy} can be derived in a similar fashion as

$$Z_{yx} = \frac{E_y}{H_x} = -\frac{\omega\mu}{k} \qquad \text{------- (3.33)}$$

By using (3.23) and the fact that $\frac{1}{\sqrt{i}} = e^{-\frac{i\pi}{4}}$ (see Appendix A for derivation), (3.32) can be written in terms of the apparent resistivity ρ

$$Z_{xy} = 2\pi\sqrt{\frac{\rho}{5T}}\cdot 10^{-3}e^{\frac{-i\pi}{4}} \quad \text{ohm} \qquad \text{------- (3.34)}$$

Since the impedance is complex, it has an amplitude and a phase. The amplitude is given by the modulus of Z

$$\left|Z_{xy}\right| = 2\pi\sqrt{\frac{\rho}{5T}}\cdot 10^{-3} \quad \text{ohm} \qquad \text{------- (3.35)}$$

and the phase by the tangency of the ratio of the imaginary part to the real part.

$$\phi_{xy} = -\frac{\pi}{4} \qquad \text{------- (3.36)}$$

For Z_{yx} the amplitude is the same as for Z_{xy} and the phase is

$$\phi_{yx} = \pi - \frac{\pi}{4} \qquad \text{------- (3.37)}$$

3.4.2. Impedance of a two-layer medium

The impedance for a two-layer medium can be derived from (3.22) and (3.25). Figure 3.4 depicts a model of a two-layer medium.

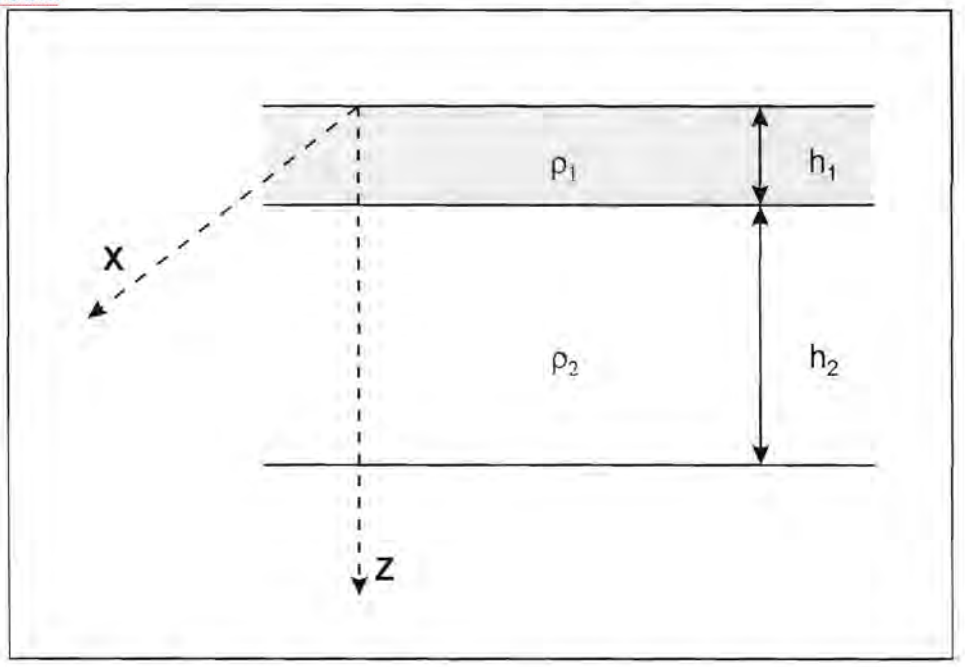

Figure 3.4 Two-layer medium

In the first layer the electric and magnetic fields are

$$E_x^{(1)} = e^{-iwt}\left(A_1 e^{ik_1 z} + B_1 e^{-ik_1 z}\right) \qquad 0 \le z \le h_1 \qquad \text{------- (3.38)}$$

and

$$H_y^{(1)} = e^{-iwt}\frac{k_1}{\omega\mu}\left(A_1 e^{ik_1 z} - B_1 e^{-ik_1 z}\right) \qquad 0 \le z \le h_1 \qquad \text{------- (3.39)}$$

The second layer is considered to be a half-space, and the electric and magnetic fields are

$$E_x^{(2)} = e^{-iwt}\left(A_2 e^{ik_2 z}\right) \qquad z \ge h_1 \qquad \text{------- (3.40)}$$

and

$$H_y^{(2)} = e^{-iwt}\frac{k_2}{\omega\mu}\left(A_2 e^{ik_2 z}\right) \qquad z \ge h_1 \qquad \text{------- (3.41)}$$

Using the impedance ratio and the boundary conditions given in (3.42) and (3.43) the impedance relation (3.44) for a two layer medium can be derived (Kaufman and Keller, 1981).

$$E_x^n = E_x^{n+1} \qquad z = h_n \qquad \text{------- (3.42)}$$

$$H_y^n = H_y^{n+1} \qquad z = h_n \qquad \text{------- (3.43)}$$

$$Z_{xy} = \frac{\omega\mu}{k_1} \frac{1+\left(\frac{1-\sqrt{\rho_1/\rho_2}}{1+\sqrt{\rho_1/\rho_2}}\right)e^{2ik_1h_1}}{1-\left(\frac{1-\sqrt{\rho 1/\rho_2}}{1+\sqrt{\rho_1/\rho_2}}\right)e^{2ik_1h_1}} \qquad \text{------- (3.44)}$$

3.4.3. Electromagnetic fields in the presence of a two-dimensional structure

After developing the impedance for a layered medium, it is important to consider what effects two-dimensional structures will have on the electromagnetic field. Two scenarios will be considered, namely

- electric field parallel to the vertical structure (E - polarisation)
- electric field perpendicular to the vertical structure (H - polarisation)

E-Polarisation

Assume the two-dimensional structure strikes in the x-direction and the primary electric field is directed along the x-axis. The primary electric field does not intersect the surface and the total electric field has only an E_x component. As a result all derivatives with respect to x are zero. Maxwell's equation describing the magnetic field due to a current distribution (3.4) therefore becomes

$$\nabla \times \mathbf{H} = \sigma\mathbf{E} \qquad \text{------- (3.45)}$$

(the displacement current is negligibly small compared to the conduction current for the frequencies and conductivities measured in magnetotellurics (Kaufman and Keller, 1981)).

Equation (3.45) reduces to

$$\sigma E_x = \frac{\partial H_z}{\partial y} - \frac{\partial H_y}{\partial z} \qquad \text{------- (3.46)}$$

and (3.3) together with $\mathbf{H} = H_0 e^{-i\omega t}$ yield

$$H_y = \frac{1}{i\omega\mu}\frac{\partial E_x}{\partial z} \qquad \text{------- (3.47)}$$

and

$$H_z = -\frac{1}{i\omega\mu}\frac{\partial E_x}{\partial y} \qquad \text{------- (3.48)}$$

Therefore, in the case of E-polarisation, the magnetic field has a vertical component.

H-Polarisation

In this case the primary electric field is directed perpendicular to the x-striking two-dimensional structure. Electric charges develop on the structure and the electric field has components E_y and E_z. The electric field does not change in the x-direction and therefore all derivatives with respect to x are zero. Ampere's law (3.45) again gives the magnetic field associated with this current distribution, with

$$\sigma E_y = \frac{\partial H_x}{\partial z} \qquad \text{------- (3.49)}$$

and

$$\sigma E_z = \frac{\partial H_x}{\partial y} \qquad \text{------- (3.50)}$$

These equations are substituted into (3.3) and yield the following equation describing the magnetic field

$$H_x = \frac{1}{i\omega\mu}\left(\frac{\partial E_z}{\partial y} - \frac{\partial E_y}{\partial z}\right) \qquad \text{------- (3.51)}$$

When the electric field is directed perpendicular to the two-dimensional structure, the magnetic field does not have a z-component.

3.4.4. Tensor impedance

From the previous section, it is clear that the relative orientation between structures in the earth and the primary electromagnetic field plays a crucial role in impedance calculations. This is further complicated by the fact that the orientation of the primary electromagnetic field changes with time and several orientations may be present at a certain time resulting in elliptical polarisation. In an attempt to deal with this problem the tensor impedance was derived (Sims et al., 1971; Kaufman and Keller, 1981). In matrix form the tensor repesentation of (3.32) and (3.33) is

$$\begin{bmatrix} E_x \\ E_y \end{bmatrix} = \begin{bmatrix} Z_{xx} & Z_{xy} \\ Z_{yx} & Z_{yy} \end{bmatrix} \begin{bmatrix} H_x \\ H_y \end{bmatrix} \qquad \text{------- (3.52)}$$

Therefore, the electric field in a certain direction may depend on magnetic fields parallel and perpendicular to it and the impedances can vary with time as the polarisation of the source field changes (Swift, 1986).

CHAPTER 4
DATA ACQUISITIONING AND PROCESSING

The collection of magnetotelluric data in the field entails setting up the sounding station and recording until adequate data have been gathered in the appropriate frequency range. Time spent on a sounding depends on the required survey depth and the level of natural electromagnetic activity. Basic processing involves a number of steps, one of the most important being to determine whether natural electromagnetic events occurred.

4.1. DATA ACQUISITIONING

4.1.1. Field Setup

It is clear from the development of the basic theory that inhomogeneities in the substructure of the earth cause secondary electric and magnetic fields that each have components in the x-, y- and z- directions. For this reason it is necessary to measure three perpendicular magnetic components and two horizontal perpendicular electric components. Two horizontal perpendicular magnetic components are also measured at a remote station away from the base station. This is based on the assumption that the noise will be different at the two stations but the events will be the same. A typical field setup is shown in Figure 4.1.

4.1.1.1. Measuring the electric field

To measure the electric field, the potential difference between two electrodes is measured. The electrodes must preferably be made of non-polarising material such as a metal immersed in one of its salts in a porous cup. The voltage difference between a pair of non-polarising electrodes is relatively stable, whereas for metal electrodes potential differences resulting

from electrochemical reactions at the metal surface can be present (Kaufman and Keller, 1981).

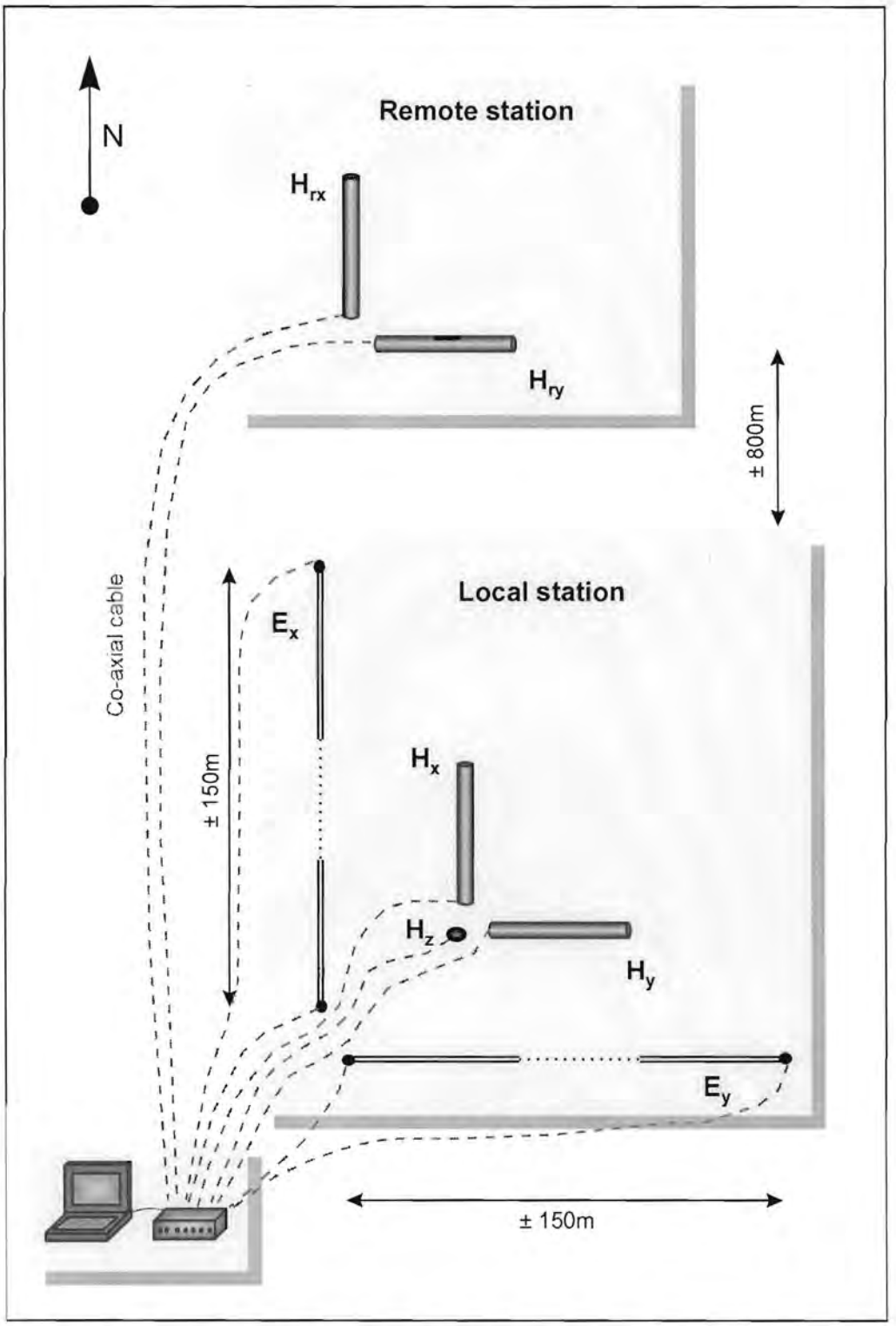

Figure 4.1. Field setup for Magnetotelluric station

Contact resistances at electrodes can cause problems. In a dry soil or bare rock the contact resistance of the electrode may be very high and the soil or rock needs to be saturated with water or sometimes even saltwater to improve the contact. It is also true that when the contact resistances are high electrostatic and electromagnetic noise cause problems.

Electrode intervals vary from site to site. According to Ohm's law potential (V) is proportional to resistance (R):

$$V = I R \qquad \text{------- (4.1)}$$

Therefore, as the resistivity of the geology increases the strength of the measured signal will increase, if the current (I) remains constant. In a conductive earth, the signal will decrease and an increase in electrode spacing is necessary to amplify the signal strength (V = E I). It is important to remember that noise will behave the same as natural signals and consequently the amount of noise present will influence the choice of electrode spacing.

Another important factor in laying out the electrodes is the geological substructure. For a small electrode spacing local variations in resistivity near the surface will negatively influence the measurements. If, for example, the electrodes are placed in a localised shallow conductor, the electric measurements will be strongly influenced by this feature while the magnetic measurements will be almost unaffected. If a longer separation is used between the electrodes, the average electric field will be more characteristic of the dominant electric field and the dominant resistivity in the surface layer.

Coaxial cables are used between the electrodes and the recording equipment. Since motion of the cables must be minimised it should be laid flat on the ground.

4.1.1.2. Measuring the magnetic field

Magnetic induction coils are used to measure the magnetic field intensity. The coil detects the rate of change of the magnetic field and the electromotive force (EMF) induced in the coil is

$$EMF = -nA\left(\frac{dB}{dt}\right)\cos\theta \qquad \text{------- (4.2)}$$

for a coil with negligible resistance, inductance and capacitance (Kaufman and Keller, 1981). In (4.2)

n = number of turns of wire

A = area of the coil (m^2)

B = magnetic induction (T)

θ = angle between the magnetic field **H** and the normal to the plane of the coil.

The voltage measured by an induction loop is proportional to the oscillation frequency or time rate of change of the magnetic field that cuts through the loop.

The coils are buried beneath the earth to minimise the effect of wind and changes in temperature. Care must be taken to level the coils perfectly in the horizontal and vertical positions for the various components respectively.

4.1.2. Data sampling

The aim of a magnetotelluric sounding is to deduce an image of changes in the electrical substructure of the earth with depth. For this reason data are sampled at different frequencies. Frequency relates to depth via the skin depth

$$\delta = \sqrt{\frac{2}{\omega\mu\sigma}} \qquad \text{------- (4.3)}$$

Data are recorded from both the electrodes and the magnetic coils in analog form and need to be digitised. The main problem with digitising a signal is frequency aliasing. The Nyquist criterion states that at least two samples must be taken over each cycle of a frequency to be certain that the frequency can be recognised. The sampling interval must therefore be chosen in such a way that all the frequencies contained in the signal can be recognised and not just those that we are interested in. A possible solution is to filter out unwanted frequencies with an analogue filter before digitising the signal. Unwanted frequencies such as 50Hz and its harmonics can be filtered out before data processing starts.

The range of frequencies finally utilised at a sounding station (and therefore the depth of investigation) depends mainly on the aim of the survey and the geo-electrical substructure. According to the Nyquist criterion the highest frequency that can be identified with a sampling period Δt is

$$f_N = \frac{1}{2\Delta t} \qquad \text{------- (4.4)}$$

For example, if the sampling frequency is 3000 Hz, the highest frequency that can be recovered would be 1500 Hz. The lowest frequency that can be measured with a specific sampling period Δt is

$$f_L = \frac{1}{(n * \Delta t) / 2} \qquad \text{------- (4.5)}$$

where n is the number of points sampled ($n = 2^m$ because the first step of processing is transformation to the frequency domain). Therefore, if we sample 2048 points at a frequency of 3000 Hz, the lowest frequency that

can be identified is approximately 3 Hz. From equation (4.5) it is clear that the range of frequencies can be improved by increasing the number of sampling points.

4.2. DATA PROCESSING

The steps involved in data processing are shown in Figure 4.2. Each of the steps will be discussed in more detail.

4.2.1. Transformation to Frequency Domain

Sampled time series data are transformed to complex amplitude spectra using Fourier transformation. The Fast Fourier Transform is the algorithm most widely used for this operation and the computational form to be implemented is

$$X(n) = \sum_{k=0}^{N-1} x_0(k) e^{\frac{-i2\pi k}{N}}, \qquad n = 0,1,\ldots,N-1 \qquad \text{------- (4.6)}$$

where $x_0(k)$ is the sampled time function.

4.2.2. Auto- and cross power spectra

The auto- and cross spectra are the frequency domain equivalents of auto-correlation and cross-correlation in the time domain. They are defined by Swift (1986) as follows:

Auto-spectra	$\langle E_x E_x^* \rangle$, $\langle E_y E_y^* \rangle$, $\langle H_x H_x^* \rangle$, $\langle H_y H_y^* \rangle$
Cross-spectra	$\langle E_x H_x^* \rangle$, $\langle E_x H_{rx}^* \rangle$, $\langle H_x E_y^* \rangle$, etc.

$E_x = E_x(\omega)$, $E_y = E_y(\omega)$, etc. are the Fourier spectra of the time domain functions and $E_x^* = E_x^*(\omega)$, $E_y^* = E_y^*(\omega)$, etc. are the complex conjugates of

the Fourier spectra. The brackets <> represent an averaging in time for finite bandwidths.

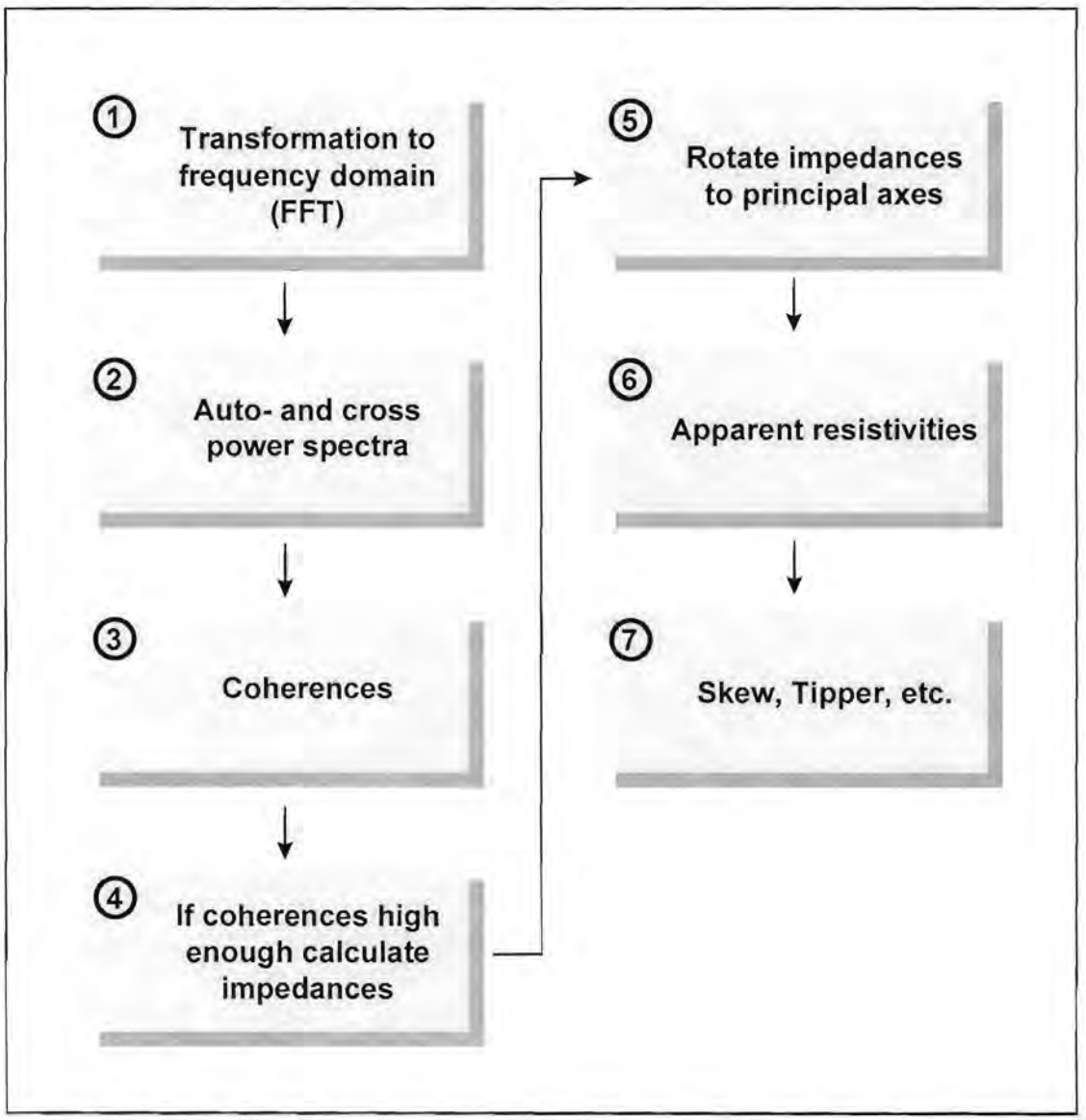

Figure 4.2. Processing steps

4.2.3. Coherences

It is necessary to determine whether a data set contains actual events or only noise. An event must appear simultaneously on at least two related

components, e.g. E_x and H_y but is usually visible on all the components. The following discussion is taken from an article on coherence functions by Reddy and Rankin (1974).

We can view the MT system as a multi-input linear system where H_x and H_y are the inputs, E_x and E_y are the outputs and Z_{zz}, Z_{xy}, Z_{yx} and Z_{yy} are the frequency response functions. Three types of coherence functions can be used to analyse the data quality:

- *Ordinary coherence*: Coherency between the output and each of the inputs, e.g. between E_x and H_x or E_x and H_y. High ordinary coherences between H_x and E_y and between H_y and E_x indicate a linear relation between the inputs and outputs.

$$\mathrm{Coh}(E_x H_x) = \frac{< E_x H_x^* >}{(< E_x E_x^* >< H_x H_x^* >)^{\frac{1}{2}}} \qquad \text{------- (4.7)}$$

- *Multiple coherence*: Coherency between the output and all of the inputs, e.g. between output E_x and inputs H_x and H_y. High multiple coherences indicate good signal to noise ratios.

$$\mathrm{Mcoh}(E_x H_x H_y) =$$

$$\frac{< H_y H_y^* >< H_x E_x^* >^2 + < H_x H_x^* >< H_y E_x^* >^2 - 2\mathrm{Re}(< H_x H_y^* >< H_y E_x^* >< E_x H_x^* >)}{< E_x E_x^* > (< H_x H_x^* >< H_y H_y^* > - < H_x H_y^* >^2)}$$

------- (4.8)

- *Partial coherence*: This is the coherency between the output and a specific input after the effect of the other inputs has been removed by least-squares prediction from the specified output and input. For e.g. between E_x and H_x after the effect of H_y has been removed by least squares prediction from E_x and H_x. High partial coherences between E_x and H_y and between E_y and H_x and corresponding low partial

coherences between E_x and H_x and between E_y and H_y indicate that the rotation angle corresponds to the principal direction. The reason for this being that in the principal direction Z_{xx} and Z_{yy} is close to zero. This means that $E_x = Z_{xx}H_x$ is close to zero and therefore the partial coherency between E_x and H_x is low.

$$Pcoh(H_xE_x) = \frac{<H_xE_x^*>}{(<E_xE_x^*><H_xH_x^*>)^{\frac{1}{2}}} \qquad \text{------- (4.9)}$$

The equation looks similar to (4.7) but it differs in that the effect of the other input (H_y in this case) has been removed. The partial coherency can also be formulated in terms of the multiple and ordinary coherences:

$$Pcoh(H_xE_x) = \frac{Mcoh(E_xH_xH_y) - Coh(H_yE_x)}{1 - Coh(H_yE_x)} \qquad \text{------- (4.10)}$$

4.2.4. Impedances

If the coherences are high enough, indicating that there may be a true event present in the data, we can proceed to calculate the impedance tensor elements. This can be done in two ways, one in which only the components measured at the local station are used and another in which the remote station components are incorporated.

4.2.4.1. Single station impedance

Z_{ij} in equation (3.52) can be estimated in a least squares way (Sims et al., 1971). Young (1962) states the principle of least squares as follows: the most probable value of a quantity is obtained from a set of measurements by choosing the value which minimises the sum of the squares of the deviations of these measurements. Deviation is defined as the difference between any measurement in the set and the mean of the set. For a set of

measurements x_i, the most probable value of x is that which minimises the quantity

$$\sum_{i=1}^{n}(x - x_i)^2$$

For this equation to be a minimum

$$\frac{d}{dx}\sum_{i=1}^{n}(x - x_i)^2 = 0 \qquad \text{------- (4.11)}$$

Apply this to (3.52) (n is the number of measurements at a specific frequency):

$$\Psi = \sum_{i=1}^{n}(E_{xi} - (Z_{xx}H_{xi} + Z_{xy}H_{yi}))^2 \qquad \text{------- (4.12)}$$

Setting the derivatives of Ψ with respect to the real and imaginary parts of Z_{xx} equal to zero yields

$$\sum_{i=1}^{n}E_{xi}H_{xi}^{*} = Z_{xx}\sum_{i=1}^{n}H_{xi}H_{xi}^{*} + Z_{xy}\sum_{i=1}^{n}H_{yi}H_{xi}^{*} \qquad \text{------- (4.13)}$$

Setting the derivatives of Ψ with respect to the real and imaginary parts of Z_{xy} equal to zero yields

$$\sum_{i=1}^{n}E_{xi}H_{yi}^{*} = Z_{xx}\sum_{i=1}^{n}H_{xi}H_{yi}^{*} + Z_{xy}\sum_{i=1}^{n}H_{yi}H_{yi}^{*} \qquad \text{------- (4.14)}$$

The solutions in (4.13) and (4.14) minimise the error caused by noise on E_x. By taking another least-squares estimate the noise on H_x can be minimised. The various least squares estimates results in the following equations:

$$<E_xE_x^*> = Z_{xx}<H_xE_x^*> + Z_{xy}<H_yE_x^*> \quad \text{----- (4.15)}$$

$$<E_xE_y^*> = Z_{xx}<H_xE_y^*> + Z_{xy}<H_yE_y^*> \quad \text{----- (4.16)}$$

$$<E_xH_x^*> = Z_{xx}<H_xH_x^*> + Z_{xy}<H_yH_x^*> \quad \text{----- (4.17)}$$

$$<E_xH_y^*> = Z_{xx}<H_xH_y^*> + Z_{xy}<H_yH_y^*> \quad \text{----- (4.18)}$$

where the terms between brackets are the auto- and cross spectra and the brackets indicate the average spectra over finite bandwidths.

By substituting (4.15) in (4.16), (4.17) and (4.18), (4.16) in (4.17) and (4.18) and (4.17) in (4.18), six estimates for the impedance tensor element Z_{xy} can be determined:

$$Z_{xy} = \frac{<E_xE_y^*><H_xE_x^*> - <E_xE_x^*><H_xE_y^*>}{<H_yE_y^*><H_xE_x^*> - <H_yE_x^*><H_xE_y^*>} \quad \text{----- (4.19)}$$

$$Z_{xy} = \frac{<E_xH_x^*><H_xE_x^*> - <E_xE_x^*><H_xH_x^*>}{<H_yH_x^*><H_xE_x^*> - <H_yE_x^*><H_xH_x^*>} \quad \text{------(4.20)}$$

$$Z_{xy} = \frac{<E_xH_y^*><H_xE_x^*> - <E_xE_x^*><H_xH_y^*>}{<H_yH_y^*><H_xE_x^*> - <H_yE_x^*><H_xH_y^*>} \quad \text{------(4.21)}$$

$$Z_{xy} = \frac{<E_xH_x^*><H_xE_y^*> - <E_xE_y^*><H_xH_x^*>}{<H_yH_x^*><H_xE_y^*> - <H_yE_y^*><H_xH_x^*>} \quad \text{----- (4.22)}$$

$$Z_{xy} = \frac{<E_xH_y^*><H_xE_y^*> - <E_xE_y^*><H_xH_y^*>}{<H_yH_y^*><H_xE_y^*> - <H_yE_y^*><H_xH_y^*>} \quad \text{----- (4.23)}$$

$$Z_{xy} = \frac{<E_xH_y^*><H_xH_x^*> - <E_xH_x^*><H_xH_y^*>}{<H_yH_y^*><H_xH_x^*> - <H_yH_x^*><H_xH_y^*>} \quad \text{----- (4.24)}$$

Six estimates for Z_{xx} can be determined in a similar way.

Following the same approach six estimates each for Z_{yx} and Z_{yy} can be determined.

4.2.4.2. Remote reference impedance calculations

The main problem in using the impedance estimates derived in the previous section is that the auto-spectra of functions that contain noise may severely bias the estimates. In order to address this problem, Gamble et al. (1979) proposed the use of a remote reference station. At this station two horizontally perpendicular magnetic components, H_{xr} and H_{yr}, are measured. The noise at this station should not correlate with the noise at the local station. Multiply the two linear relations in (3.52) with H_{xr}^* and H_{yr}^*

$$< E_x H_{xr}^* >= Z_{xx} < H_x H_{xr}^* > + Z_{xy} < H_y H_{xr}^* > \quad \text{----- (4.25)}$$

$$< E_x H_{yr}^* >= Z_{xx} < H_x H_{yr}^* > + Z_{xy} < H_y H_{yr}^* > \quad \text{----- (4.26)}$$

$$< E_y H_{xr}^* >= Z_{yx} < H_x H_{xr}^* > + Z_{yy} < H_y H_{xr}^* > \quad \text{----- (4.27)}$$

$$< E_y H_{yr}^* >= Z_{yx} < H_x H_{yr}^* > + Z_{yy} < H_y H_{yr}^* > \quad \text{----- (4.28)}$$

Solve these four equations for the impedance tensor elements:

$$Z_{xx} = \frac{< E_x H_{xr}^* >< H_y H_{yr}^* > - < E_x H_{yr}^* >< H_y H_{xr}^* >}{< H_x H_{xr}^* >< H_y H_{yr}^* > - < H_x H_{yr}^* >< H_y H_{xr}^* >} \quad \text{----- (4.29)}$$

$$Z_{xy} = \frac{< E_x H_{yr}^* >< H_x H_{xr}^* > - < E_x H_{xr}^* >< H_x H_{yr}^* >}{< H_x H_{xr}^* >< H_y H_{yr}^* > - < H_x H_{yr}^* >< H_y H_{xr}^* >} \quad \text{----- (4.30)}$$

$$Z_{yx} = \frac{< E_y H_{xr}^* >< H_y H_{yr}^* > - < E_y H_{yr}^* >< H_y H_{xr}^* >}{< H_x H_{xr}^* >< H_y H_{yr}^* > - < H_x H_{yr}^* >< H_y H_{xr}^* >} \quad \text{----- (4.31)}$$

$$Z_{yy} = \frac{< E_y H^*_{yr} >< H_x H^*_{xr} > - < E_y H^*_{xr} >< H_x H^*_{yr} >}{< H_x H^*_{xr} >< H_y H^*_{yr} > - < H_x H^*_{yr} >< H_y H^*_{xr} >} \quad \text{----- (4.32)}$$

4.2.5. Rotation of impedance tensor

The impedance estimates in the previous section were calculated for the measuring axes x, y. In a two-dimensional earth the electric field in one direction may depend on magnetic field variations both parallel and perpendicular. The ideal is for the x-axis to point north in a one dimensional case or parallel to the strike in a two dimensional case (Hobbs, 1992). In the two dimensional case this will minimise the effects of the E_xH_x and E_yH_y terms. However, the strike direction of the two-dimensional structures may vary with depth and for this reason data are measured with x directed along magnetic north. The next step in data processing is to rotate the calculated impedance elements to the principal axes (parallel and perpendicular to strike) using the following equations:

$$Z_{x'x'}(\alpha) = \tfrac{1}{2}((Z_{xx} + Z_{yy}) + (Z_{xx} - Z_{yy})\cos 2\alpha + (Z_{xy} + Z_{yx})\sin 2\alpha \quad \text{----- (4.33)}$$

$$Z_{x'y'}(\alpha) = \tfrac{1}{2}((Z_{xy} - Z_{yx}) + (Z_{xy} + Z_{yx})\cos 2\alpha + (Z_{yy} - Z_{xx})\sin 2\alpha \quad \text{----- (4.34)}$$

$$Z_{y'x'}(\alpha) = \tfrac{1}{2}((Z_{yx} - Z_{xy}) + (Z_{yx} + Z_{xy})\cos 2\alpha + (Z_{yy} - Z_{xx})\sin 2\alpha \quad \text{----- (4.35)}$$

$$Z_{y'y'}(\alpha) = \tfrac{1}{2}((Z_{xx} + Z_{yy}) - (Z_{xx} - Z_{yy})\cos 2\alpha - (Z_{xy} + Z_{yx})\sin 2\alpha \quad \text{----- (4.36)}$$

The principal axes are those which maximise $Z_{x'y'}$ and $Z_{y'x'}$ (principal impedances) or minimise $Z_{x'x'}$ and $Z_{y'y'}$ (auxiliary impedances). The impedance elements are rotated a few degrees at a time until the desired maximum or minimum is found.

Rotation of the data assuming a two dimensional earth as described above was proposed by Swift (1986). More recently various authors have given attention to the effect of three dimensional conductivity distributions on the impedance tensor (e.g. Bahr, 1988, 1991; Groom and Bailey, 1989, 1991).

The three dimensionality of the earth's electrical structure will ensure that the diagonal elements of the tensor never disappear. Several decomposition schemes for the measured impedance tensor have been proposed by these authors. Bahr (1988, 1991) chose what he called the principal superimposition model to be a local three dimensional anomaly over a regional two dimensional structure. He used certain parameters to classify different distortion types and subsequently decide whether decomposition of the impedance tensor is necessary (Bahr, 1991). Figure 4.3(a) shows a schematic summary of his distortion classification process. The equations referred to in this diagram appear in figure 4.3(b).

4.2.6. Apparent resistivity

The final processing step is the calculation of the apparent resistivity as a function of frequency using Cagnaird's (1953) formula

$$\rho_{ij} = \frac{1}{5f}\left|Z_{ij}\right|^2 \qquad i,j = x,y \qquad \text{------- (4.37)}$$

The apparent resistivities are shown on a log-log graph as a function of frequency. Spies and Eggers (1986) noted that curves calculated with equation (4.37) usually show an oscillation at low frequencies. Since these oscillations are not present in the time domain they concluded that the oscillations are artefacts of the frequency domain representation and suggested using some alternative forms of (4.37)

$$\rho_{ij} = \frac{2}{5f}\left[\mathrm{Re}(Z)\right]^2 \qquad i,j = x,y \qquad \text{------- (4.38)}$$

$$\rho_{ij} = \frac{2}{5f}\left[\mathrm{Im}(Z)\right]^2 \qquad i,j = x,y \qquad \text{------- (4.39)}$$

$$\rho_{ij} = \frac{1}{5f}\left[\mathrm{Im}(Z^2)\right] \qquad i,j = x,y \qquad \text{------- (4.40)}$$

$$\rho_{ij} = \frac{1}{5f}\left|Z^2\right| \qquad i,j = x,y \qquad \text{------- (4.41)}$$

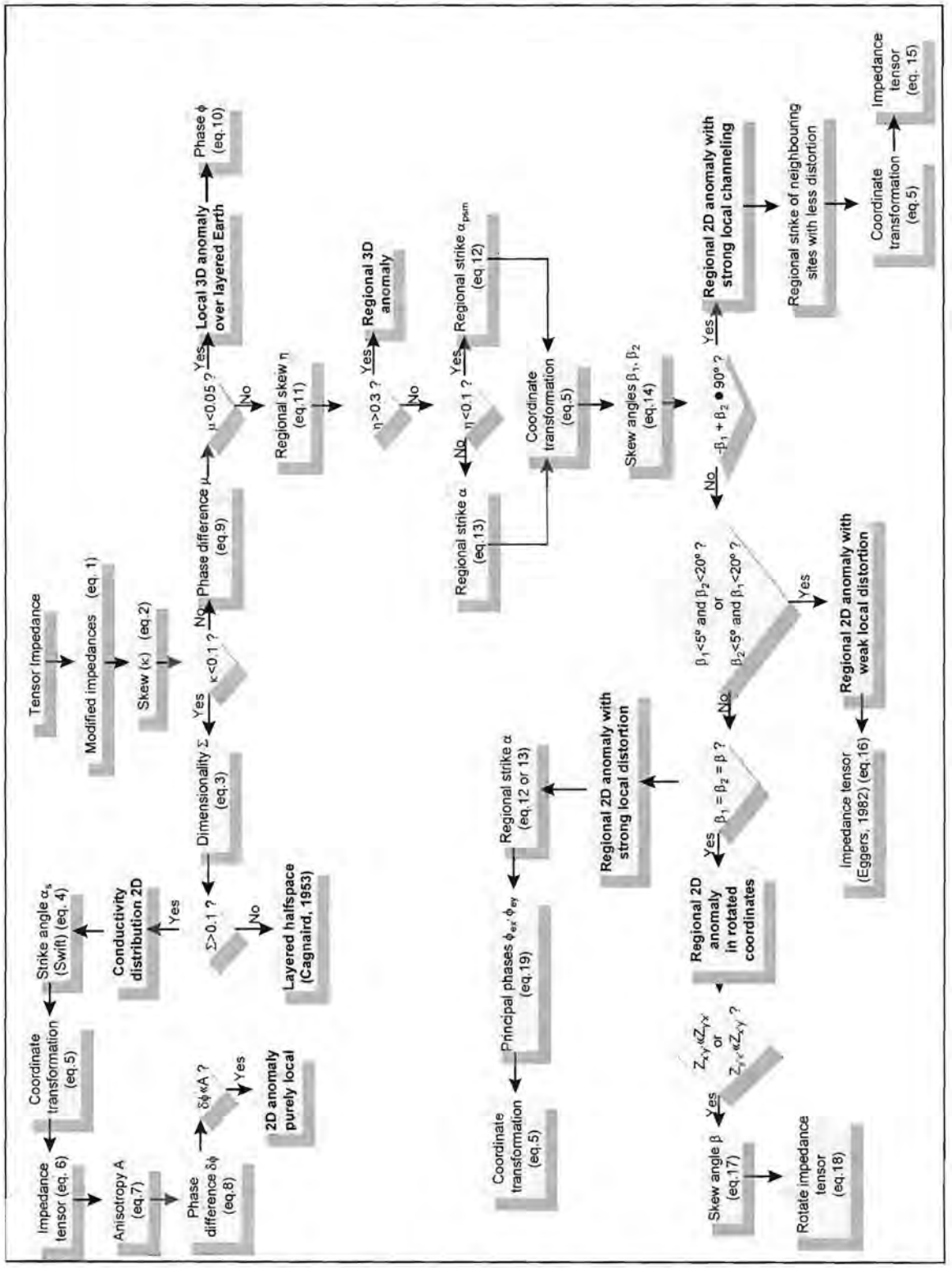

Figure 4.3(a). A flow diagram showing the calculation of distortion parameters (Bahr, 1991).

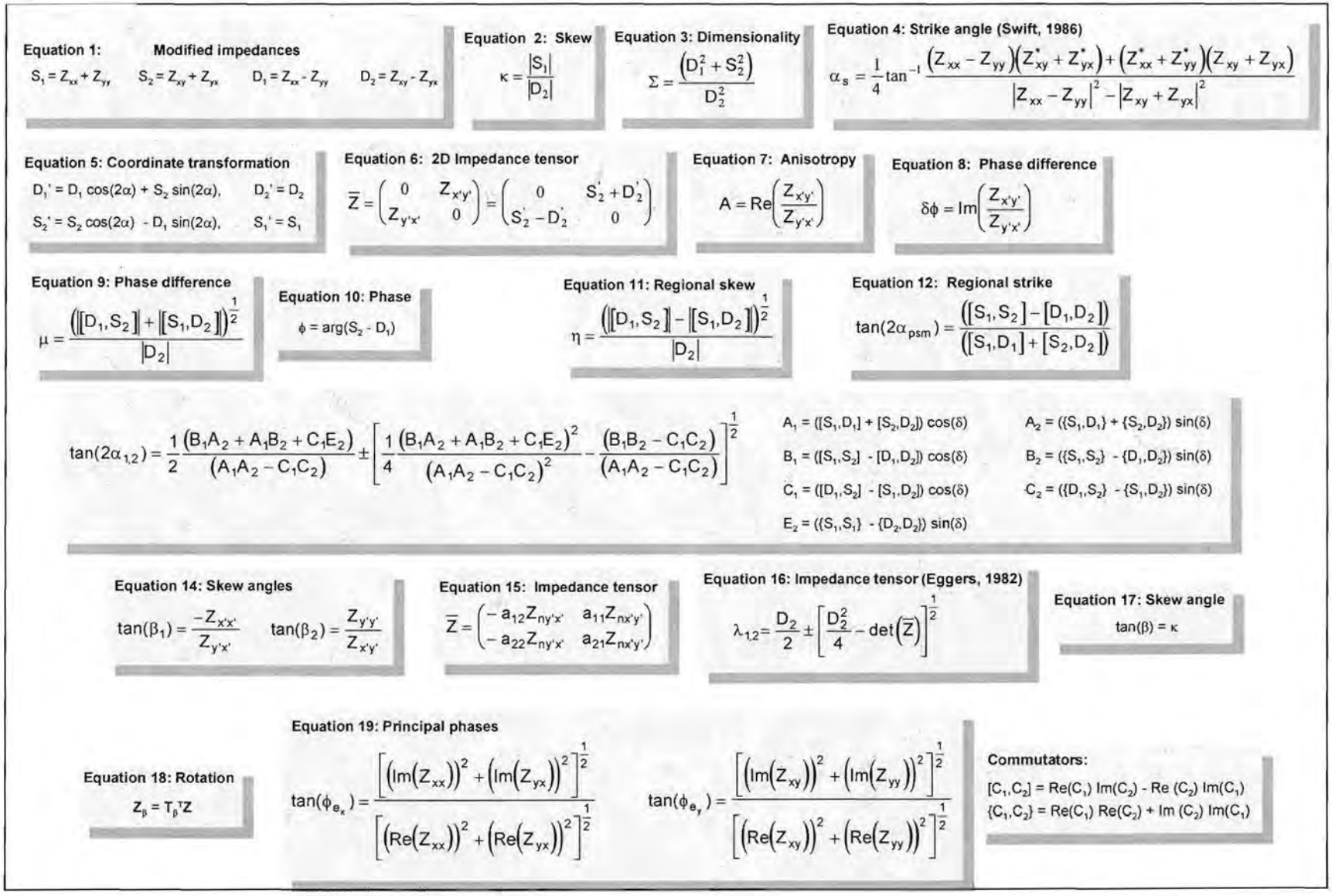

Figure 4.3(b). Equations used in Figure 4.3(a)

4.2.7. Other parameters calculated during processing

A number of additional parameters can be calculated from the impedance tensor and can assist in gaining a better understanding of the earth's electrical substructure.

4.2.7.1. Skewness

When the impedance tensor has been rotated to the principal direction, Z_{xx} and Z_{yy} will be very small if the earth is laterally uniform or two-dimensional, but larger when the earth has a three dimensional structure (Vozoff, 1972). At the same time the difference between the elements Z_{xy} and Z_{yx} is large when the earth is strongly two-dimensional and small otherwise. The ratio

$$S = \frac{|Z_{xx} + Z_{yy}|}{|Z_{xy} - Z_{yx}|} \qquad \text{------- (4.42)}$$

is known as the 'skewness' ratio. If S is large the structure of the earth appears to be three-dimensional for that specific frequency range.

4.2.7.2. Tipper

We saw in equations (3.47), (3.48) and (3.51) that the magnetic field does not have a vertical component when the electric field is directed perpendicular to the strike direction (H-polarisation). Therefore, the vertical magnetic component can be used to determine the strike direction of the two-dimensional structure (the horizontal direction in which the magnetic field is most highly coherent with H_z is perpendicular to the strike). In defining the 'Tipper' parameter we assume that H_z is linearly related to H_x and H_y (Vozoff, 1972). At each frequency

$$H_z = AH_x + BH_y \qquad \text{------- (4.43)}$$

where A and B are unknown complex coefficients. These coefficients (A,B) can be thought of as 'tipping' part of the horizontal magnetic field into the vertical and is therefore called the tipper. The tipper (T) is defined as

$$|T| = (|A|^2 + |B|^2)^{\frac{1}{2}} \qquad \text{------- (4.44)}$$

with a phase

$$\delta = \frac{(A_r^2 + A_i^2)\arctan(\frac{A_i}{A_r}) + (B_r^2 + B_i^2)\arctan(\frac{B_i}{B_r})}{T^2} \qquad \text{------- (4.45)}$$

CHAPTER 5

STATISTICAL REDUCTION OF DATA

5.1. GENERAL

In chapter 3 we derived the basic equations used in MT (eq. 3.52). In reality, in the presence of noise the equations look as follows

$$E_x = Z_{xx}H_x + Z_{xy}H_y + r \qquad \text{----- (5.1)}$$

$$E_y = Z_{xy}H_x + Z_{yy}H_y + r \qquad \text{----- (5.2)}$$

where r represents the noise component. In the field *N* data sets are collected at a specific frequency. The above equations in matrix form are

$$\left[E_{x_i}\right] = \left[H_{x_i}\ H_{y_i}\right]\begin{bmatrix} Z_{xx} \\ Z_{xy} \end{bmatrix} + \left[r_i\right] \qquad \text{----- (5.3)}$$

$$\left[E_{y_i}\right] = \left[H_{x_i}\ H_{y_i}\right]\begin{bmatrix} Z_{yx} \\ Z_{yy} \end{bmatrix} + \left[r_i\right] \qquad \text{----- (5.4)}$$

In general the equations are written as

$$\mathbf{x} = \mathbf{U}\beta + \mathbf{r} \qquad \text{----- (5.5)}$$

with **x** an Nx1 matrix representing the electric field components, **U** an Nx2 matrix containing the measured magnetic field components, β the 2x1 impedance matrix and **r** an Nx1 matrix containing the noise component. Since the impedance tensor is indicative of the properties of the underlying geology, there is only one tensor for *N* sets of data recordings at a particular frequency. If the data were noise free and consisted only of true natural electromagnetic events, it would be sufficient to do only one recording per frequency. In reality noise contamination is an ever-present problem in magnetotelluric data collection and consequently it is necessary to record several data sets at a specific frequency. From a statistical point of view the aim is to determine the impedance tensor that most probably represents the electrical properties of the underlying earth.

In order to determine the impedance value, it is necessary to minimise the error between observed and calculated values, for example between $E_{observed}$ and

$E_{calcualted}$ (as calculated using equation (3.52)). Figure 5.1 shows a schematic diagram of this process.

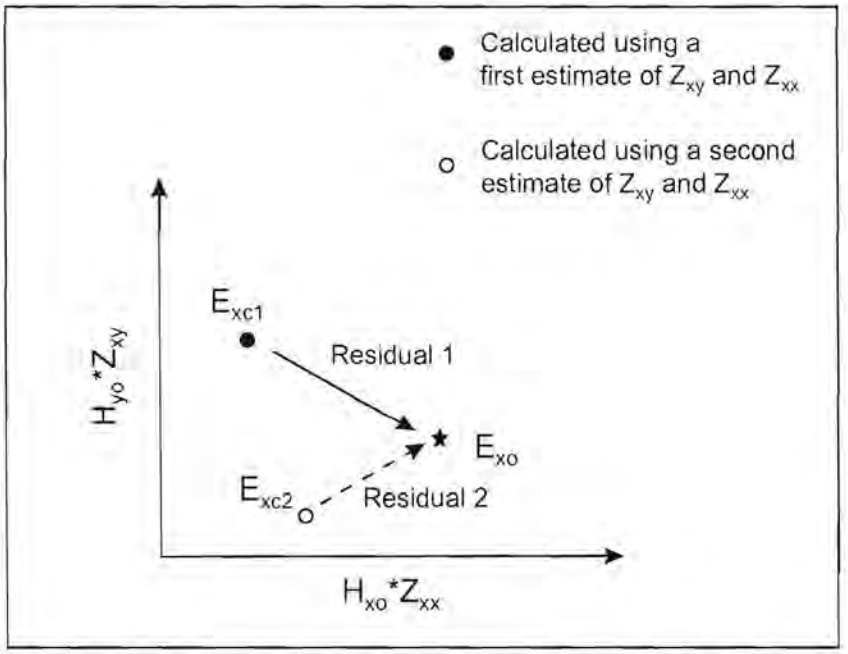

Figure 5.1 Visualisation of the minimisation of a residual

The objective is to minimise the residuals between N calculated and N observed electrical components for an estimate of Z_{xx} and Z_{xy}.

5.2. L_1 AND L_2 NORMS

A possible solution to this problem is to use the Least Squares method to determine β. The principle of least squares was outlined in section 4.2.4.1. as the most probable value of a quantity obtained from a set of measurements by choosing the value that minimises the sum of the squares of the deviations of these measurements (Young, 1962). For a set of measurements x_i the most probable value of x is that which minimises the quantity

$$\sum_{i=1}^{n}(x-x_i)^2 \qquad \text{----- (5.6)}$$

with x a variable that can be varied to obtain the minimum value of the function. For this function to be a minimum the following condition must be satisfied:

$$\frac{d}{dx}\sum_{i=1}^{N}(x-x_i)^2 = 0 \qquad \text{----- (5.7)}$$

The derivative of a sum of terms is equal to the sum of the derivatives, therefore

$$x = \frac{1}{N}\sum_{i=1}^{N} x_i \qquad \text{----- (5.8)}$$

The most probable value of x turns out to be the mean of the observations. This minimisation is called the L_2 norm. A major problem with this method is the effect of one poor observation on the mean. The technique works best if the errors are normally distributed. A first step to improve the robustness of the method is to work with the median instead of the mean. This is achieved by minimising the summed absolute values instead of the summed squared differences and is known as the L_1 norm:

$$\begin{aligned} &\frac{d}{dx}\sum_{i-1}^{N}|x - x_i| = 0 \\ &\sum_{i=1}^{N}\frac{d}{dx}|x - x_i| = 0 \qquad \text{----- (5.9)} \\ &\sum_{i=1}^{N}\text{sign}(x - x_i) = 0 \end{aligned}$$

sign is +1 when the argument is positive, -1 when the argument is negative and somewhere in between when the argument is zero (Claerbout, 1976). For N odd x is equal to the middle order statistic $x_{(\lfloor N/2 \rfloor+1)}$ where $\lfloor\ \rfloor$ denotes the integer part while for N even the median is chosen as $(x_{\lfloor N/2 \rfloor}+x_{(\lfloor N/2 \rfloor+1)})/2$ (Chave et al., 1987). Before the median can be computed the data have to be ordered in ascending order.

5.3. ROBUST M-ESTIMATION

From the discussion it is clear that the L_1 norm is not as sensitive as the L_2 norm, but it is still prone to the effect of outliers. Weighted medians go some way to improving the robustness of the impedance estimation procedure, minimising

$$\sum_{i=1}^{N}|w_i||x - x_i| \qquad \text{----- (5.10)}$$

with w_i the weight factor, but is still too vulnerable to bad data points. Furthermore, the Least Squares estimate is only really adequate when the errors in the input data have a Gaussian distribution (Egbert and Booker, 1986). It is

possible to test whether the errors are Gaussian distributed by making use of Quantile-Quantile plots (Q-Q plots)

5.3.1. Q-Q Plots

A way of examining the distribution of the error data is by drawing Q-Q plots. The Q-Q plot is achieved by plotting observed residuals against the values expected if the residuals were normally distributed (Johnson and Wichern, 1998). The observed residuals must be ordered (written in ascending order). The inverse of the Gaussian distribution function (ϕ^{-1}) gives the expected residuals.

Plot the i^{th} value of the N observed residuals r_i against $\phi^{-1}(i/N)$. If the points fall on a straight line with unit slope, the residuals have a normal (Gaussian) distribution.

To determine the residual expected from a Gaussian error, calculate (i-½)/N and consult a table that depicts the areas under a normal curve (Table A3. Walpole and Myers, 1989) for a value that corresponds to (i-½)/N.

However, impedance tensors still have to be estimated regardless of the error distribution. According to Johnson and Wichern (1998), it is possible to transform non-normal data so that it has a more Gaussian distribution. This is in effect the approach suggested by Sutarno and Vozoff (1989,1991) where they minimise a function of the residuals and not the residuals themselves.

A very important fact to realise is that in all the above we have made use of the principle of maximum likelihood, namely the assumption that the set of measurements we obtained was the most probable set of measurements (Young, 1962).

With the classical least squares approach, impedance tensor estimates can be determined by minimising the error component in equation (5.5) (Sutarno and Vozoff, 1989, 1991).

$$\sum_{i=1}^{N}(x_i - \sum_{j=1}^{2} U_{ij}\beta_j)^2 \rightarrow \min \qquad \text{----- (5.11)}$$

Find the value of β that minimises (5.11), that is, solve for the derivative equal to 0.

$$\sum_{i=1}^{N}(x_i - \sum_{j=1}^{2} U_{ij}\beta_j)U_{ij} = 0 \qquad \text{----- (5.12)}$$

In matrix form equation (5.12) becomes

$$(\tilde{x} - \tilde{U}\hat{\beta})\tilde{U} = 0$$
$$\tilde{U}^T\tilde{x} - \tilde{U}^T\tilde{U}\hat{\beta} = 0$$
$$\tilde{U}^T\tilde{U}\hat{\beta} = \tilde{U}^T\tilde{x}$$
$$\hat{\beta} = (\tilde{U}^T\tilde{U})^{-1}\tilde{U}^T\tilde{x} \qquad \text{----- (5.13)}$$

Huber (1981) solves the problem of robustness by minimising a sum of less rapidly increasing functions of the residuals instead of minimising a sum of squares:

$$\sum_{i=1}^{N}\rho(r_i) = \sum_{i=1}^{N}\rho\left(x_i - \sum_{j=1}^{2} U_{ij}\beta_j\right) = \min \qquad \text{----- (5.14)}$$

ρ(t) is known as a loss function and should be chosen so that the influence function $\psi(t) = \frac{d\rho(t)}{dt}$ is continuous and bounded.

$$\sum_{i=1}^{N}\psi(r_i) = \sum_{i=1}^{N}\psi\left(x_i - \sum_{j=1}^{2} U_{ij}\beta_j\right)U_{ik} = 0, \quad k = 1,2 \qquad \text{----- (5.15)}$$

To ensure that the solution to (5.14) is scale invariant it is necessary to introduce a scaling parameter. Equations (5.14) and (5.15) are substituted by

$$\sum_{i=1}^{N}\rho\left(\frac{r_i}{s}\right) = \sum_{i=1}^{N}\rho\left(\frac{x_i - \sum_{j=1}^{2} U_{ij}\beta_j}{s}\right) \rightarrow \min \qquad \text{----- (5.16)}$$

$$\sum_{i=1}^{N}\psi\left(\frac{r_i}{s}\right)=\sum_{i=1}^{N}\psi\left(\frac{x_i-\sum_{j=1}^{2}U_{ij}\beta_j}{s}\right)U_{ik}=0,\quad k=1,2 \qquad \text{----- (5.17)}$$

Chave et al. (1987) propose two possible choices for the scaling parameter, namely

$$\hat{S}=\frac{s_{MAD}}{\sigma_{MAD}} \qquad \text{----- (5.18)}$$

$$\hat{S}=\frac{s_{IQ}}{\sigma_{IQ}} \qquad \text{----- (5.19)}$$

s_{MAD} is the median value of the absolute residuals (median absolute deviation (MAD))

$$s_{MAD} = \text{median}(|r_i - \text{median}(r)|) \qquad \text{----- (5.20)}$$

and σ_{MAD} is the expected value of the MAD for the appropriate probability density function. In equation (5.19) the subscript IQ marks the interquartile distance. s_{IQ} is the spacing between the 75% and 25% points of the sample distribution, or the centre range containing half of the probability (Chave et al., 1987)

$$s_{IQ}=r_{\left(\frac{3N}{4}\right)}-r_{\left(\frac{N}{4}\right)} \qquad \text{----- (5.21)}$$

σ_{IQ} is the corresponding theoretical value and is equal to twice the MAD for symmetric distributions.

Egbert and Booker (1986) follow a slightly different approach in determining the scale factor. They compute an initial estimate from the root mean square residual

$$\hat{s}_0=\sqrt{\frac{1}{(2N-4)}\sum_{i=1}^{2N}r_{i0}^{\,2}} \qquad \text{----- (5.22)}$$

Using the actual rms of the residuals r_{in} for the n^{th} iteration makes the estimate extremely vulnerable to the effect of outliers. By replacing sample averages by expectations, the scale estimate for the n^{th} iteration becomes

$$\hat{s}_0=\sqrt{\frac{1}{\beta(2N-4)}\sum_{i=1}^{2N}\left(E_{in}^{meas}-E_{n}^{pred}\right)^2} \qquad \text{----- (5.23)}$$

with β=0.7784.

For the loss function Huber (1981) uses a convex function that has a positive minimum at 0. It is based on a density function that has a Gaussian centre and Laplacian tails and is defined as follows:

$$\rho(t) = \begin{cases} \frac{1}{2}t^2 & |t| < t_0 \\ t_0|t| - \frac{1}{2}t_0^2 & |t| \geq t_0 \end{cases} \qquad \text{----- (5.24)}$$

t_0 is the tuning constant and value of 1.5 gives at least 95% efficiency for outlier-free normal data (Chave et al., 1987).

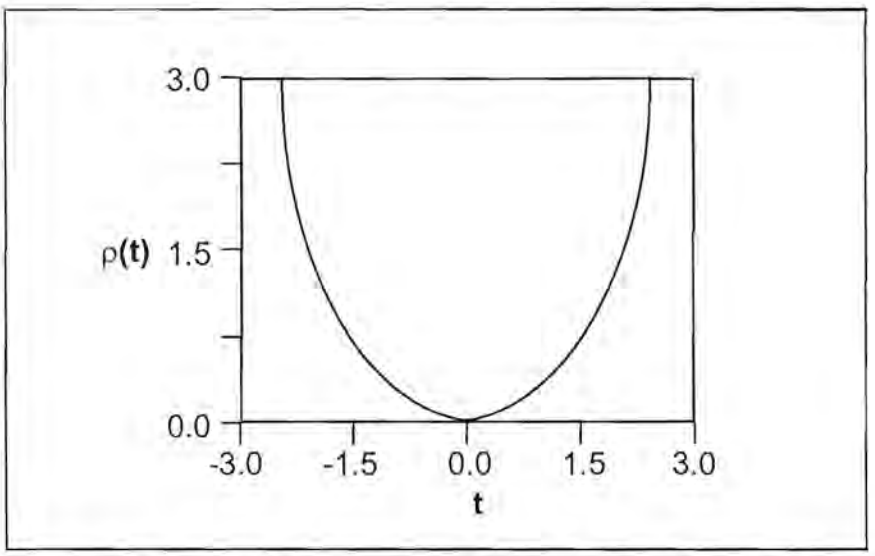

Figure 5.2. The Huber loss function (Sutarno and Vozoff,1989)

The influence function is

$$\psi(t) = \begin{cases} t & -t_0 < t < t_0 \\ t_0 & t \geq t_0 \\ -t_0 & t \leq -t_0 \end{cases} \qquad \text{----- (5.25)}$$

In order to achieve the best possible solution for the impedance tensor, the robust linear regression problem can be converted into a weighted least squares problem. Division of the influence function by the scaled residuals produces the weight function. Through substituting the influence function in equation (5.15) with the

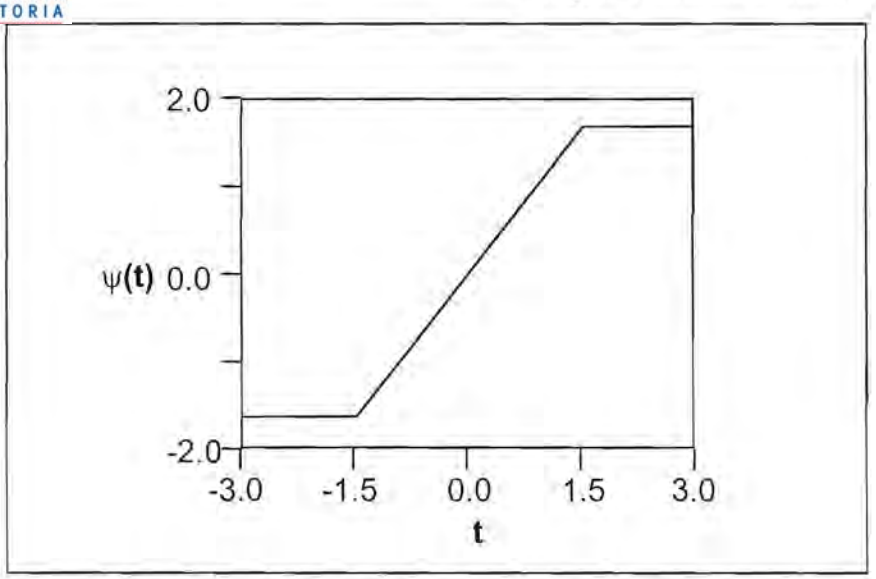

Figure 5.3. The Huber influence function (Sutarno and Vozoff, 1989)

weighted function and writing it in matrix form, the problem reduces to solving the following equation iteratively:

$$\tilde{U}^T\tilde{W}\tilde{r} = 0$$
$$\tilde{U}^T\tilde{W}(\tilde{x} - \tilde{U}\hat{\beta}) = 0$$
$$\tilde{U}^T\tilde{W}\tilde{U}\hat{\beta} = \tilde{U}^T\tilde{W}\tilde{x}$$
$$\hat{\beta} = (\tilde{U}^T\tilde{W}\tilde{U})^{-1}\tilde{U}^T\tilde{W}\tilde{x} \qquad \text{----- (5.26)}$$

For the loss function in (5.24), the Huber weight function reduces to

$$W(t) = \begin{cases} 1 & |t| < t \\ \dfrac{t_0}{|t|} & |t| \geq t_0 \end{cases} \qquad \text{----- (5.27)}$$

Equation (5.26) is solved iteratively, choosing the least squares estimate as an initial solution. From this the predicted outputs and residuals are calculated using equations (5.1 and 2) and (5.28) respectively.

$$r_i = x_i^{meas} - x_i^{pred} \qquad i = 1,\ldots,N \qquad \text{----- (5.28)}$$

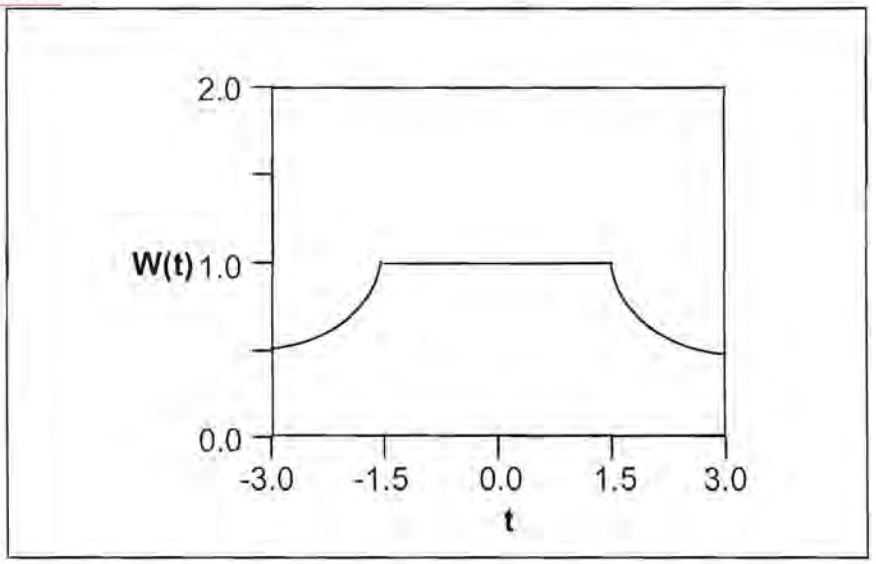

Figure 5.4. The Huber weight function (Sutarno and Vozoff, 1989)

Next, the scale parameter and Huber weights are determined and used to solve (5.26). The new impedance tensor estimate is then used to calculate the predicted outputs and the process is repeated until the estimates converge.

Sutarno and Vozoff (1991) states that "the Huber weights fall off slowly for large residuals and provide inadequate protection against severe residuals". They suggest the use of Thomson weights for a few iterations after convergence with the Huber weights. Thomson weights are described by the function

$$W(t) = e^{-e^{\alpha(|t|-\alpha)}} \qquad \text{------ (5.29)}$$

α determines the scale at which down weighting begins. Egbert and Booker (1986) use a value of 2.8 for α. Chave et al. (1987) describes the N^{th} quantile of the appropriate probability distribution as an excellent choice for α. Furthermore, if outliers have been eliminated, the residuals are χ^2 distributed. This distribution with two degrees of freedom is equivalent to the exponential distribution and thus has the pdf

$$f(t) = \frac{1}{2} e^{\frac{-t}{2}} \qquad t \geq 0 \qquad \text{----- (5.30)}$$

with $\sigma_{MAD} = 2\sinh^{-1}(0.5) \approx 0.9624$ and $\square_{IQ} = 2 \log 3 \approx 2.1972$ (Chave et al., 1987). The quantiles of the exponential distribution are given by

$$Q_j = 2\log\left(\frac{N}{N-j+0.5}\right) \qquad j = 1,\ldots,N. \qquad \text{----- (5.31)}$$

According to Sutarno and Vozoff (1991), if outliers have been eliminated the magnitudes of the residuals are Rayleigh-distributed with pdf

$$f(t) = te^{\frac{-t^2}{2}} \qquad t \geq 0 \qquad \text{----- (5.32)}$$

and $\sigma_{MAD} = 0.44845$. The quantiles are given by

$$Q_j = \sqrt{2\log\left(\frac{N}{N-j+0.5}\right)} \qquad j = 1,\ldots,N. \qquad \text{----- (5.33)}$$

With magnetotelluric data, equations (5.1) and (5.2) consists of complex numbers. Sutarno and Vozoff (1989) suggest two ways of handling complex data:

- regard the data as having independent Gaussian real and imaginary parts and apply separate weights to them,
- use the magnitude of the complex numbers and apply identical weights to the real and imaginary parts.

The second method is preferable since it is rotationally invariant (Sutarno and Vozoff, 1991). Equation (5.26) then becomes

$$\hat{\beta} = (\tilde{U}^*\tilde{W}\tilde{U})^{-1}\tilde{U}^*\tilde{W}\tilde{x} \qquad \text{----- (5.34)}$$

where * denotes the Hermitian conjugate.

5.4. ADAPTIVE L_p NORM

An alternative approach has been developed to deal with the problem of non-Gaussian distributed errors. Kijko (1994) proposes that it is not always necessary to use the L_1 or L_2 norm to minimise residuals, but that one can use the L_p norm where p can be a real value not necessarily equal to 1 or 2. He goes further to develop an adaptive procedure whereby the value of p is automatically determined from the quality of the data. The technique was developed for use with seismological data but can easily be applied to magnetotelluric data.

Instead of minimising equation (5.6), the following misfit function is minimised

$$\sum_{i=1}^{n} |x - x_i|^p \qquad \text{------ (5.35)}$$

where $1 \leq p < \infty$. The value of p depends on the distribution of the residuals and is therefore related to the kurtosis of the residual distribution. Press et al. (1992) define the kurtosis as a measurement of the peakedness or flatness of a distribution relative to the normal distribution. A distribution with a sharp peak is known as 'leptokurtic' and the term 'platykurtic' describes a flat distribution. The kurtosis (β_2) is given by

$$\beta_2 = \frac{\mu_4}{\mu_2^2} \qquad \text{------ (5.36)}$$

where μ_2 and μ_4 are the second- and fourth order central moments.

Several authors suggested different ways to determine the value of p using the kurtosis. Money et al. (1982) used the equation

$$\hat{p} = \frac{9}{\hat{\beta}_2^2} + 1 \qquad \text{------ (5.37)}$$

where $1 \leq \hat{p} < \infty$. Sposito et al. (1983) developed a different equation

$$\hat{p} = \frac{6}{\hat{\beta}_2^2} \qquad \text{------ (5.38)}$$

with $1 \leq \hat{p} \leq 2$.

Therefore, when data are severely contaminated, the error distribution will have long tails, resulting in a large kurtosis and subsequently a small value for p.

Kijko (1994) developed an adaptive algorithm for determining an estimate for the p-value.

5.5. APPLICATION OF STATISTICAL REDUCTION TECHNIQUES TO SYNTHETIC DATA

The statistical reduction methods discussed in the previous sections will first be applied to synthetic data. Hattingh (1989) describes the construction of a unit apparent resistivity curve. He generates electric field data by multiplying real

magnetic field data with unit impedance (equation (3.52)). The resultant apparent resistivity versus frequency curve will plot as a straight line on double logarithmic paper.

5.5.1. Synthetic data with Gaussian distributed random errors

For the first test, noise with a Gaussian distribution was added to the data. Figure 5.4 shows the apparent resistivity and phase versus frequency curves. Noise added to the two curves both had a zero mean, but different standard deviations.

The Q-Q plots for these data sets (Figure 5.6) plot on roughly straight lines, confirming that the noise is normally distributed. The correlation coefficients between the observed and expected residuals are 0.89516 and 0.896132 for noise with standard deviations of 0.0001 and 0.2 respectively.

Figures 5.7 to 5.12 show the curves fitted to the data using the L_1 norm, L_2 norm, adaptive L_p norm and robust M-estimation techniques. In the calculation of the L_1, L_2 and adaptive L_p norms, an algorithm for the downhill simplex method taken from Press et al. (1992) was used to minimise the impedance variables. Nelder and Mead (1965) introduced this method of minimising multidimensional functions.

The L_1 and L_2 norm methods yield very similar results (Figures 5.7 and 5.8). Curves estimated by these two techniques approximate the original data displayed in Figure 5.5 very well.

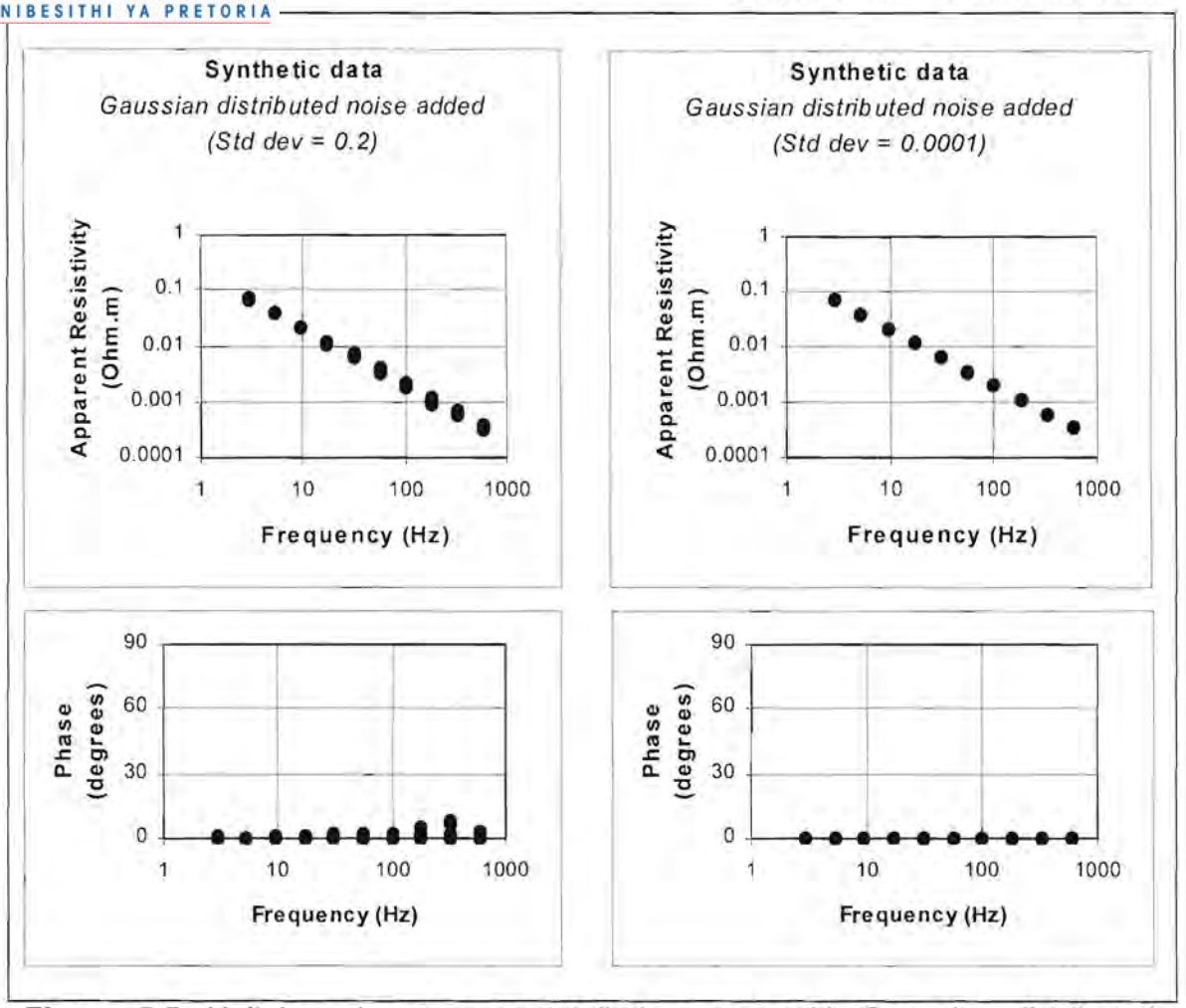

Figure 5.5. Unit impedance magnetotelluric curves with Gaussian distributed noise added.

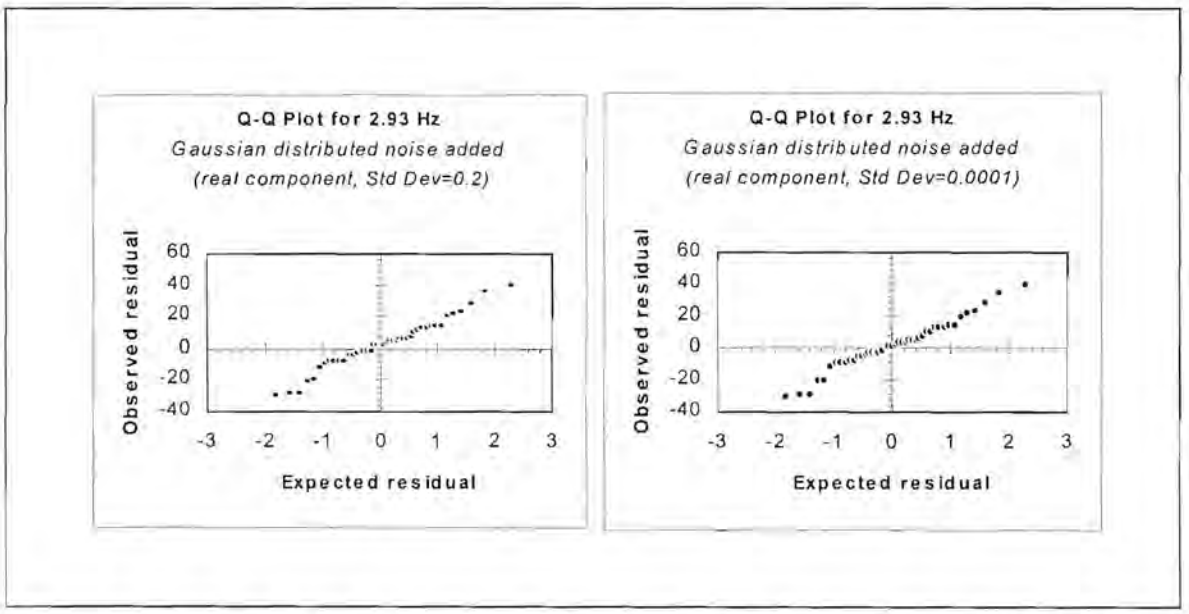

Figure 5.6. Q-Q plots of the synthetic data with Gaussian distribution noise added

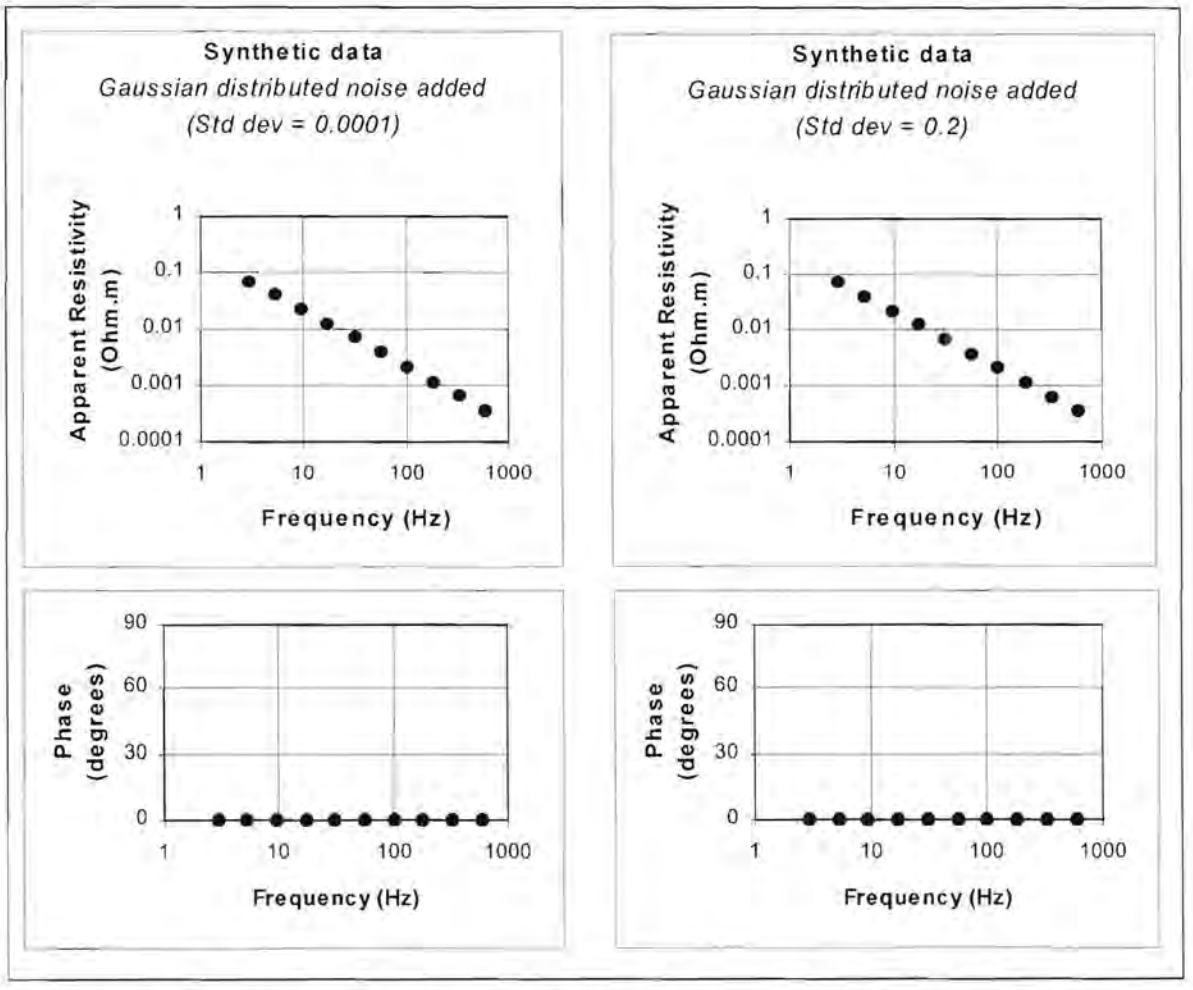

Figure 5.7. Apparent resistivity versus frequency curves produced by the L_1 norm estimation technique for the synthetic data (with Gaussian distributed noise) displayed in Figure 5.5.

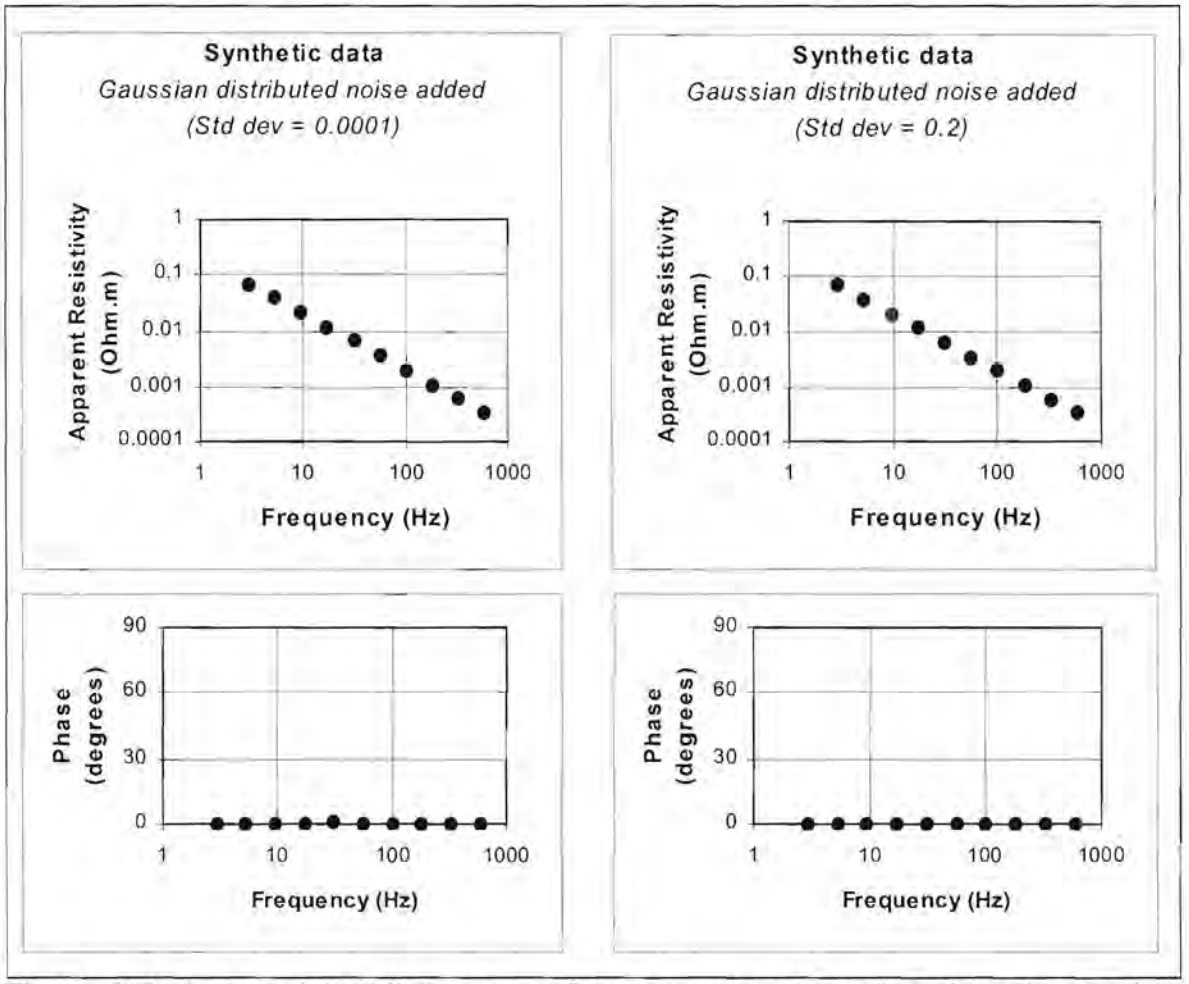

Figure 5.8. Apparent resistivity versus frequency curves produced by the least squares (L_2) estimation technique for the synthetic data (with Gaussian distributed noise) displayed in Figure 5.5.

The adaptive L_p norm technique yielded similar results to the L_1 and L_2 norms. The curves in Figure 5.9 were calculated using the formula of Money et al. (1982) to calculate exponent p. Figures 5.10.1 to 5.10.10 show the values of p calculated for each frequency during the estimation of the apparent resistivity and phase versus frequency curves.

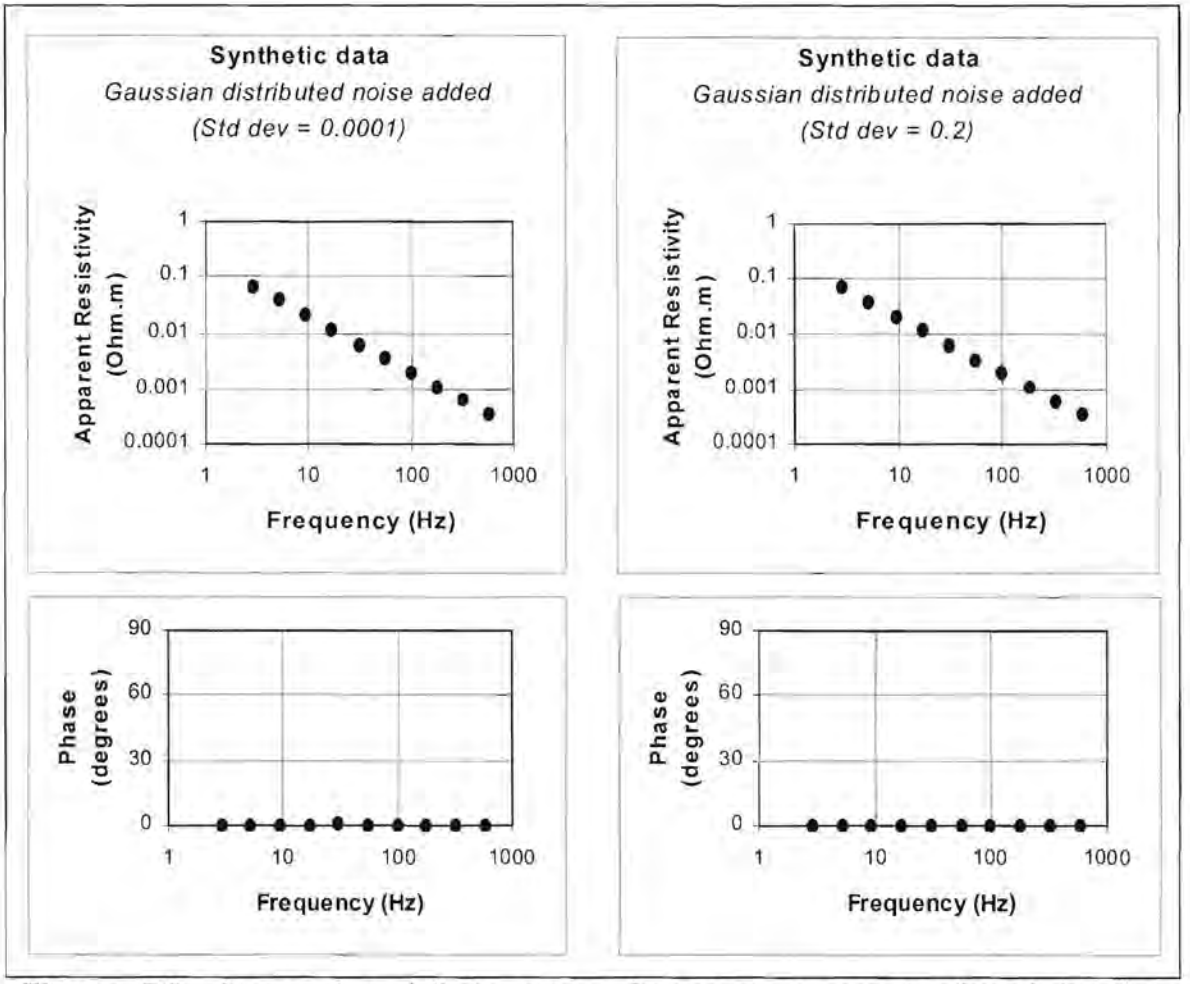

Figure 5.9. Apparent resistivity versus frequency curves produced by the adaptive L_p norm technique for the synthetic data (with Gaussian distributed noise) displayed in Figure 5.5. The formula suggested by Money et al. (1982) was used to calculate the exponent p.

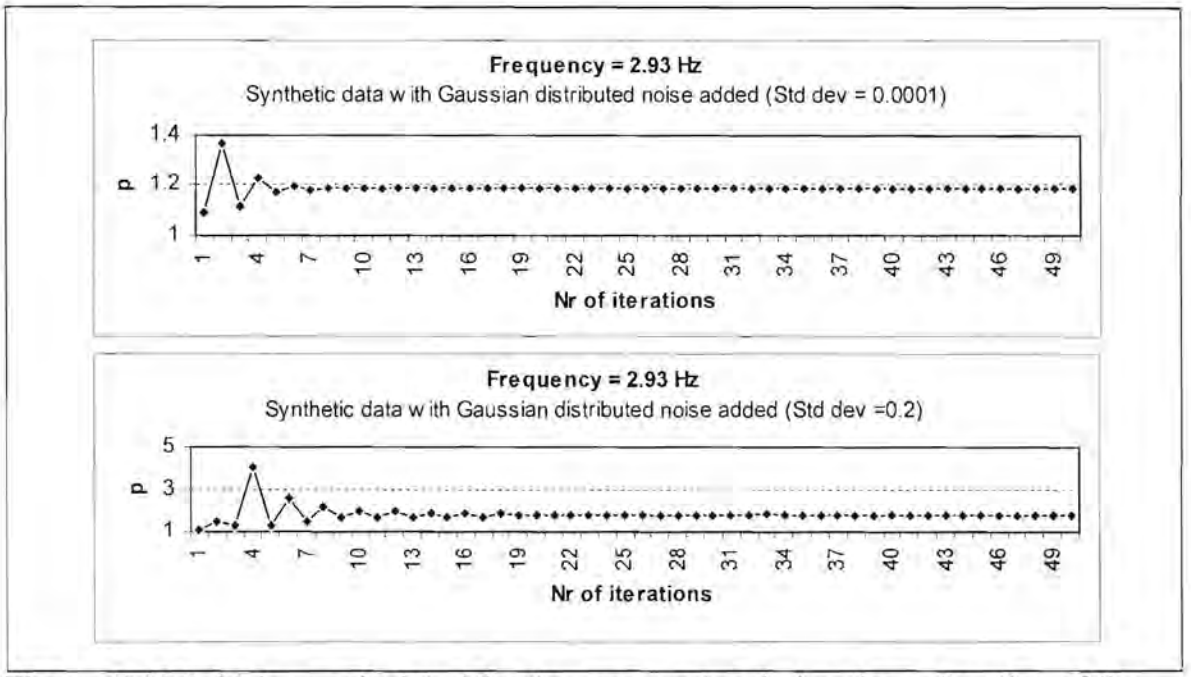

Figure 5.10.1. Values calculated for the exponent p during the estimation of the apparent resistivity values displayed in Figure 5.9 at 2.93 Hz

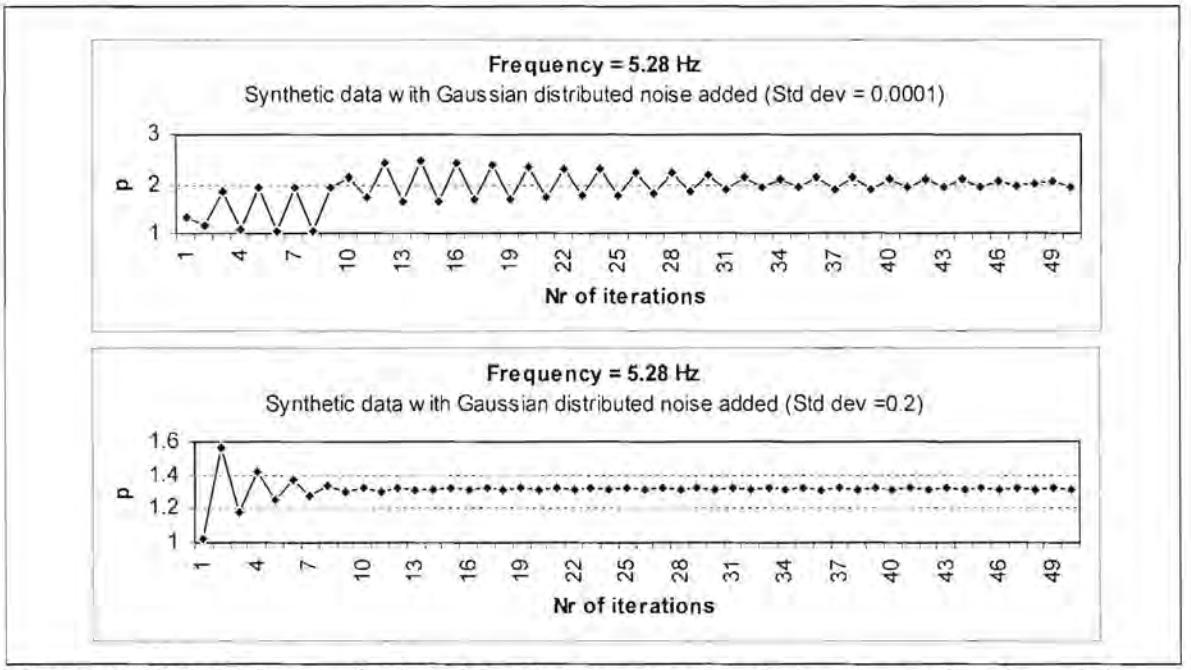

Figure 5.10.2. Values calculated for the exponent p during the estimation of the apparent resistivity values displayed in Figure 5.9 at 5.28 Hz

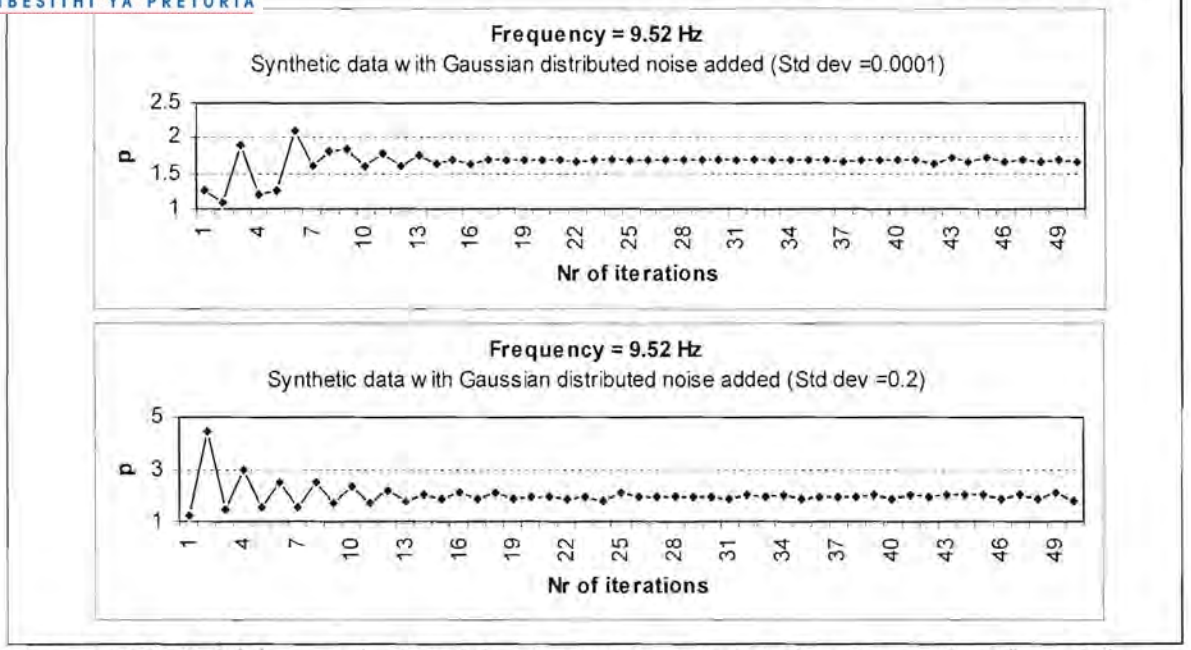

Figure 5.10.3. Values calculated for the exponent p during the estimation of the apparent resistivity values displayed in Figure 5.9 at 9.52 Hz

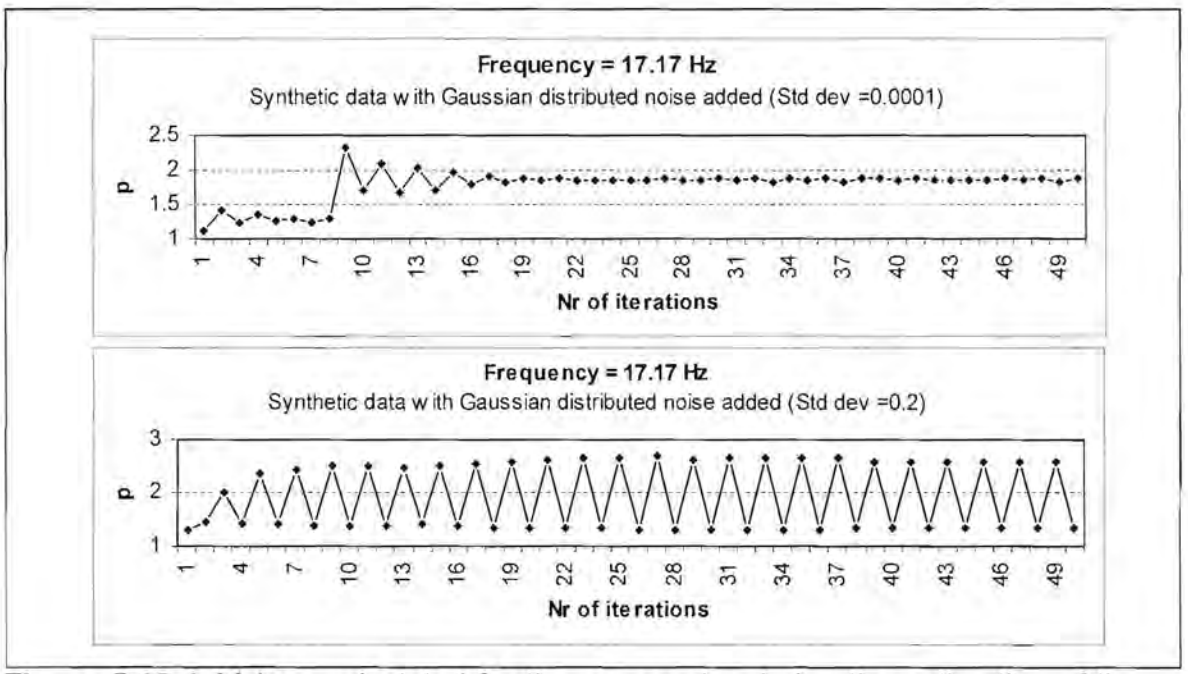

Figure 5.10.4. Values calculated for the exponent p during the estimation of the apparent resistivity values displayed in Figure 5.9 at 17.17 Hz

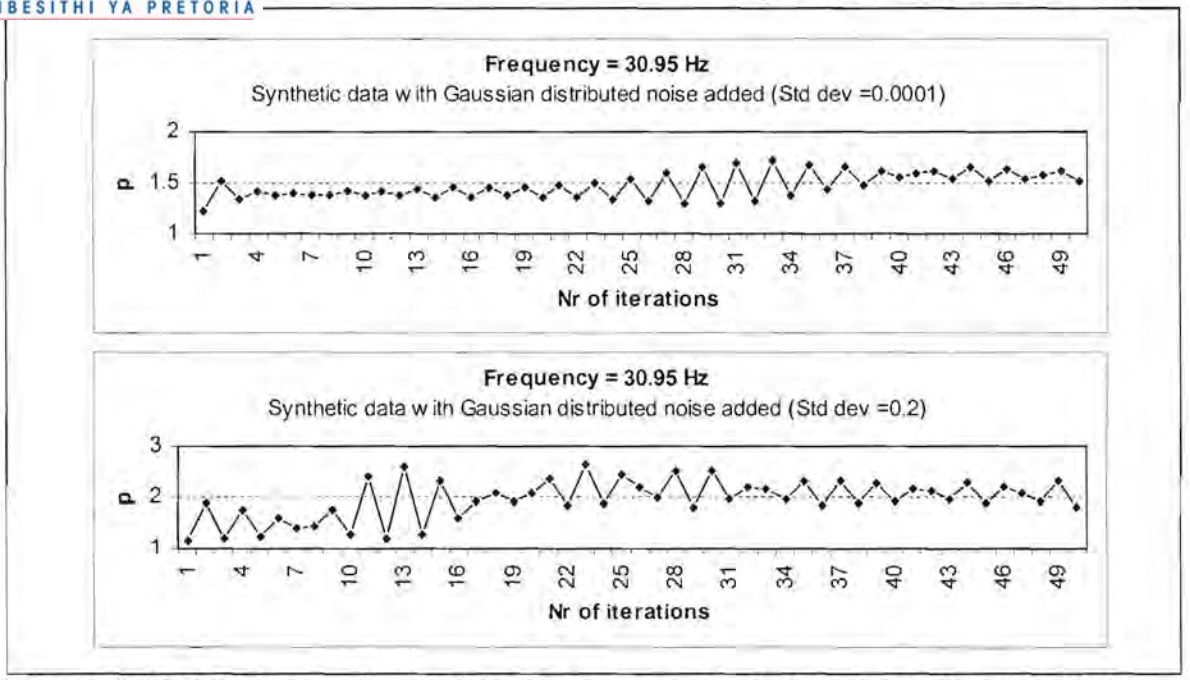

Figure 5.10.5. Values calculated for the exponent p during the estimation of the apparent resistivity values displayed in Figure 5.9 at 30.95 Hz

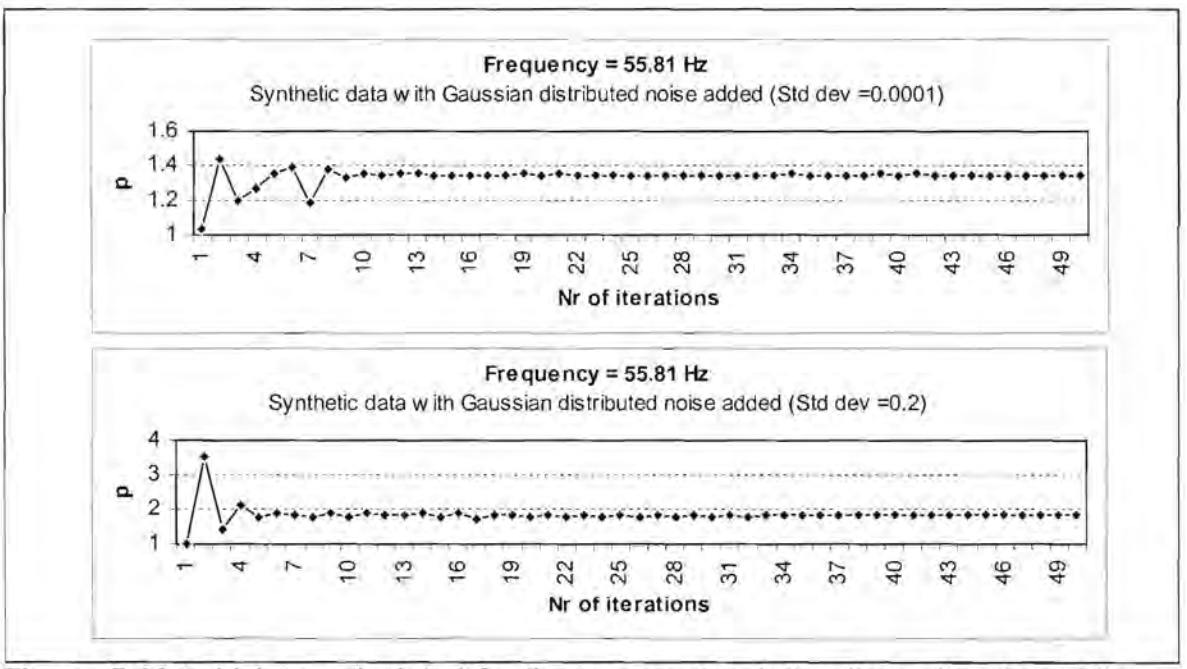

Figure 5.10.6. Values calculated for the exponent p during the estimation of the apparent resistivity values displayed in Figure 5.9 at 55.81Hz

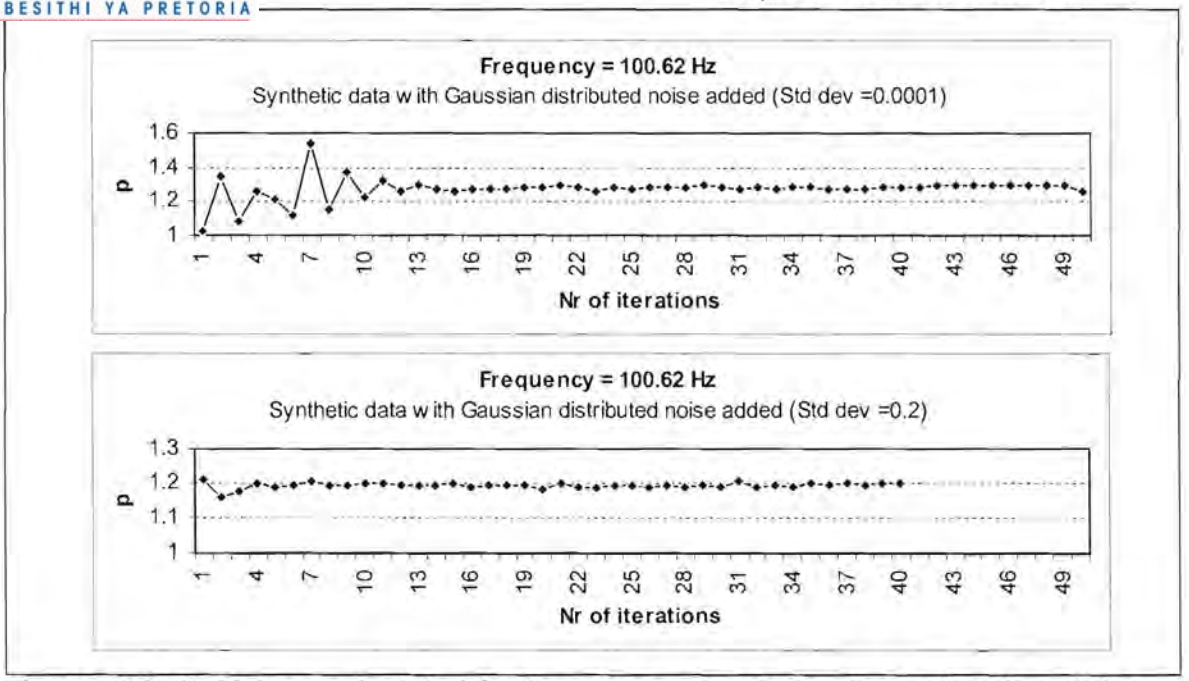

Figure 5.10.7. Values calculated for the exponent p during the estimation of the apparent resistivity values displayed in Figure 5.9 at 100.62 Hz

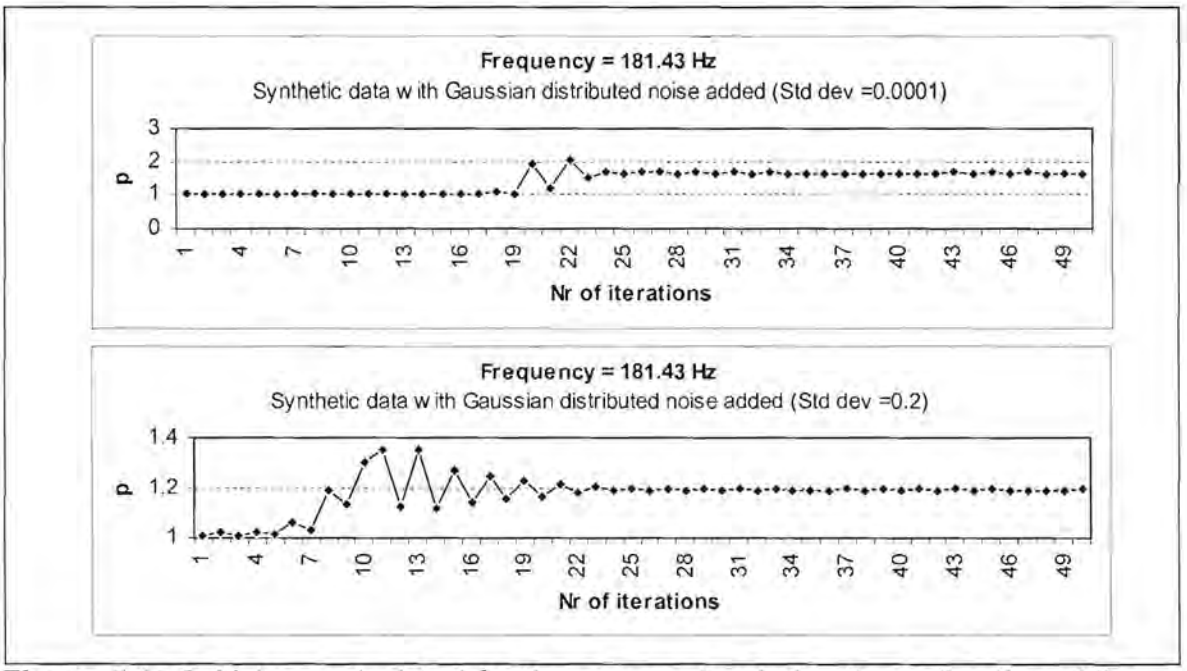

Figure 5.10.8. Values calculated for the exponent p during the estimation of the apparent resistivity values displayed in Figure 5.9 at 181.43 Hz

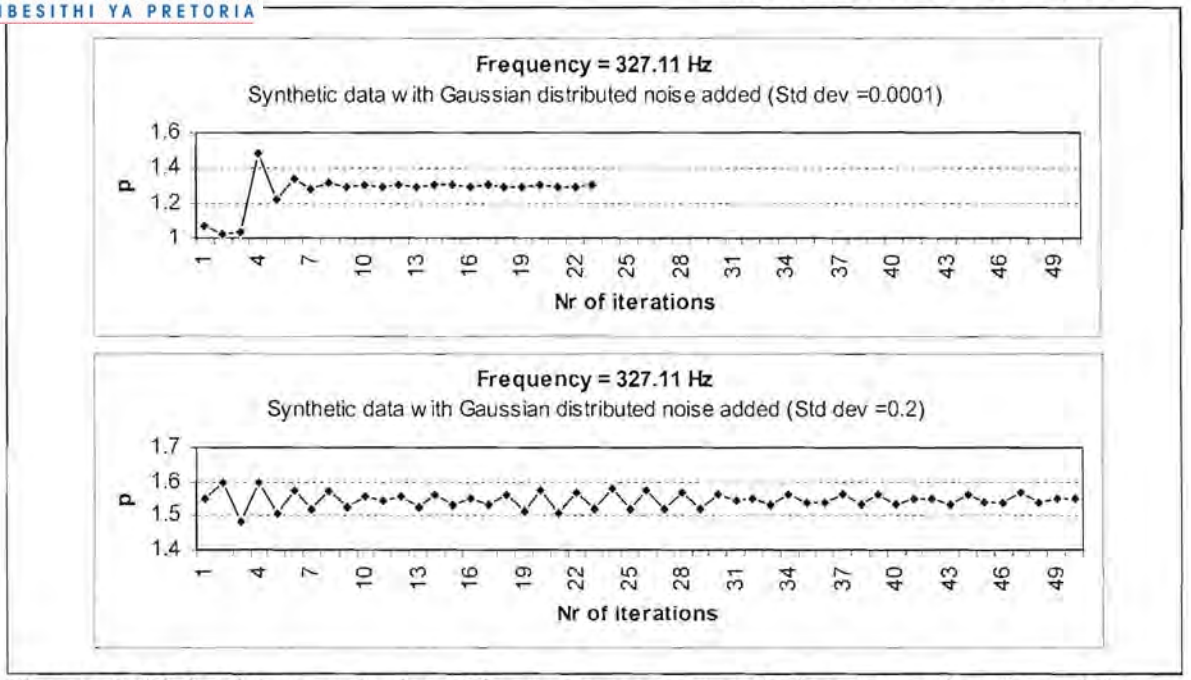

Figure 5.10.9. Values calculated for the exponent p during the estimation of the apparent resistivity values displayed in Figure 5.9 at 327.11 Hz

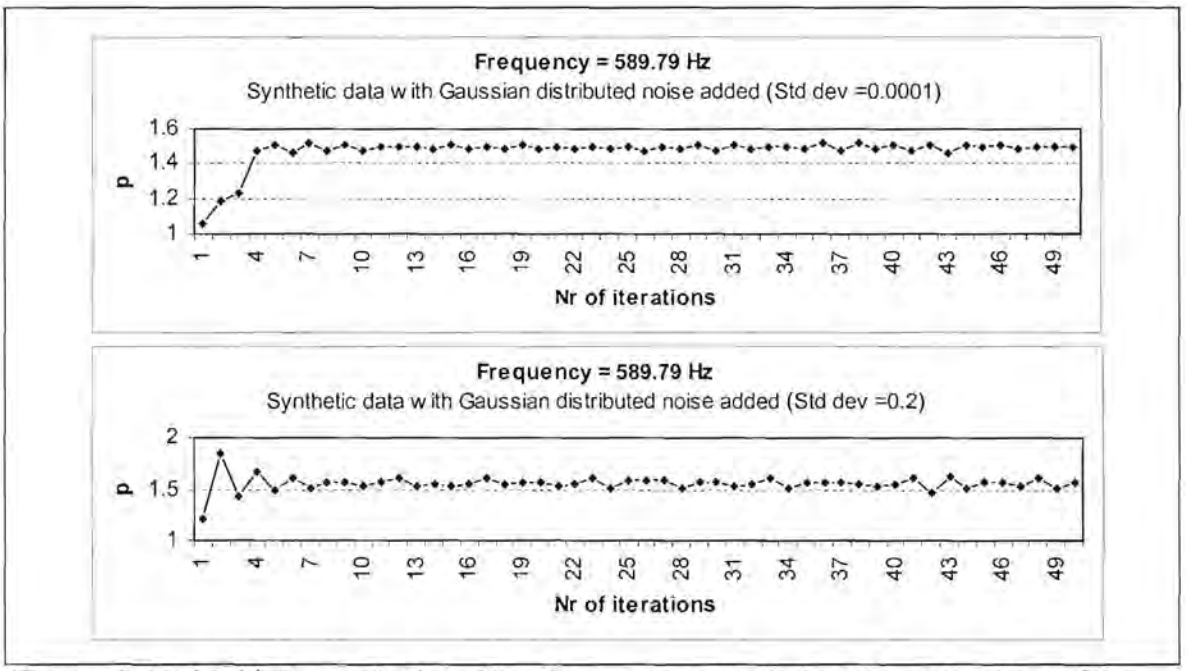

Figure 5.10.10. Values calculated for the exponent p during the estimation of the apparent resistivity values displayed in Figure 5.9 at 589.79 Hz

Using the formula suggested by Sposito et al. (1983) in equation (5.38) to calculate the exponent p, yield the apparent resistivity versus frequency curves shown in Figure 5.11. The results are again of high quality as would be expected for noise with a normal distribution. Figures 5.12.1 to 5.12.10 show the values of p calculated during the adaptive L_p norm process.

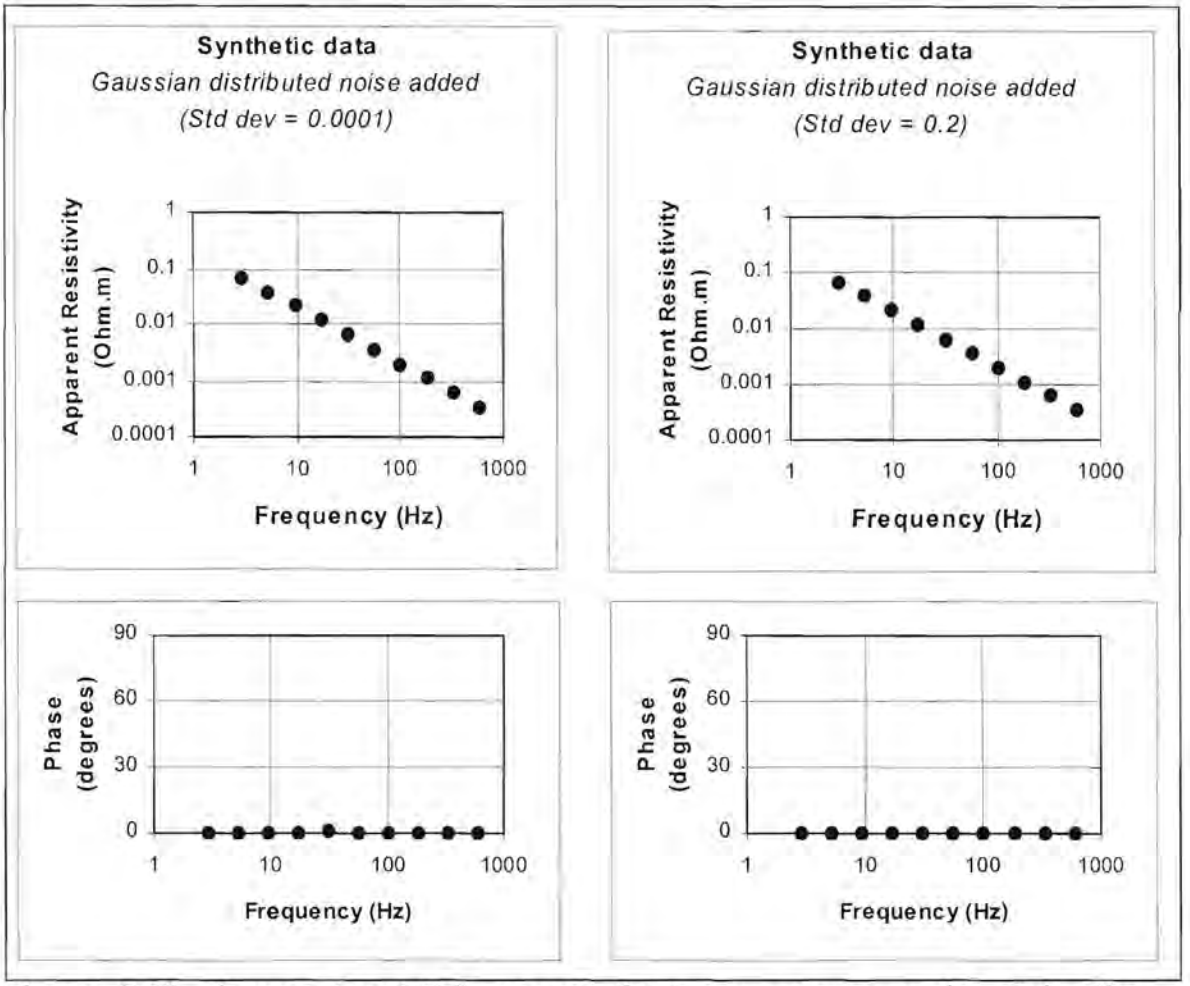

Figure 5.11. Apparent resistivity versus frequency curves produced by the adaptive L_p norm technique for the synthetic data (with Gaussian distributed noise) displayed in Figure 5.5. The formula suggested by Sposito et al. (1983) was used to calculate the exponent p.

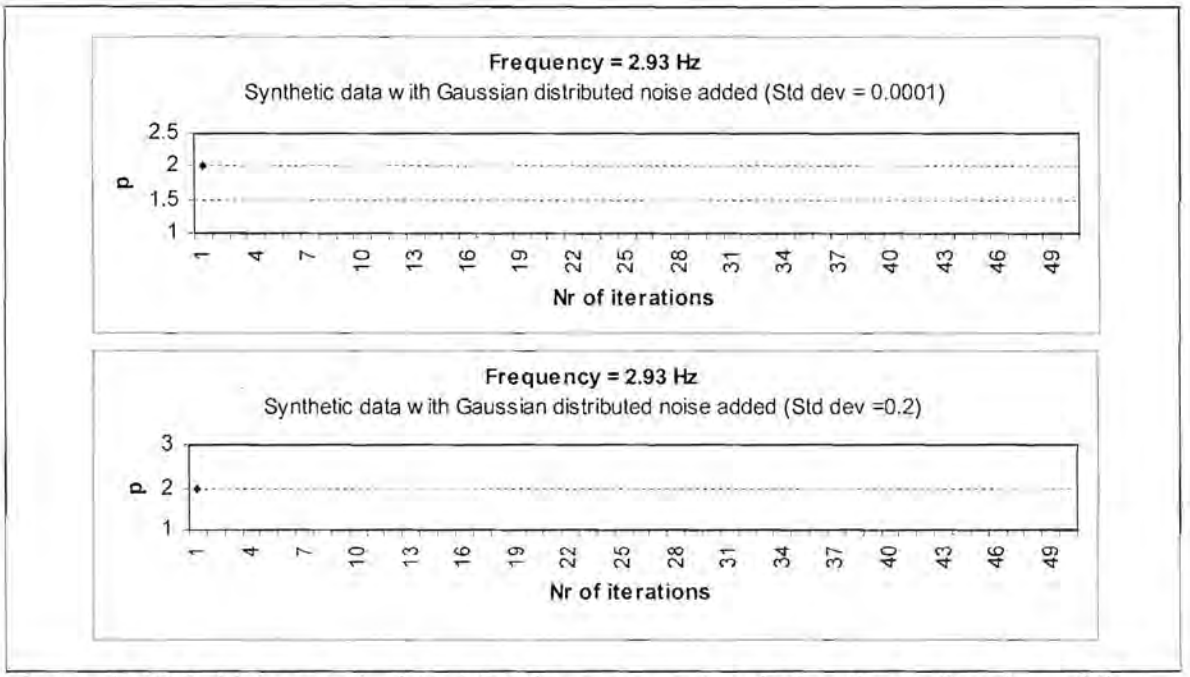

Figure 5.12.1. Values calculated for the exponent p during the estimation of the apparent resistivity values displayed in Figure 5.11 at 2.93 Hz

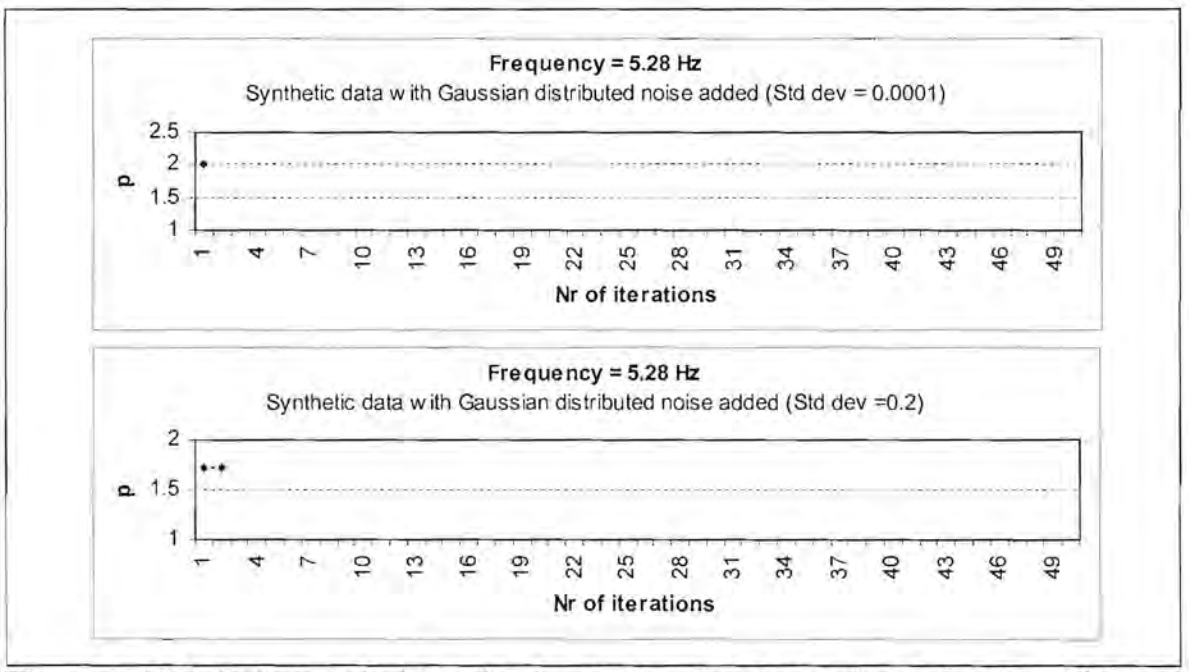

Figure 5.12.2. Values calculated for the exponent p during the estimation of the apparent resistivity values displayed in Figure 5.11 at 5.28 Hz

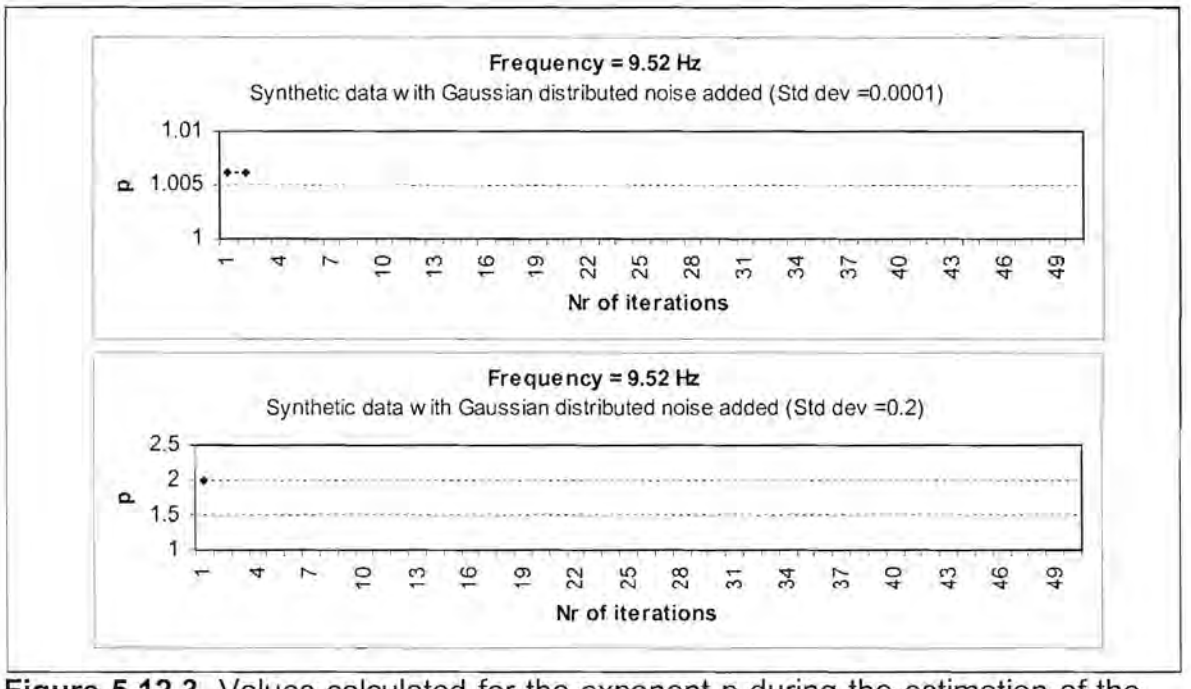

Figure 5.12.3. Values calculated for the exponent p during the estimation of the apparent resistivity values displayed in Figure 5.11 at 9.52 Hz

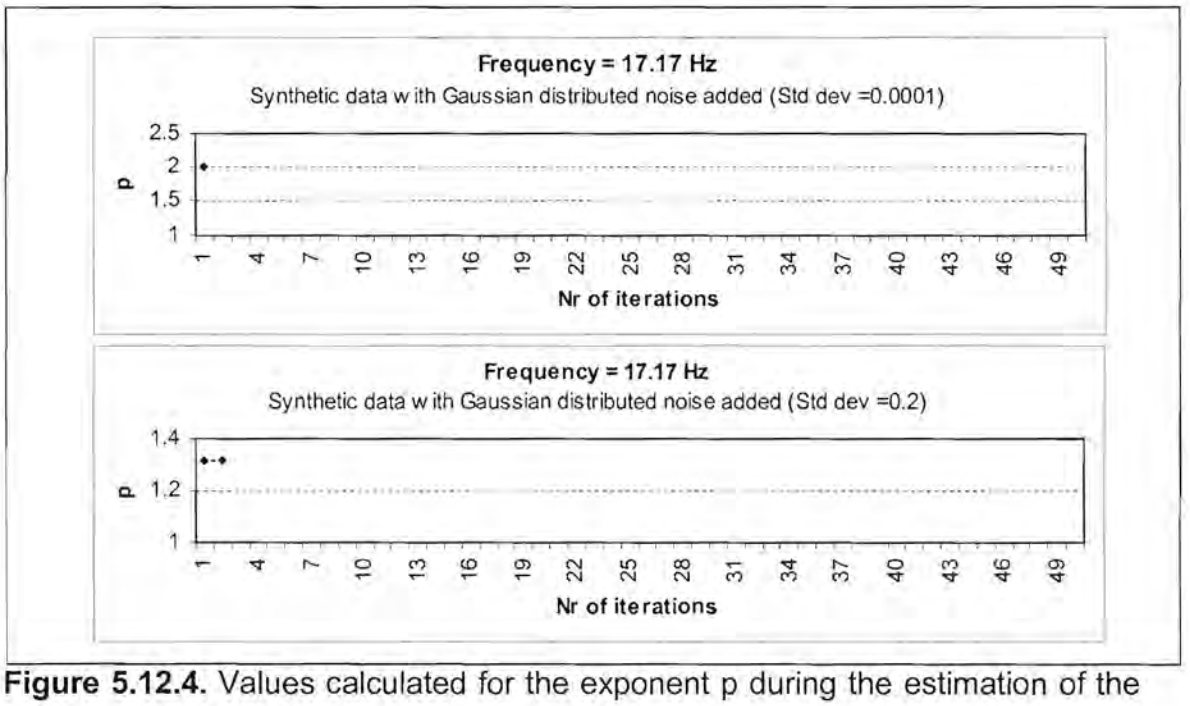

Figure 5.12.4. Values calculated for the exponent p during the estimation of the apparent resistivity values displayed in Figure 5.11 at 17.17 Hz

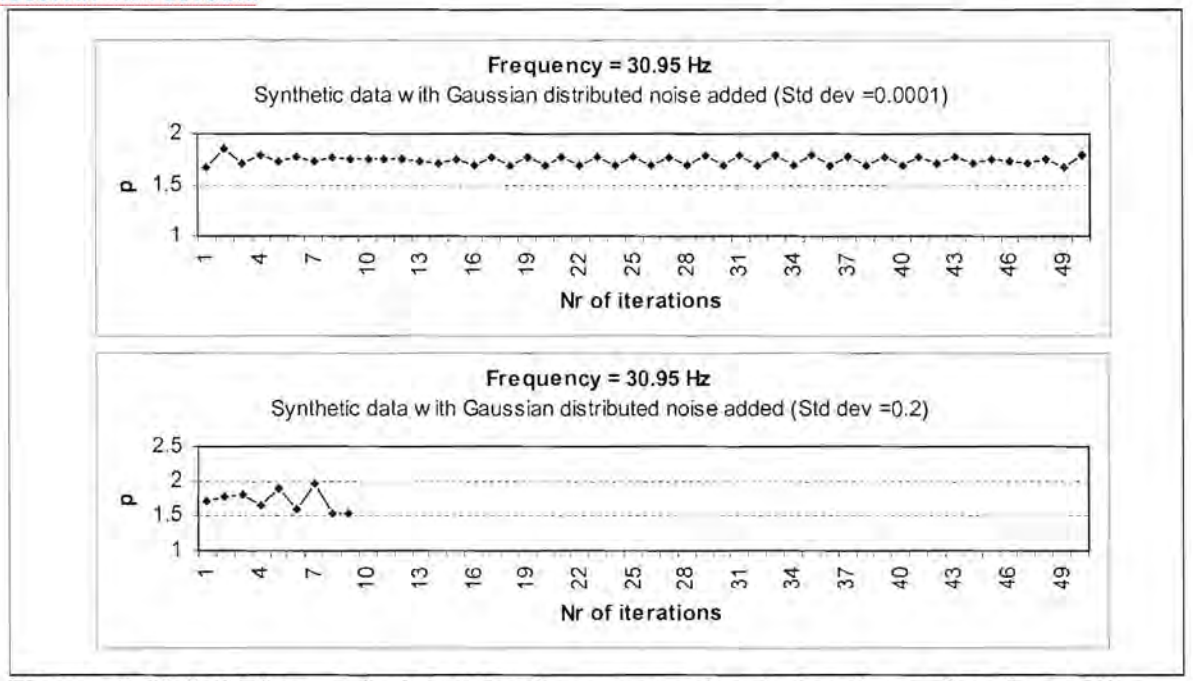

Figure 5.12.5. Values calculated for the exponent p during the estimation of the apparent resistivity values displayed in Figure 5.11 at 30.95 Hz

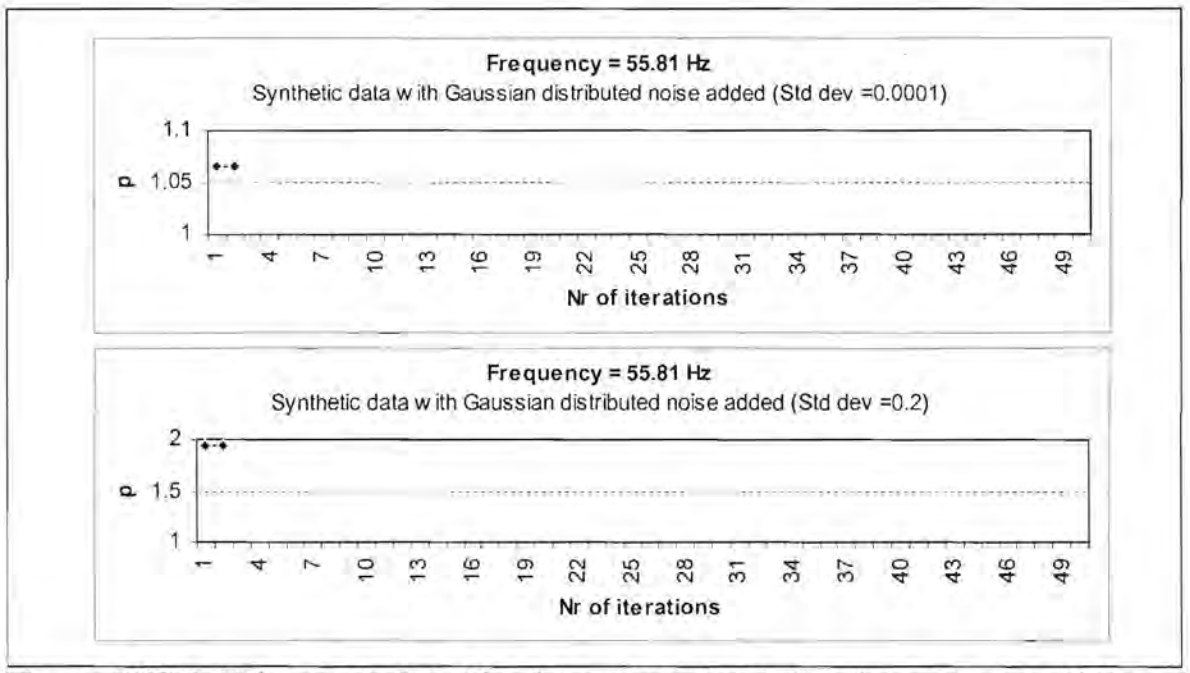

Figure 5.12.6. Values calculated for the exponent p during the estimation of the apparent resistivity values displayed in Figure 5.11 at 55.81 Hz

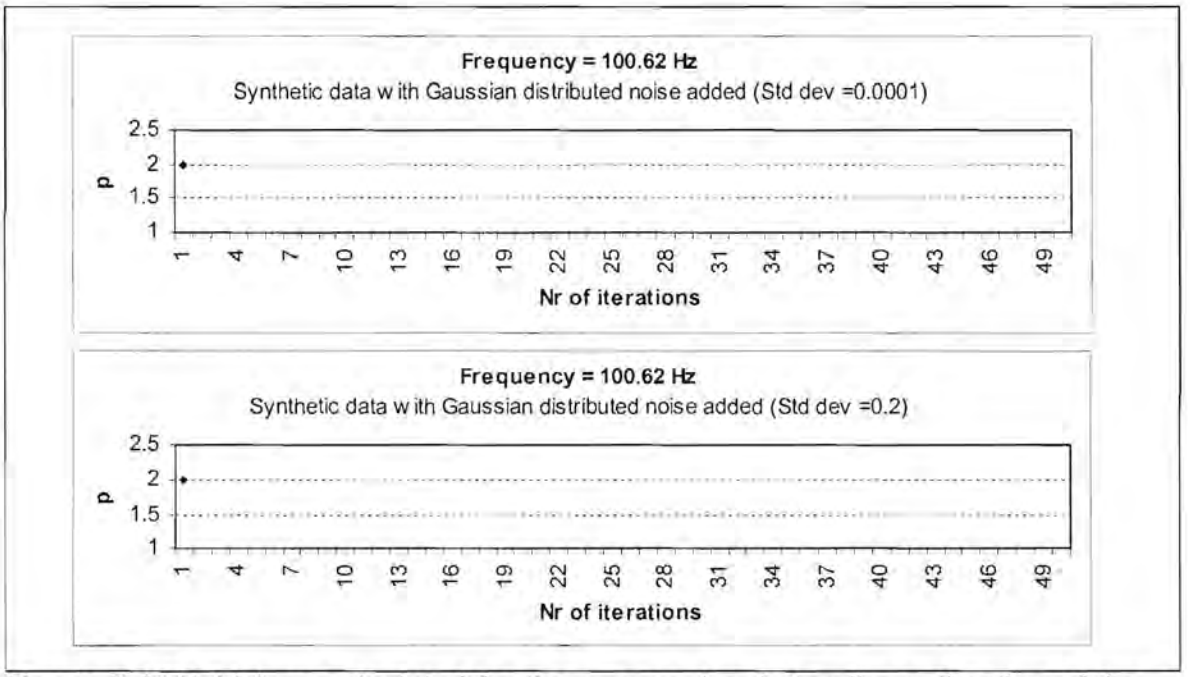

Figure 5.12.7. Values calculated for the exponent p during the estimation of the apparent resistivity values displayed in Figure 5.11 at 100.62 Hz

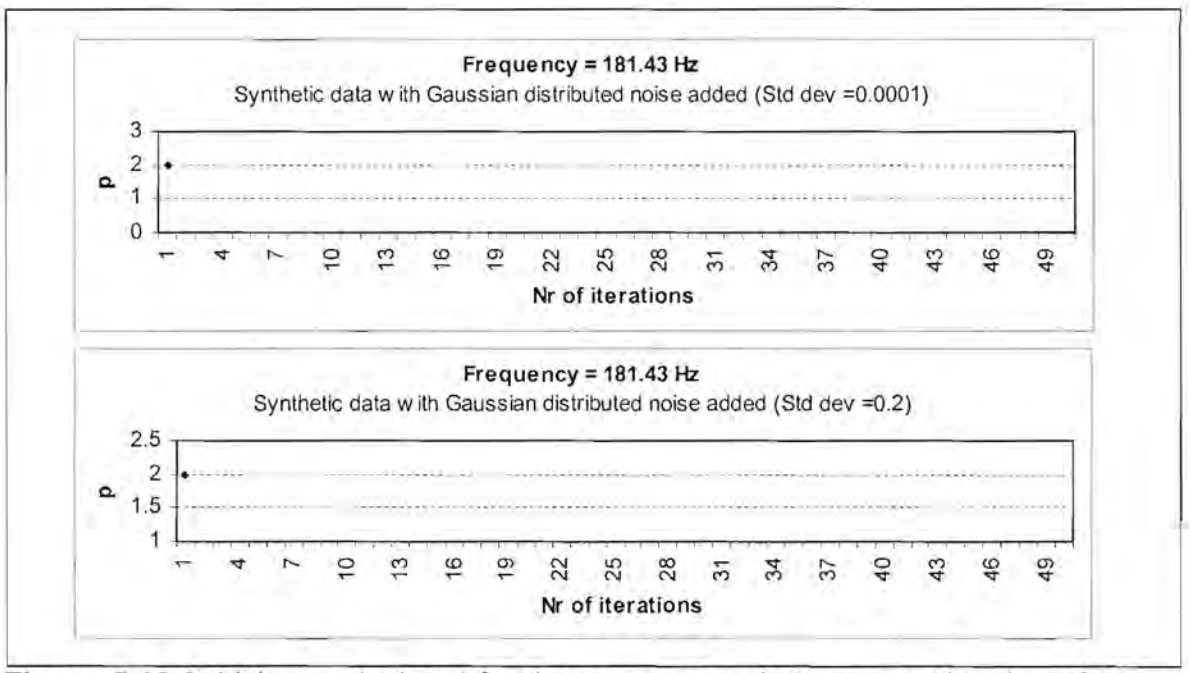

Figure 5.12.8. Values calculated for the exponent p during the estimation of the apparent resistivity values displayed in Figure 5.11 at 181.43 Hz

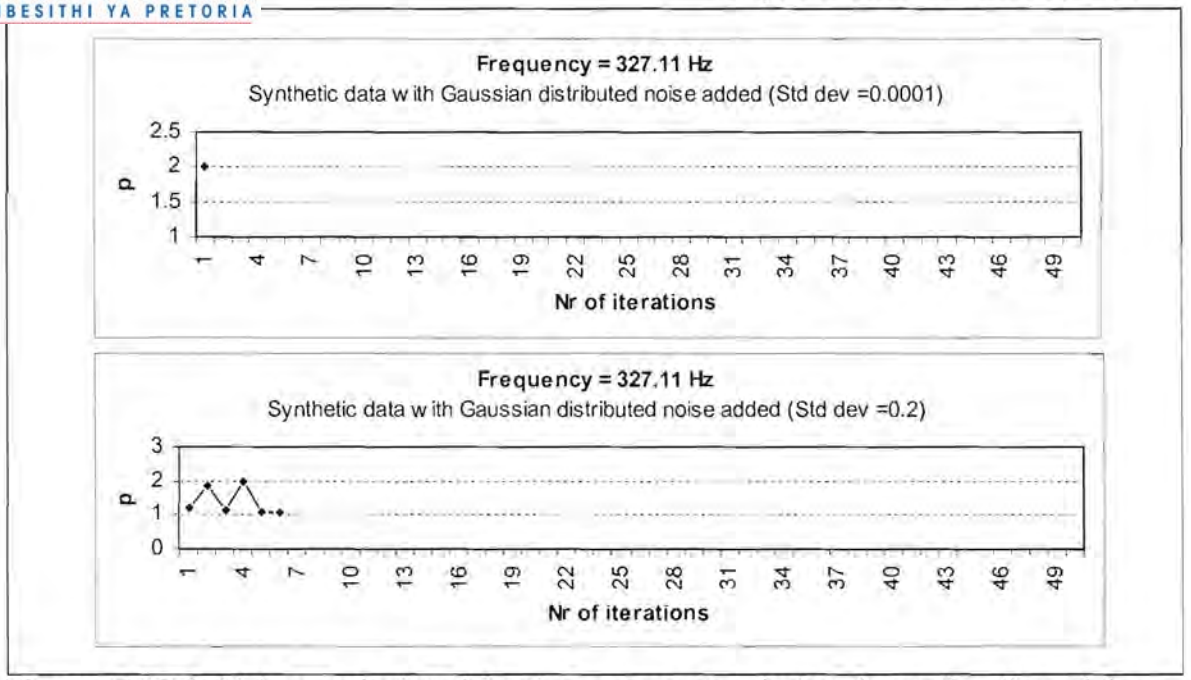

Figure 5.12.9. Values calculated for the exponent p during the estimation of the apparent resistivity values displayed in Figure 5.11 at 327.11 Hz

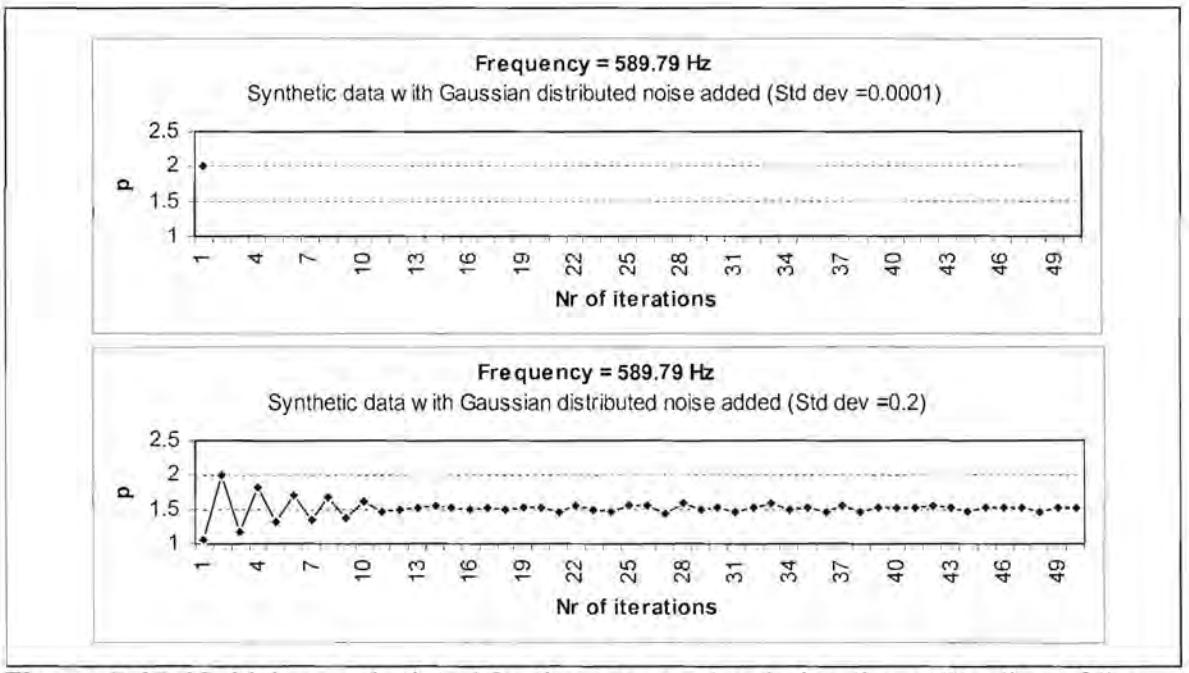

Figure 5.12.10. Values calculated for the exponent p during the estimation of the apparent resistivity values displayed in Figure 5.11 at 589.79 Hz

The amount of iterations is markedly less when Sposito's formula is used in the estimation of p. A main reason for this is that equation (5.38) does not allow p to be greater than two. The adaptive procedure is terminated when p becomes too large.

The minimisation using the Robust M estimation technique also yielded very good results (Figure 5.13), similar to the L_1, L_2 and adaptive L_p norm methods.

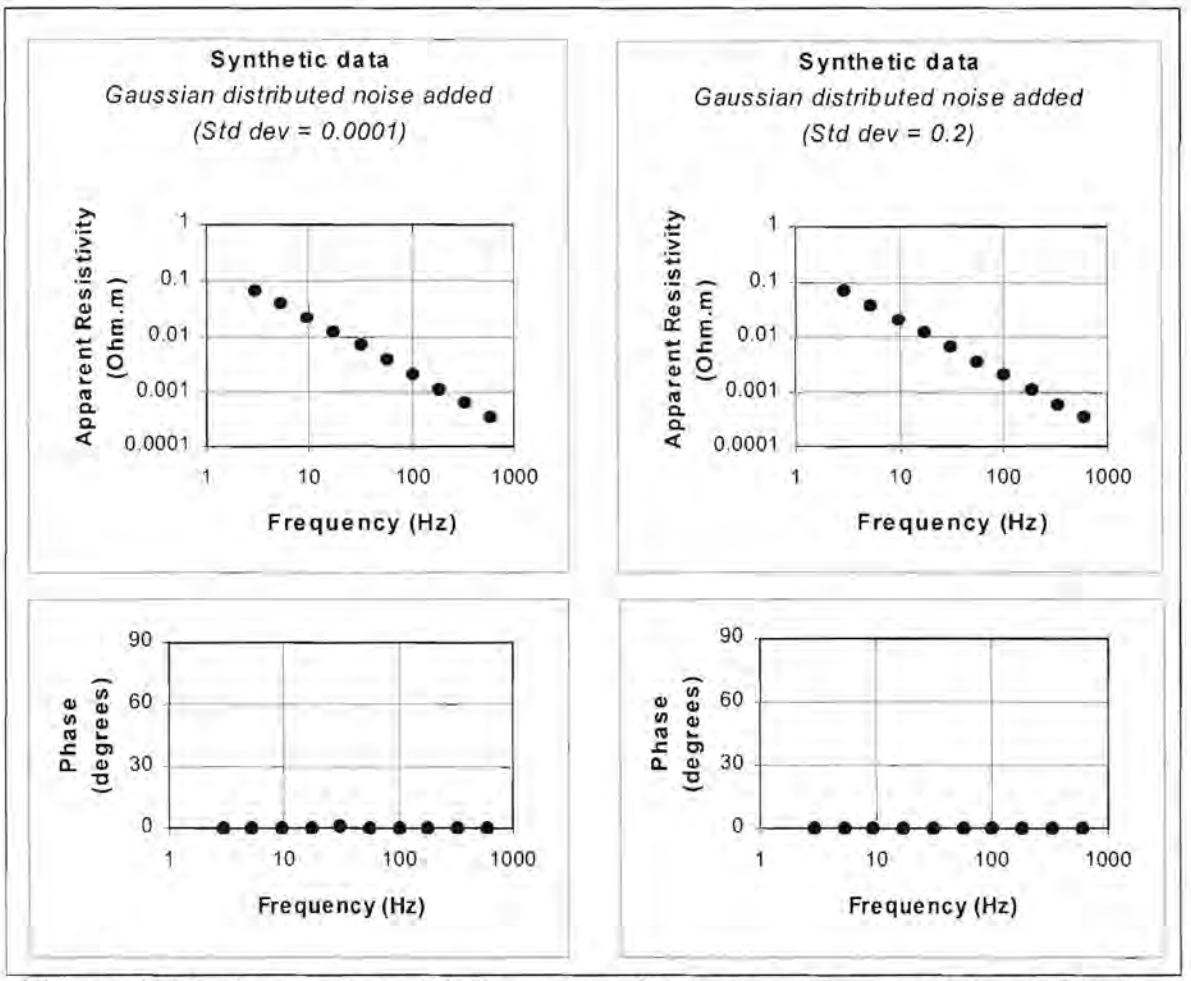

Figure 5.13. Apparent resistivity versus frequency curves produced by the Robust M estimation technique for the synthetic data (with Gaussian distributed noise) displayed in Figure 5.5.

All of the tested statistical reduction methods yielded good results for data containing normally distributed errors, as would be expected. An increase in standard deviation of the noise did not affect the quality of the estimated curves.

5.5.2. Synthetic data with non-Gaussian distributed random errors

Figure 5.14 shows two curves, both with Gaussian distributed random noise added. In this case the mean is 0.0 and the standard deviation is 1.0 for both

curves. Random noise without a specific distribution was added to the data in the first curve. This introduced outliers to the data.

Figure 5.14. Apparent resistivity versus frequency curves using the unit impedance with Gaussian and randomly distributed noise added.

The Q-Q plots for these two data sets calculated at a frequency where outliers are clearly visible (Figure 5.15) confirm that the noise in the first curve does not have a perfect normal distribution. The correlation coefficients between the observed and expected residuals are 0.771726 for the curve with the randomly distributed errors, and 0.984253 for the data containing only normally distributed errors.

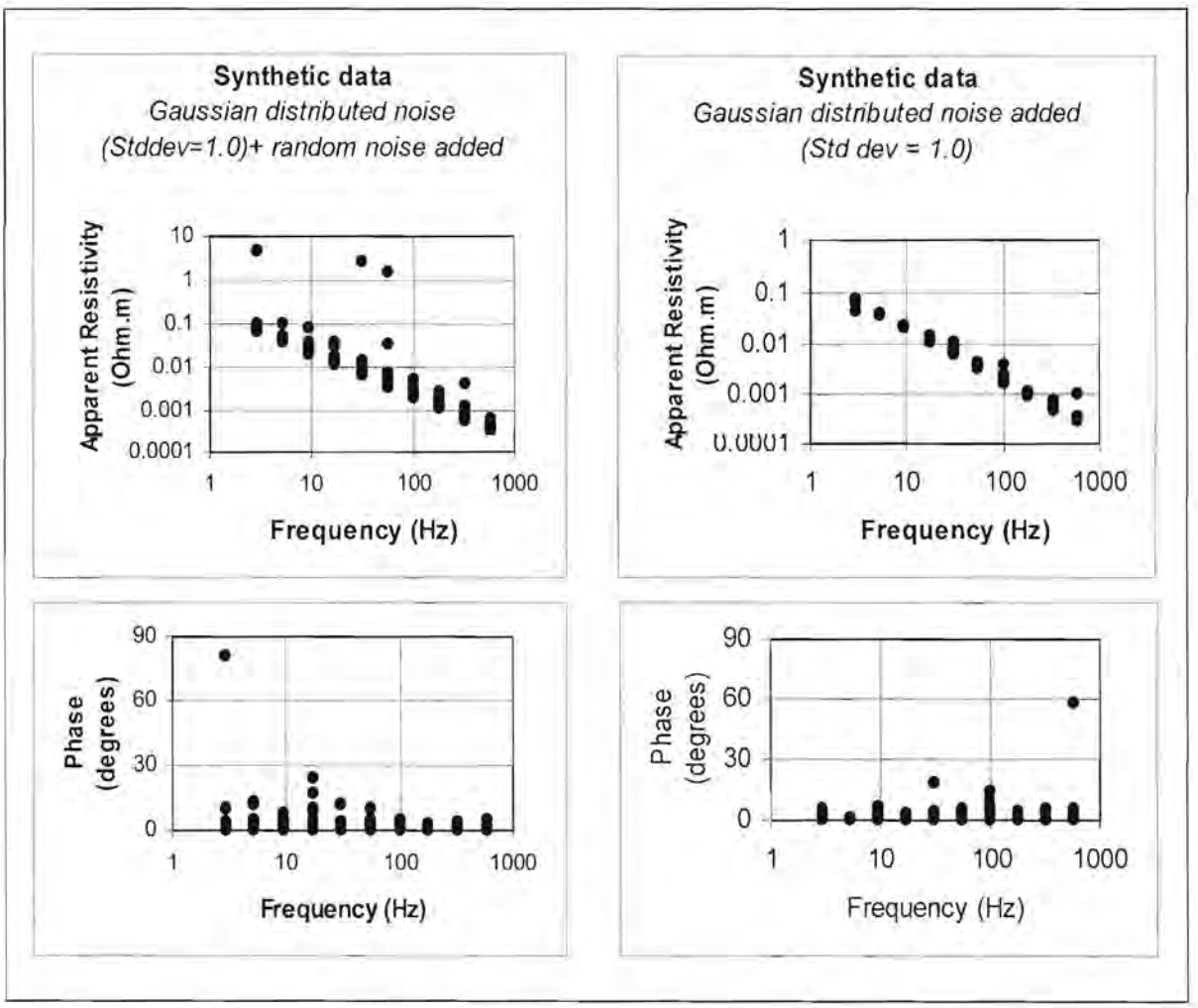

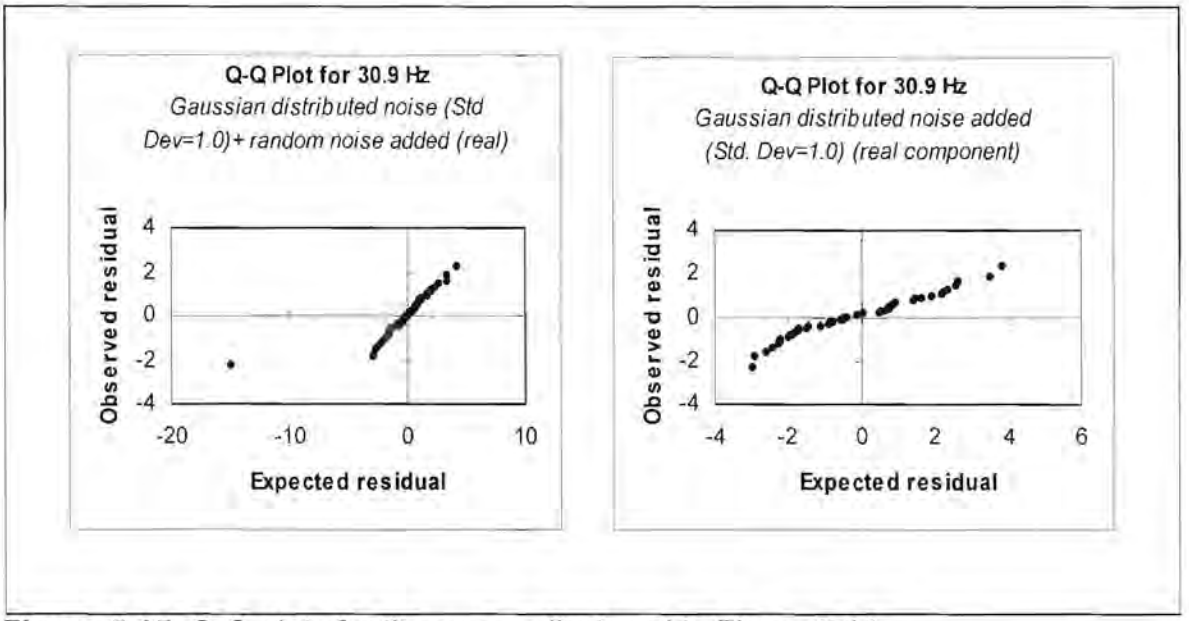

Figure 5.15. Q-Q plots for the curves displayed in Figure 5.14.

The curves fitted to the data using the L_1 and L_2 norms yield very different results (Figures 5.16 and 5.17). The L_1 norm produces a good fit for the apparent resistivity curve and a mediocre fit for the phase curve. In contrast with this the L_2 norm results in a very bad fit for both apparent resistivities and phases compared to the L_1 norm. Phases calculated for the data containing only Gaussian distributed noise also show larger misfits at higher frequencies.

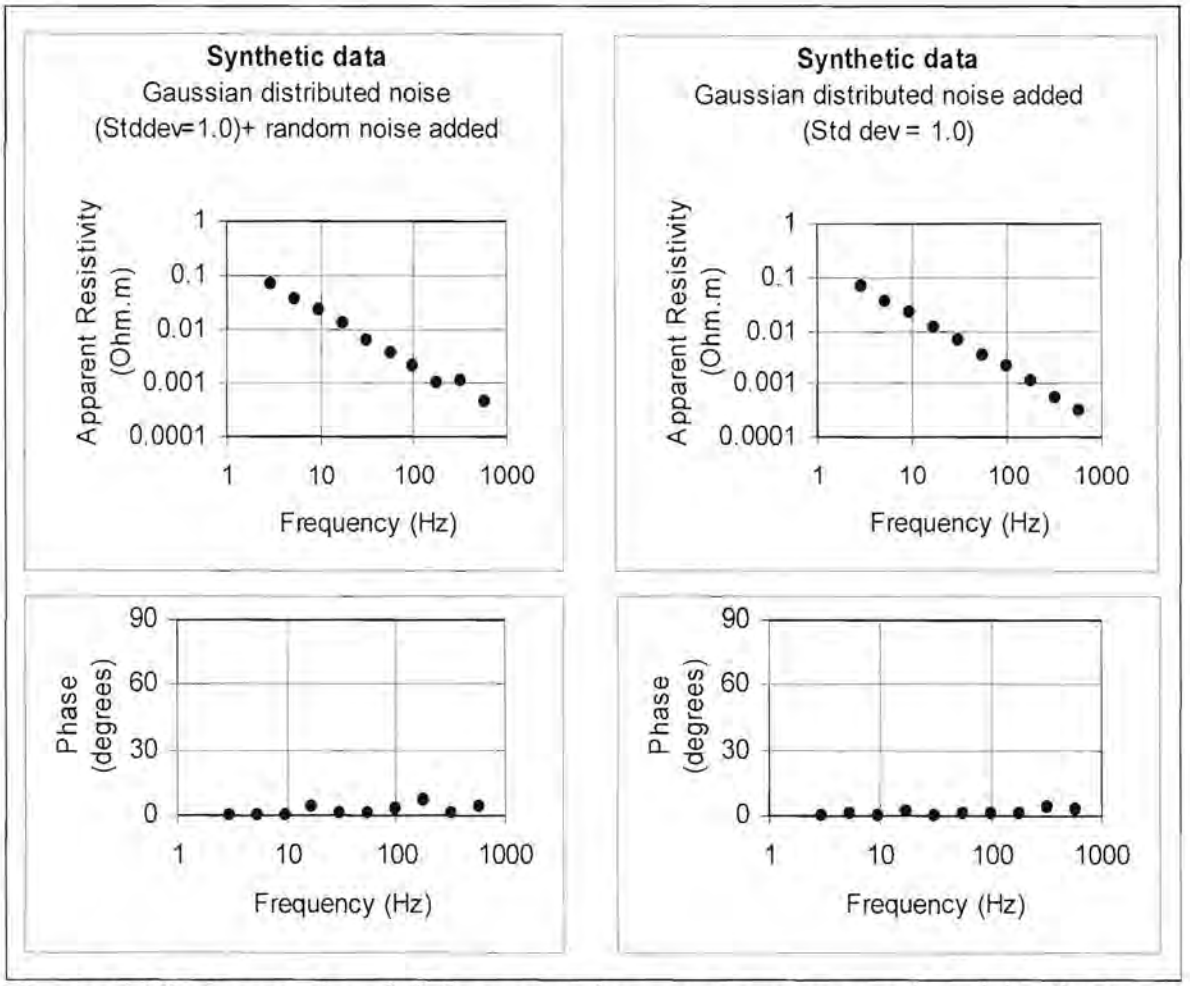

Figure 5.16. Apparent resistivity versus frequency curves produced by the L_1 norm estimation technique for the synthetic data displayed in Figure 5.14.

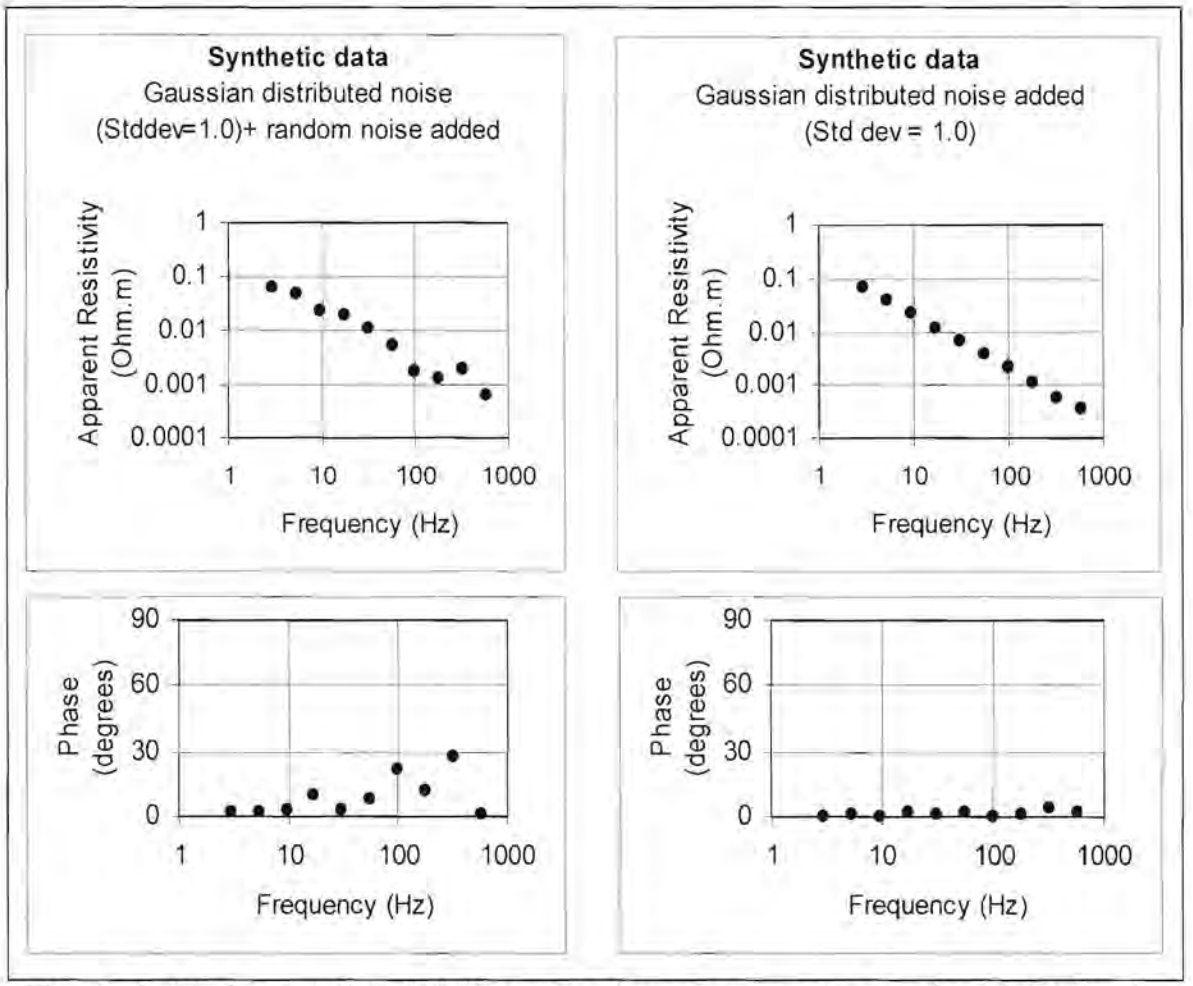

Figure 5.17. Apparent resistivity versus frequency curves produced by the L_2 norm estimation technique for the synthetic data displayed in Figure 5.14.

Results obtained with the adaptive L_p norm procedure and using Money et al.'s method of calculating p (equation 5.37) are depicted in Figure 5.18. The apparent resistivity curve is very similar to the curve estimated with the L_1 norm. The phase data again yield better results than the L_2 norm but worse results than the L_1 norm. Figures 5.19.1 to 5.19.10 show the value for p calculated during each iteration.

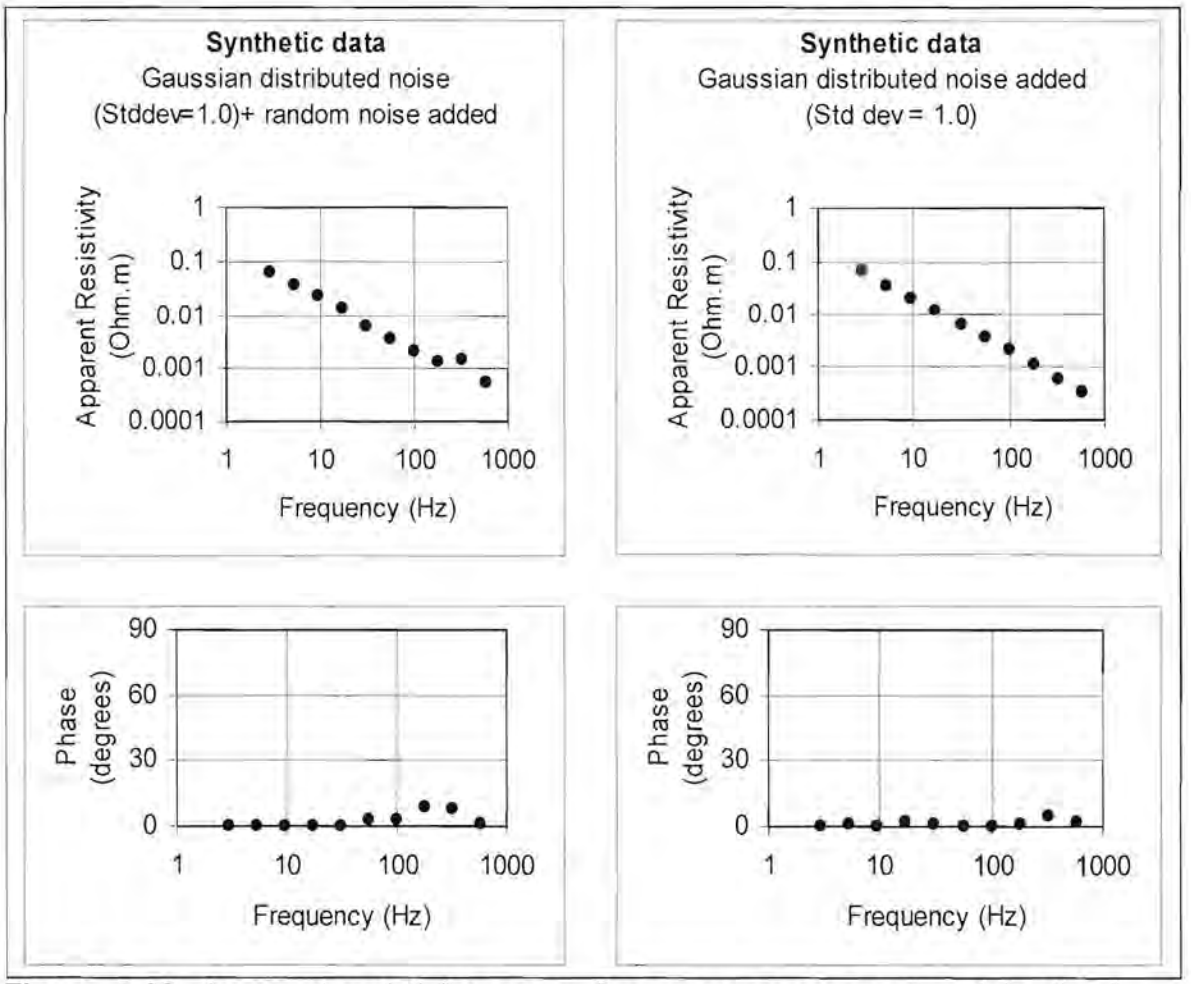

Figure 5.18. Apparent resistivity versus frequency curves produced by the L_p norm estimation technique for the synthetic data displayed in Figure 5.14. Money et al.'s (1982) equation was used to calculate p.

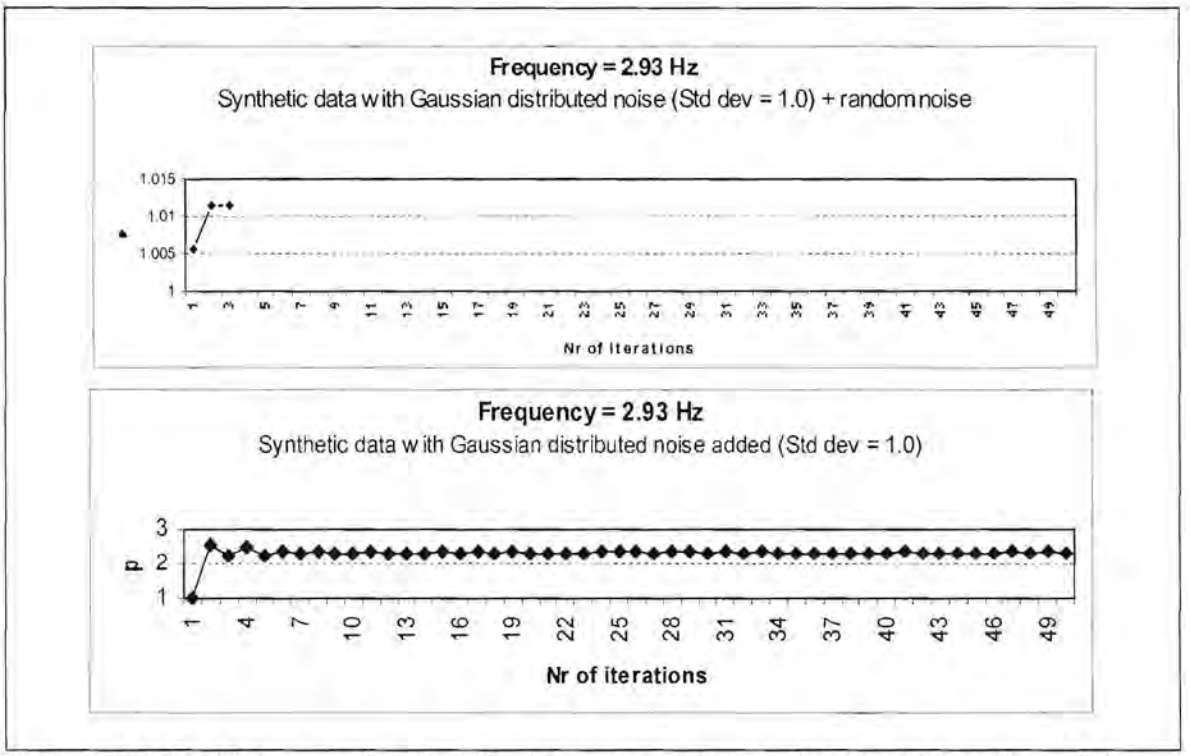

Figure 5.19.1. Values calculated for the exponent p during the estimation of the apparent resistivity values displayed in Figure 5.18 at 2.93 Hz

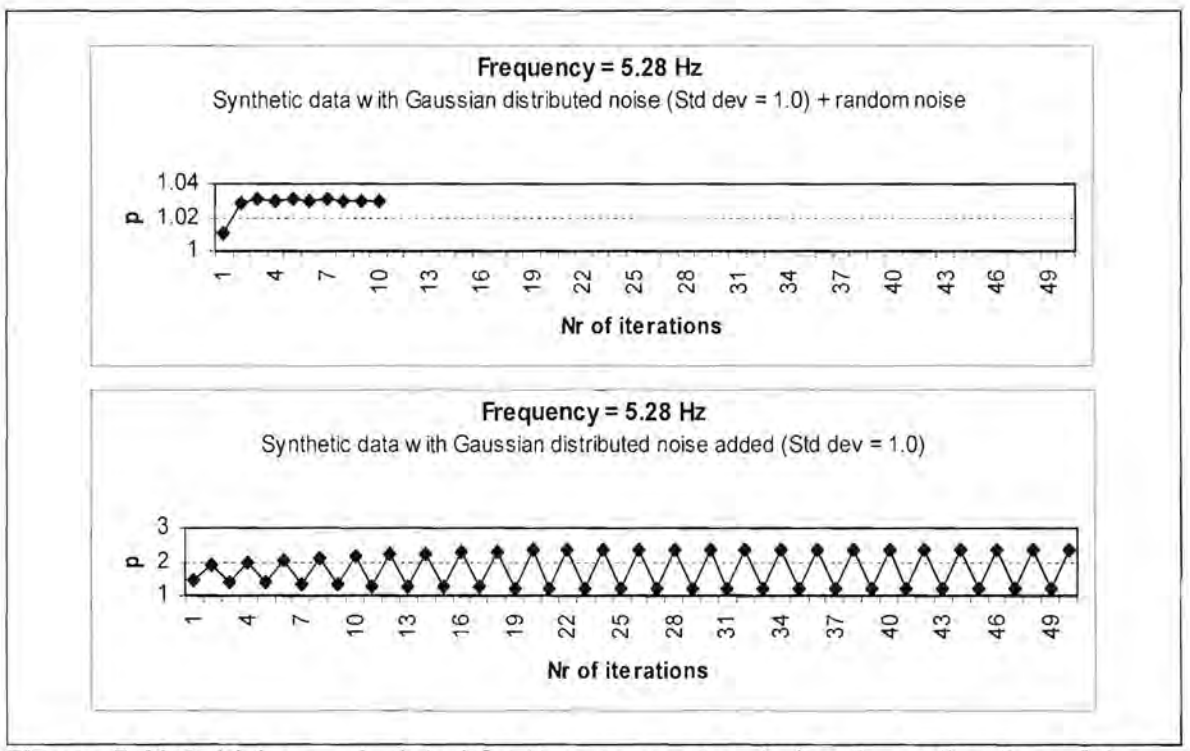

Figure 5.19.2. Values calculated for the exponent p during the estimation of the apparent resistivity values displayed in Figure 5.18 at 5.28 Hz

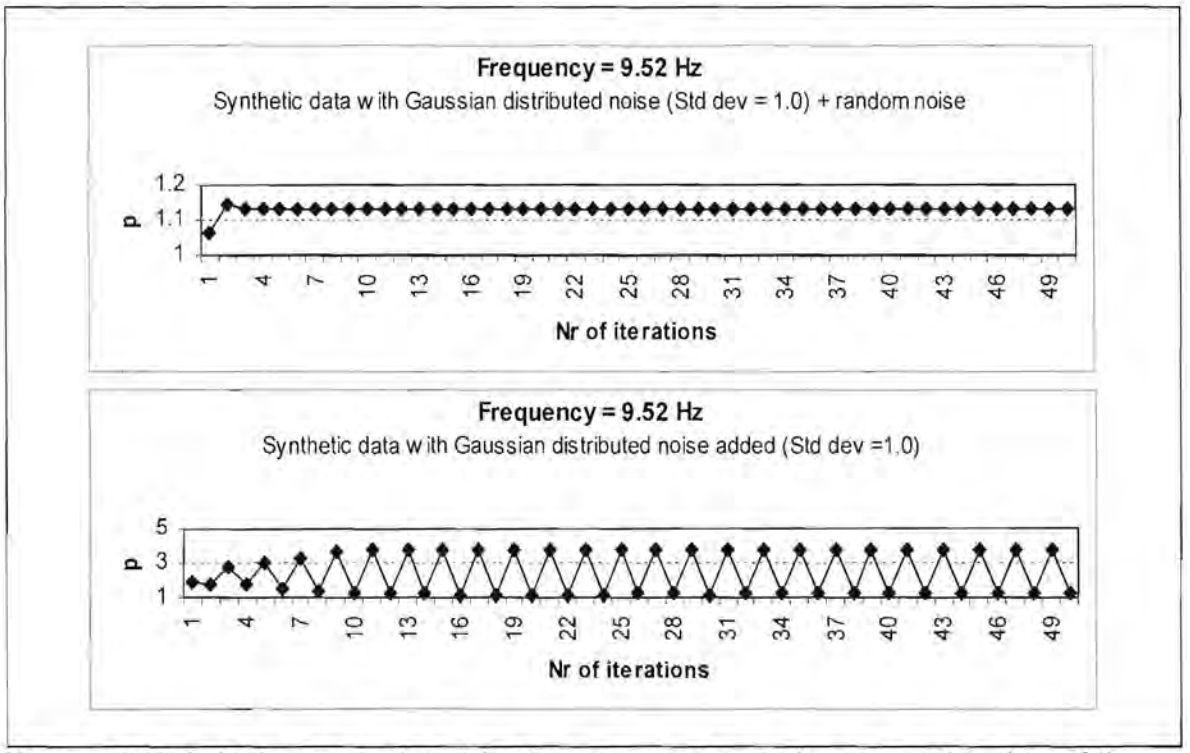

Figure 5.19.3. Values calculated for the exponent p during the estimation of the apparent resistivity values displayed in Figure 5.18 at 9.52 Hz

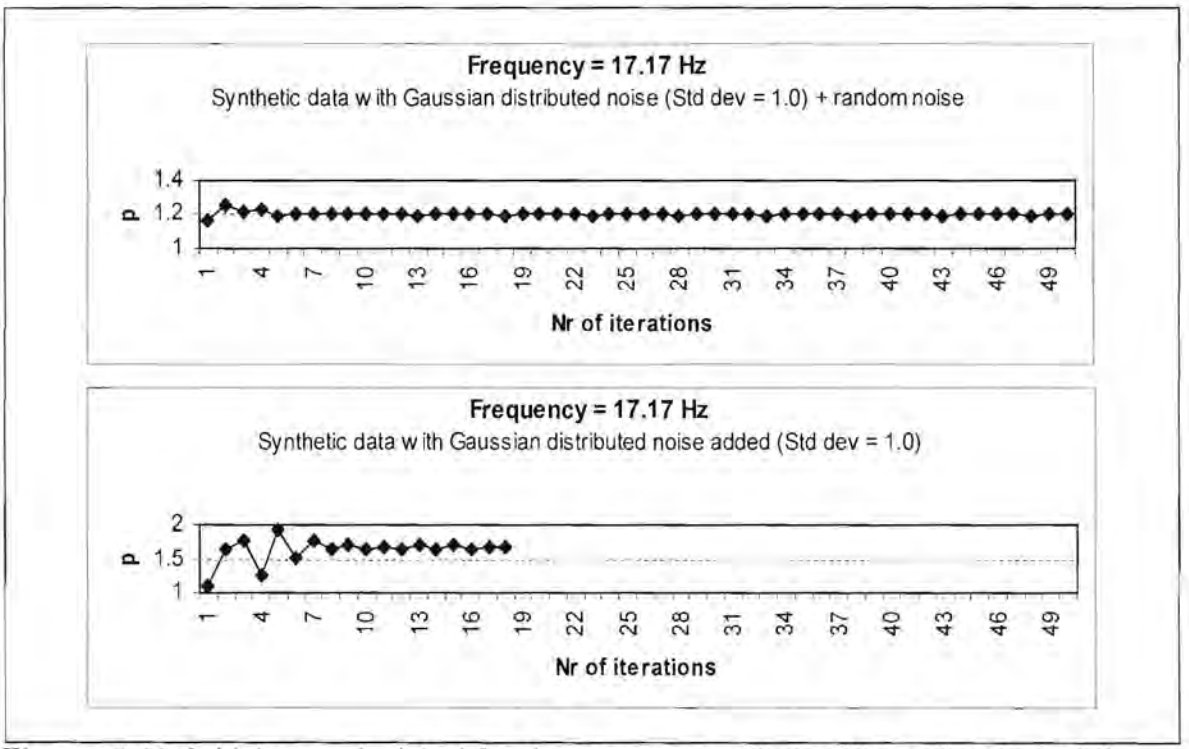

Figure 5.19.4. Values calculated for the exponent p during the estimation of the apparent resistivity values displayed in Figure 5.18 at 17.17 Hz

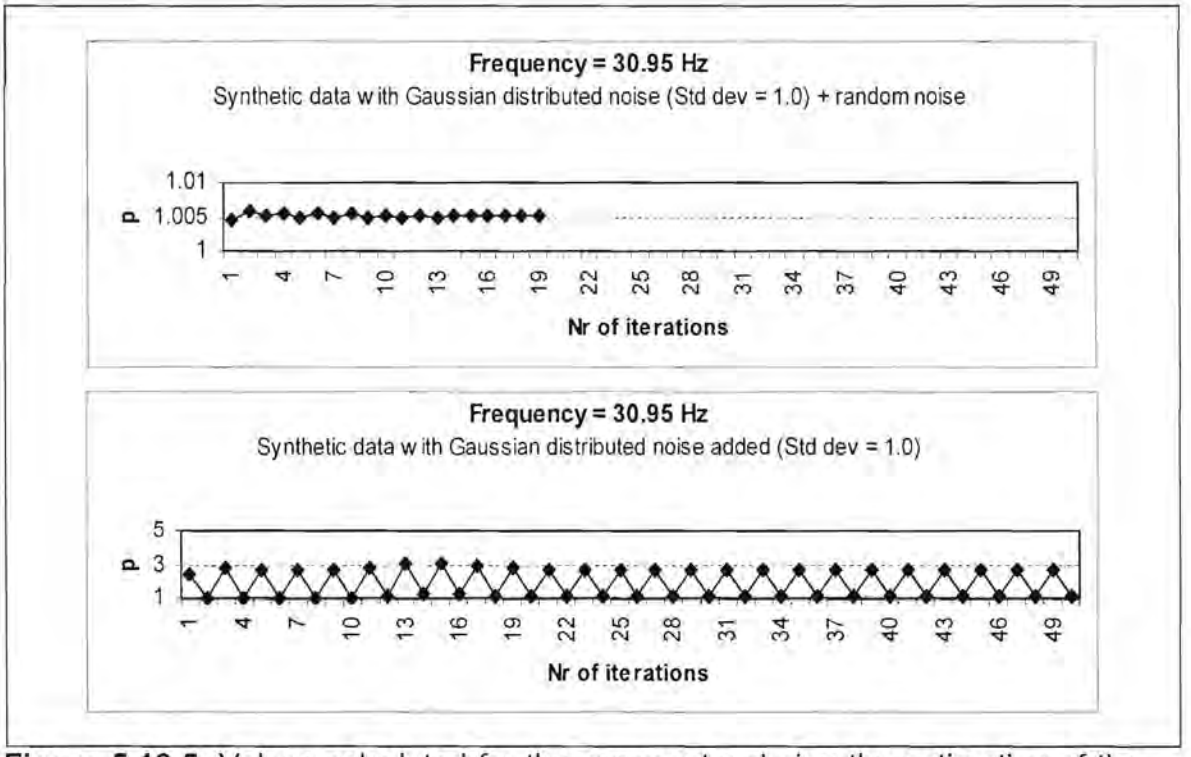

Figure 5.19.5. Values calculated for the exponent p during the estimation of the apparent resistivity values displayed in Figure 5.18 at 30.95 Hz

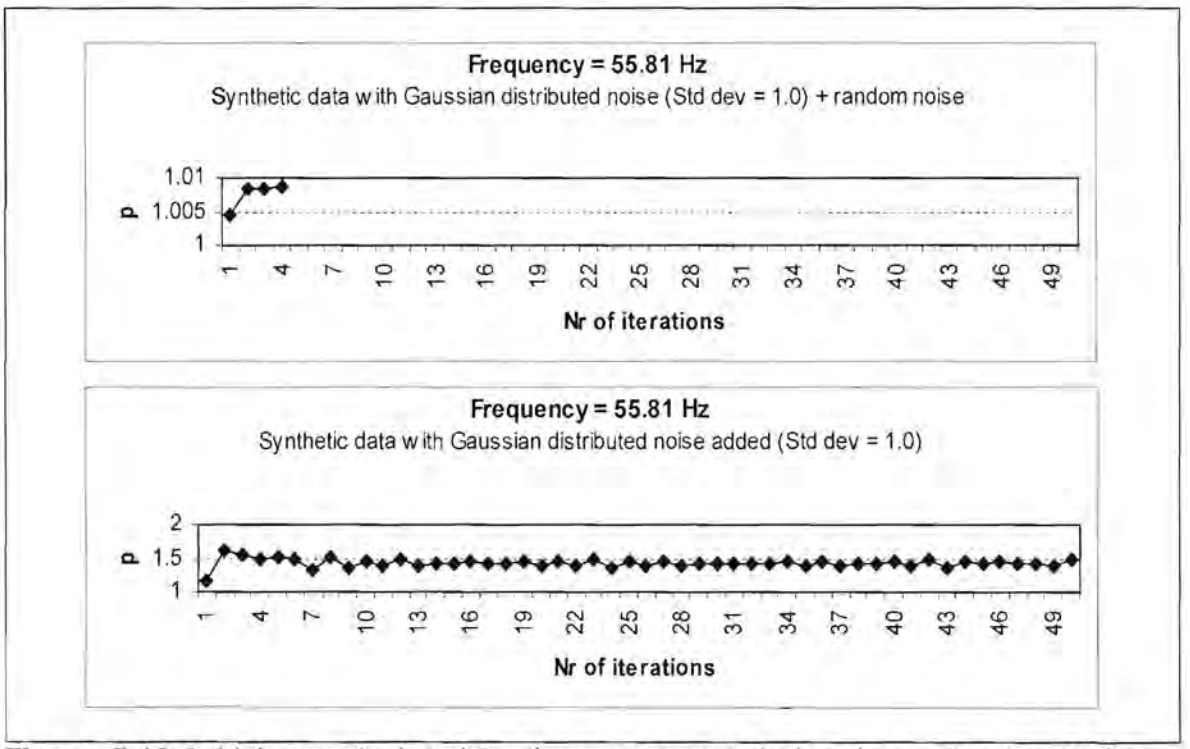

Figure 5.19.6. Values calculated for the exponent p during the estimation of the apparent resistivity values displayed in Figure 5.18 at 55.81 Hz

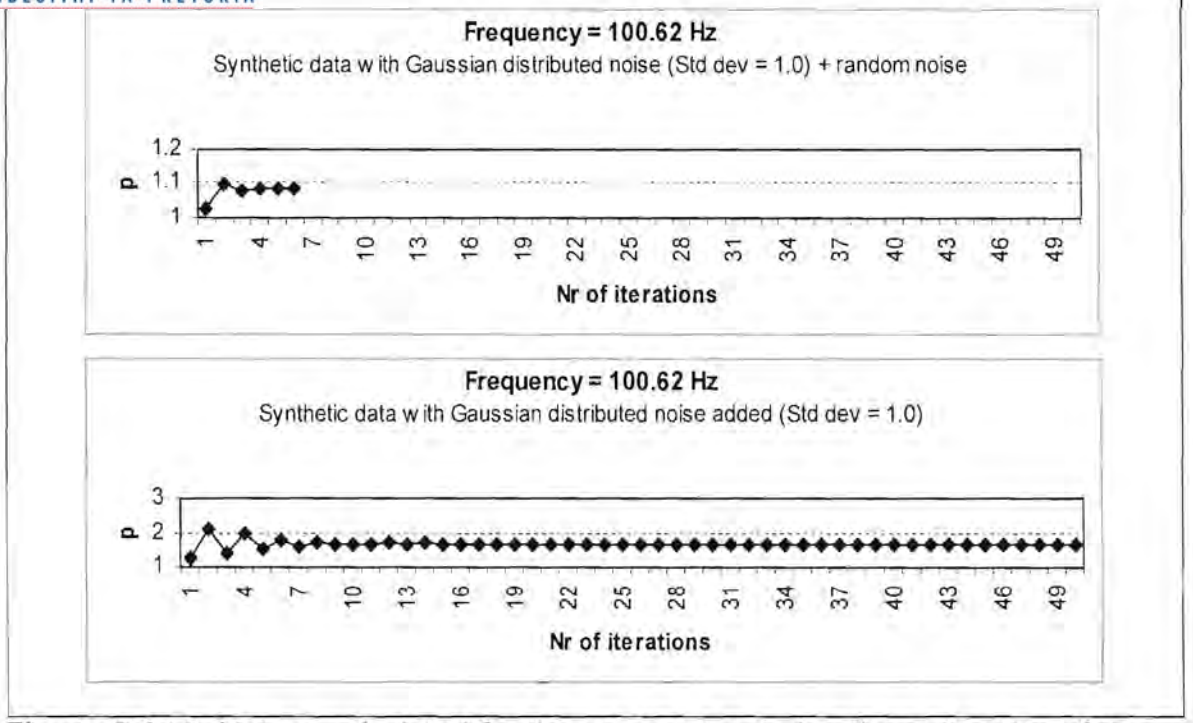

Figure 5.19.7. Values calculated for the exponent p during the estimation of the apparent resistivity values displayed in Figure 5.18 at 100.62 Hz

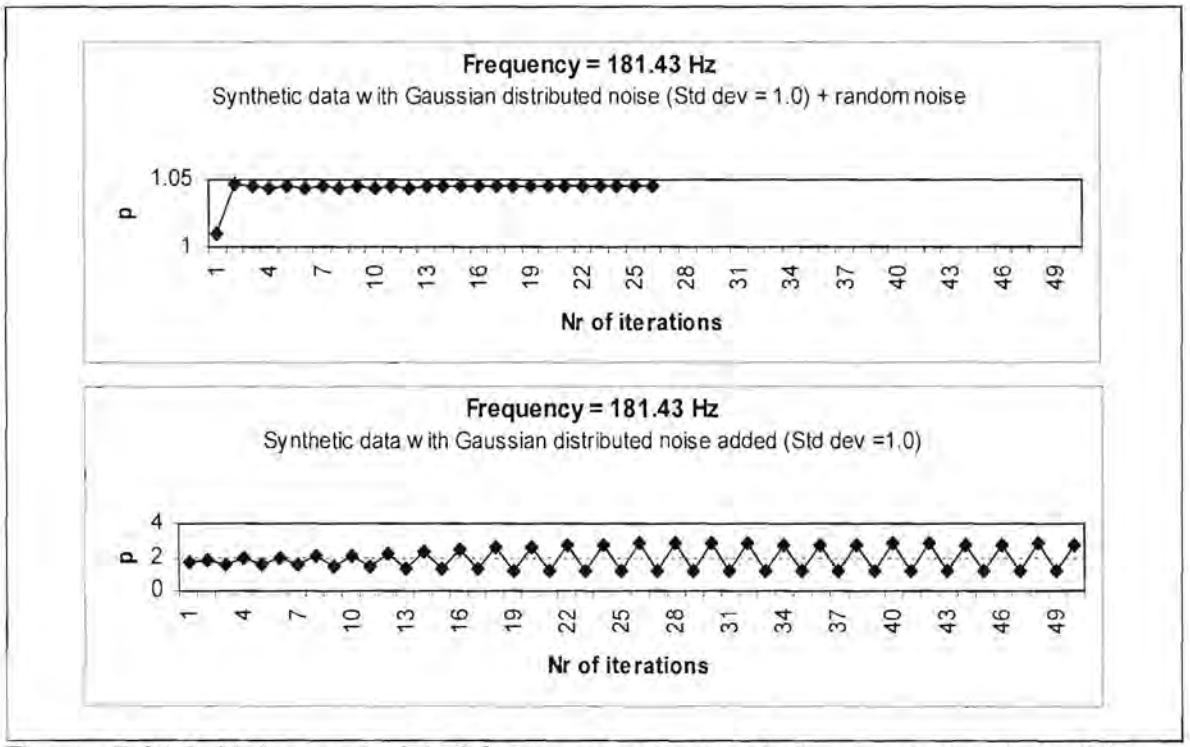

Figure 5.19.8. Values calculated for the exponent p during the estimation of the apparent resistivity values displayed in Figure 5.18 at 181.43 Hz

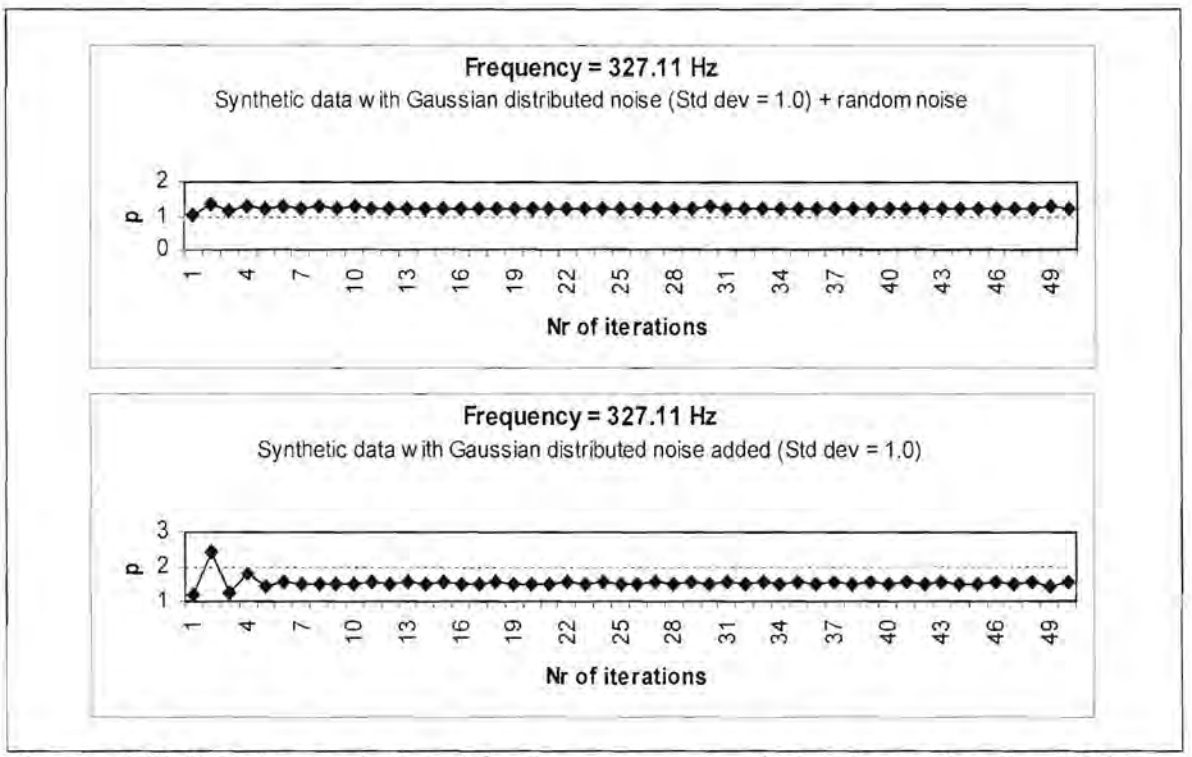

Figure 5.19.9. Values calculated for the exponent p during the estimation of the apparent resistivity values displayed in Figure 5.18 at 327.11 Hz

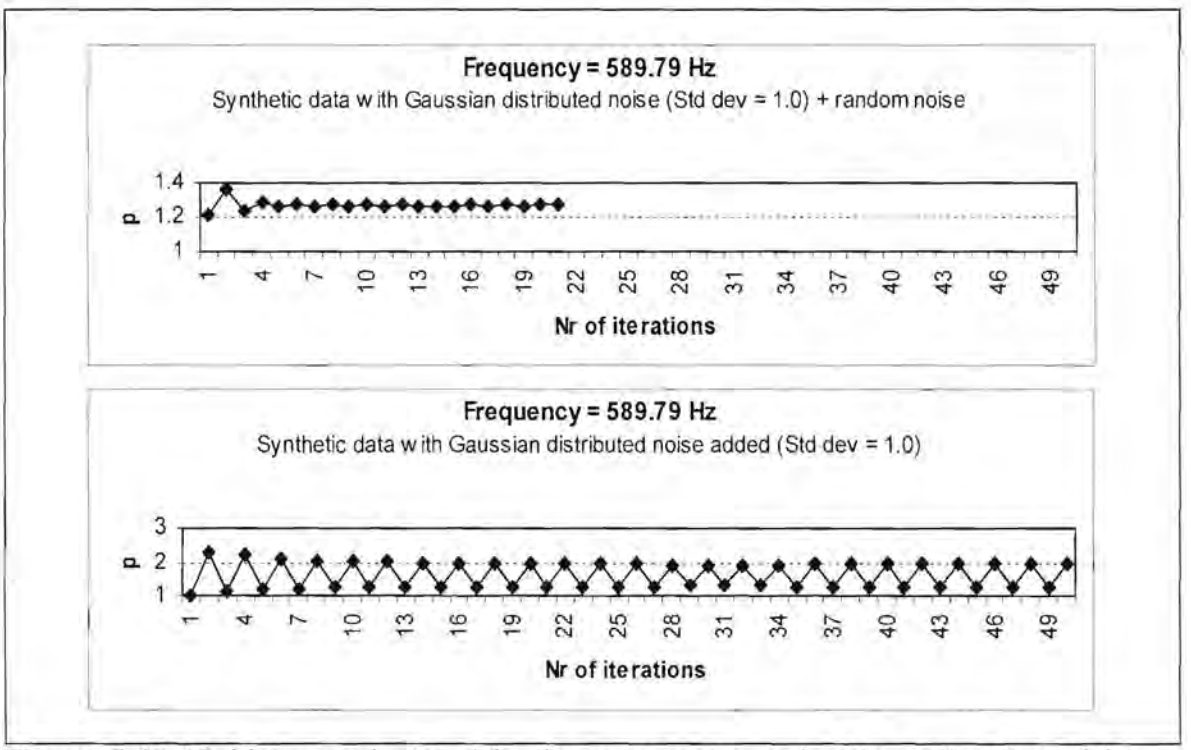

Figure 5.19.10. Values calculated for the exponent p during the estimation of the apparent resistivity values displayed in Figure 5.18 at 589.79 Hz

Figure 5.20 shows the results of using the adaptive L_p norm estimation technique and Sposito et al.'s (1983) formula (Equation 5.38) to calculate p.

Where non-Gaussian distributed noise was added, the results are very poor and correlate very well with the curves obtained from the least squares method. The reason for this becomes clear when one looks at the values of p calculated for each iteration in Figures 5.21.1 to 5.21.10. At most frequencies the adaptation procedure was terminated after only a few iterations because the values calculated for p were greater than 2, and this is not allowed when using equation (5.38).

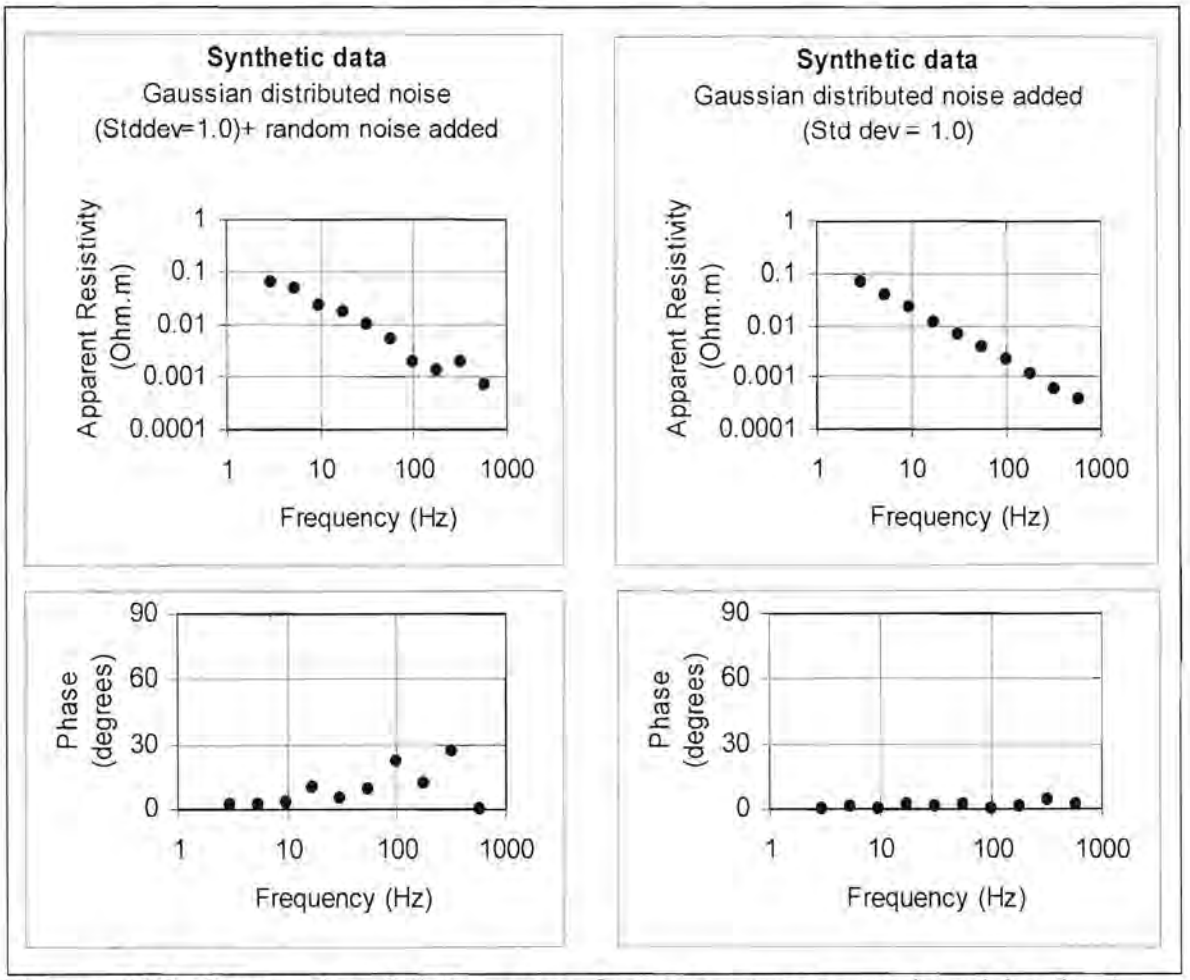

Figure 5.20. Apparent resistivity versus frequency curves produced by the L_p norm estimation technique for the synthetic data displayed in Figure 5.14. Sposito's (1983) equation was used to calculate p.

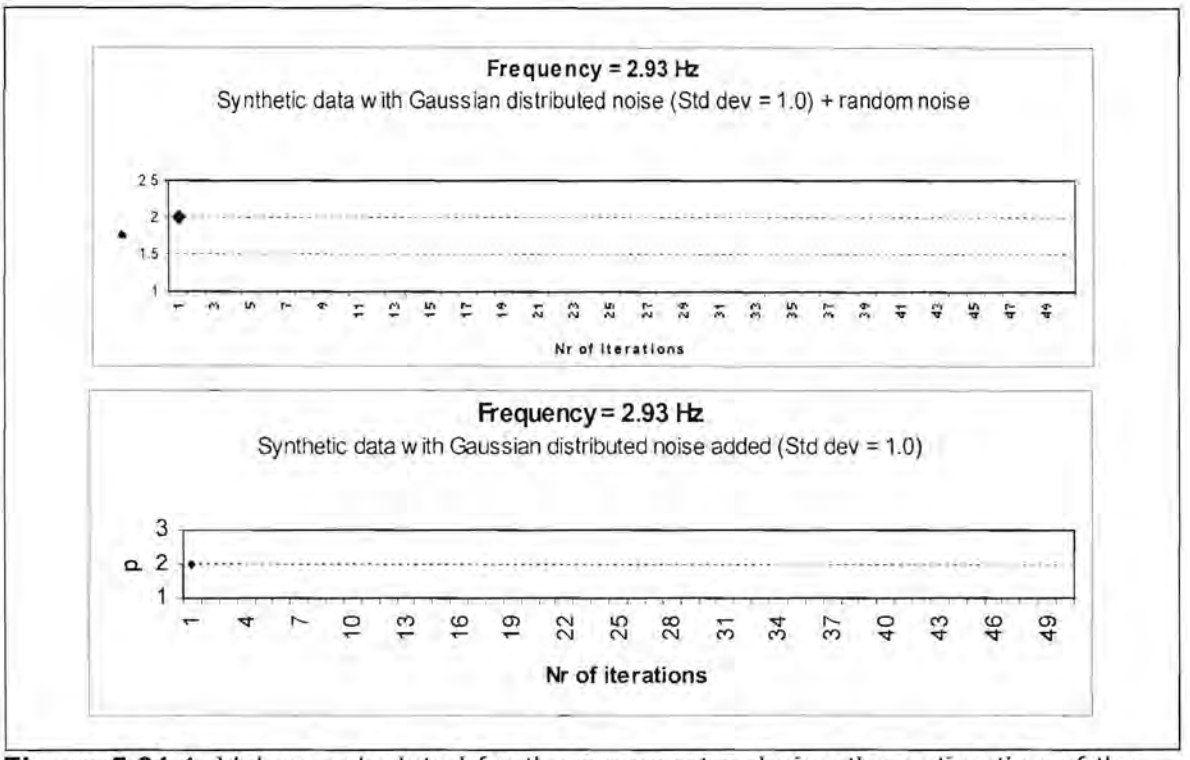

Figure 5.21.1. Values calculated for the exponent p during the estimation of the apparent resistivity values displayed in Figure 5.20 at 2.93 Hz

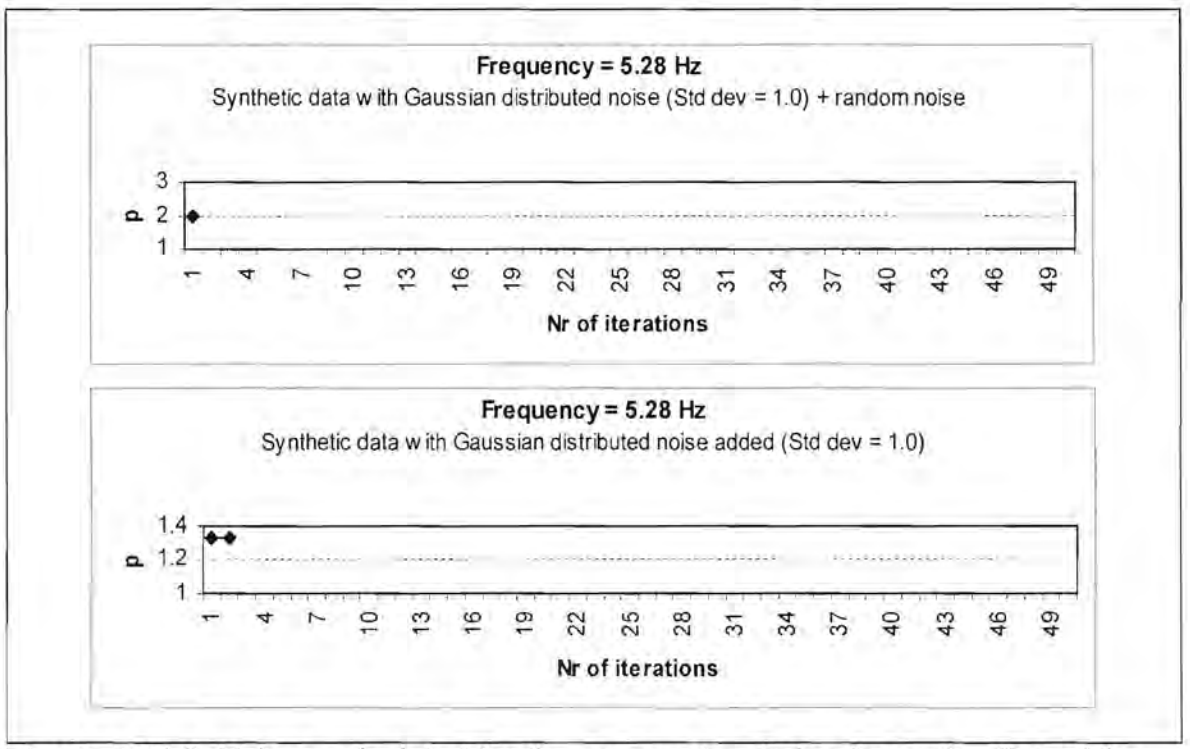

Figure 5.21.2. Values calculated for the exponent p during the estimation of the apparent resistivity values displayed in Figure 5.20 at 5.28 Hz

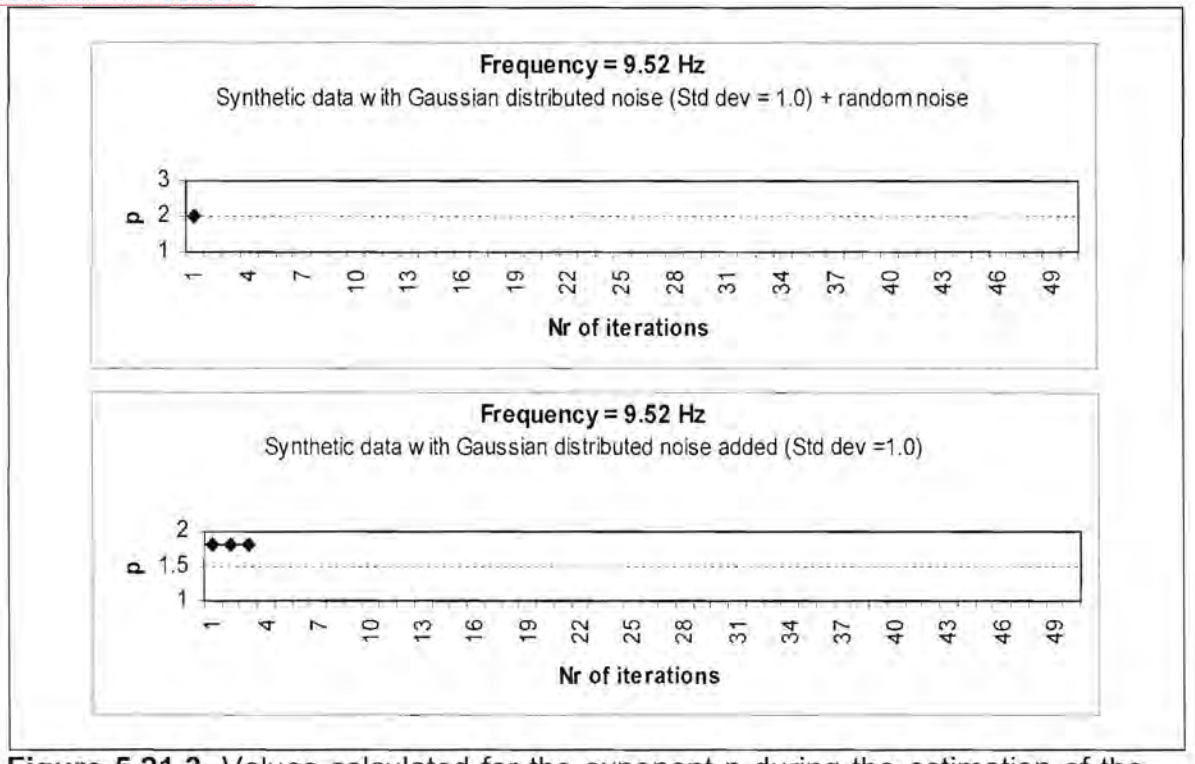

Figure 5.21.3. Values calculated for the exponent p during the estimation of the apparent resistivity values displayed in Figure 5.20 at 9.52 Hz

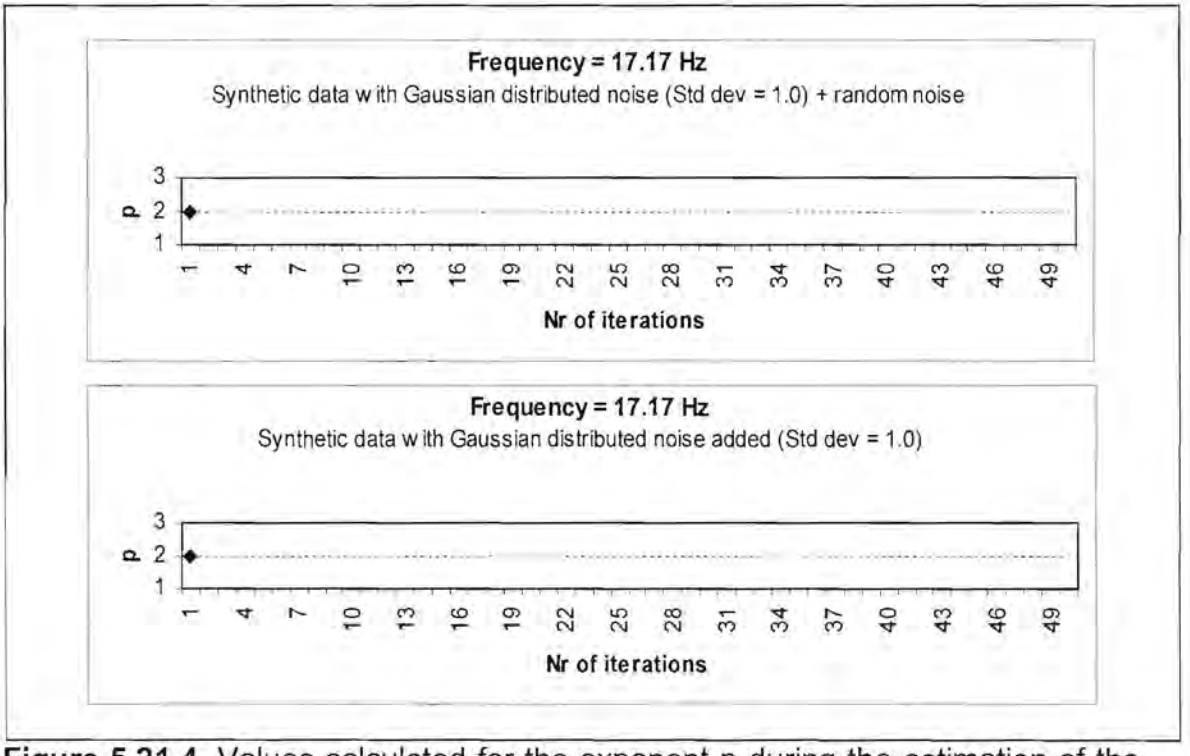

Figure 5.21.4. Values calculated for the exponent p during the estimation of the apparent resistivity values displayed in Figure 5.20 at 17.17 Hz

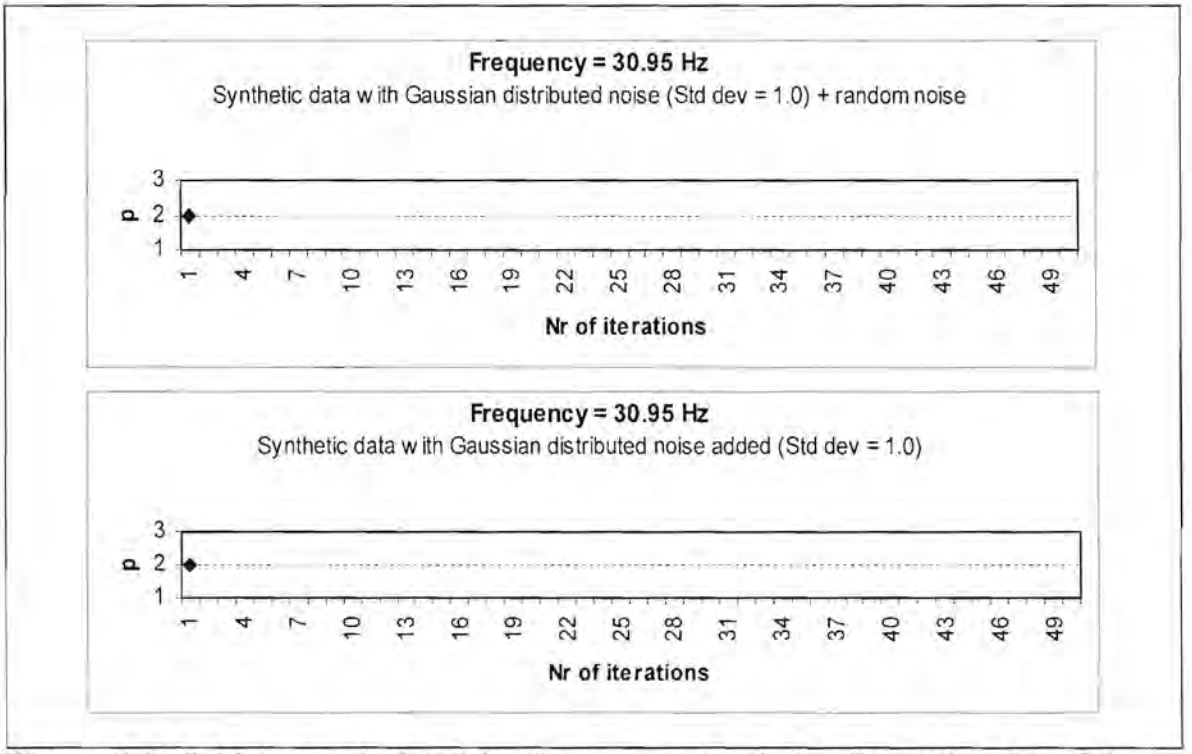

Figure 5.21.5. Values calculated for the exponent p during the estimation of the apparent resistivity values displayed in Figure 5.20 at 30.95 Hz

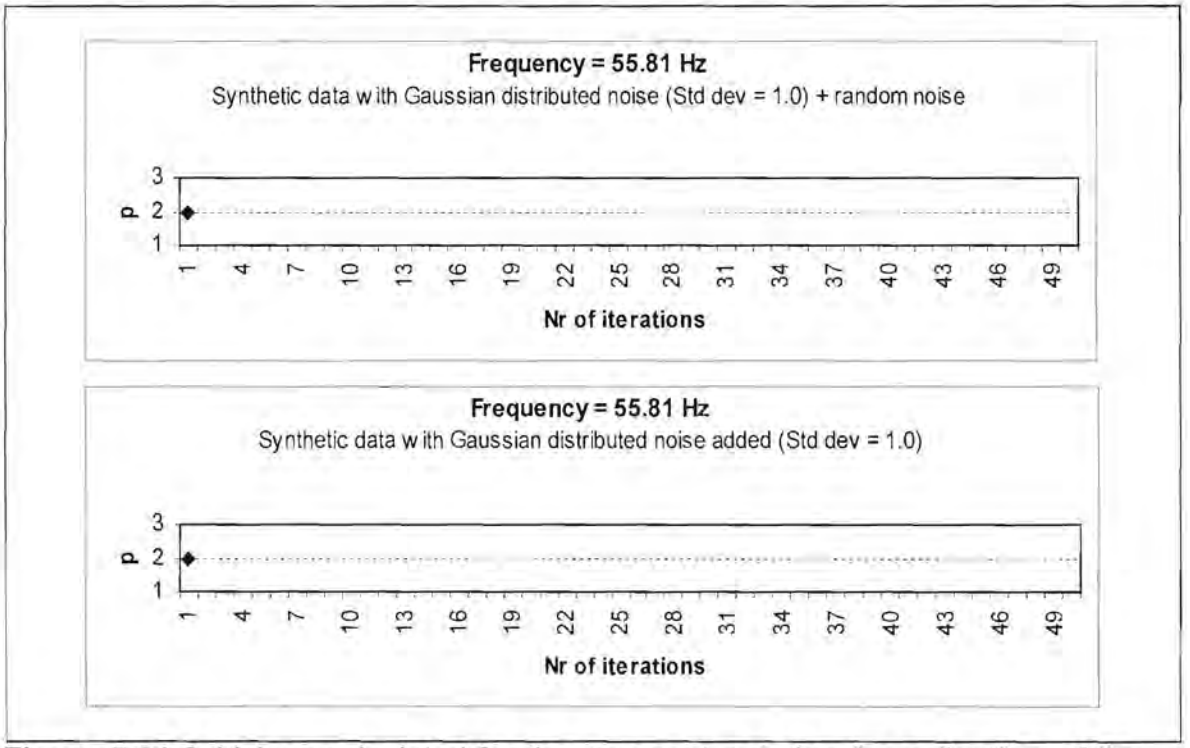

Figure 5.21.6. Values calculated for the exponent p during the estimation of the apparent resistivity values displayed in Figure 5.20 at 55.81 Hz

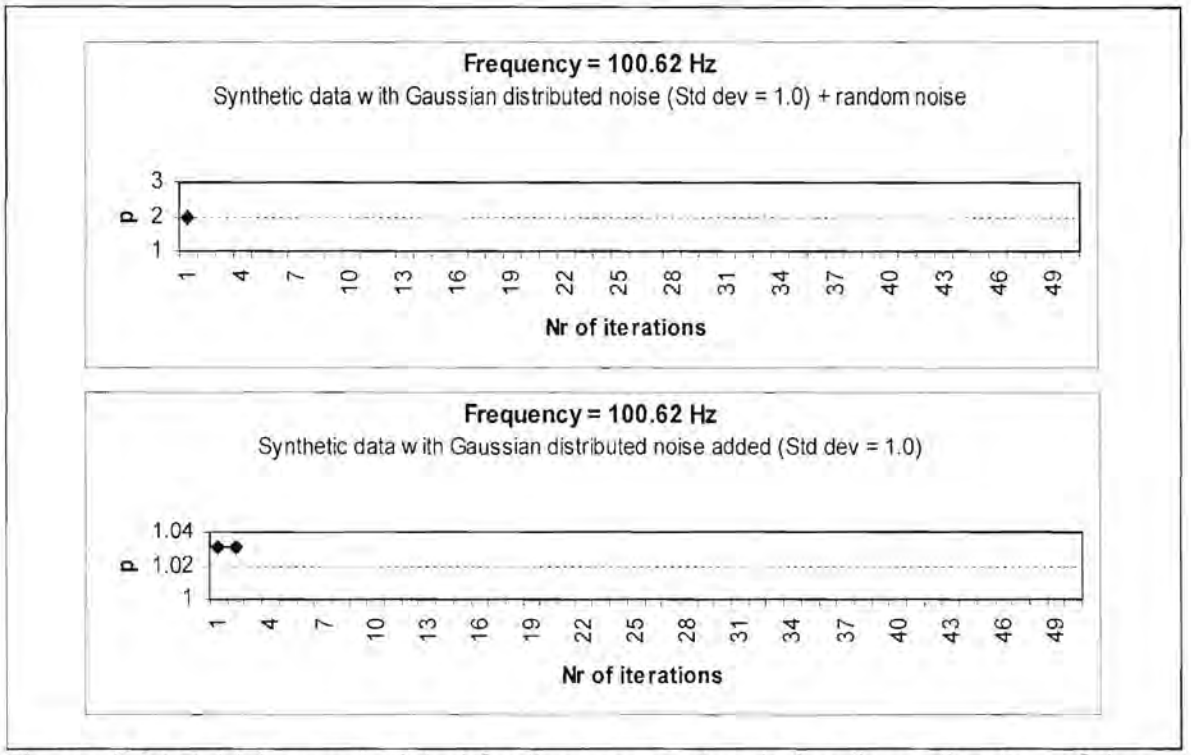

Figure 5.21.7. Values calculated for the exponent p during the estimation of the apparent resistivity values displayed in Figure 5.20 at 100.62 Hz

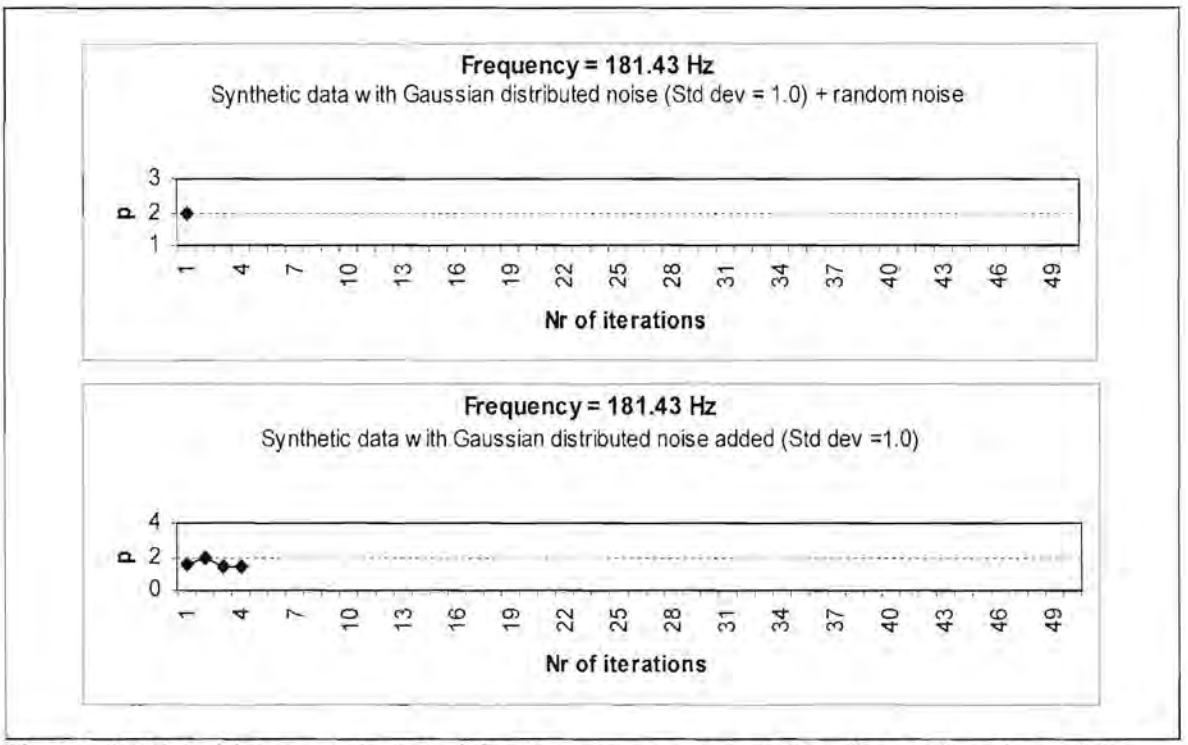

Figure 5.21.8. Values calculated for the exponent p during the estimation of the apparent resistivity values displayed in Figure 5.20 at 181.43 Hz

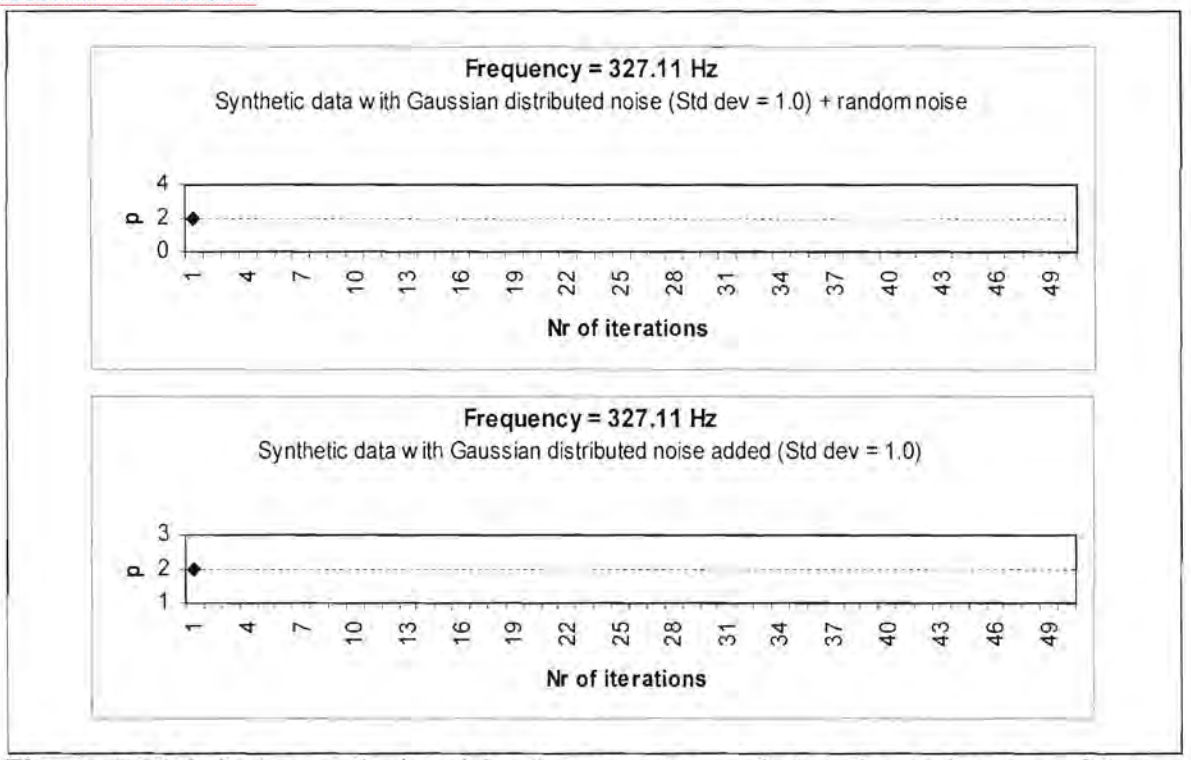

Figure 5.21.9. Values calculated for the exponent p during the estimation of the apparent resistivity values displayed in Figure 5.20 at 327.11 Hz

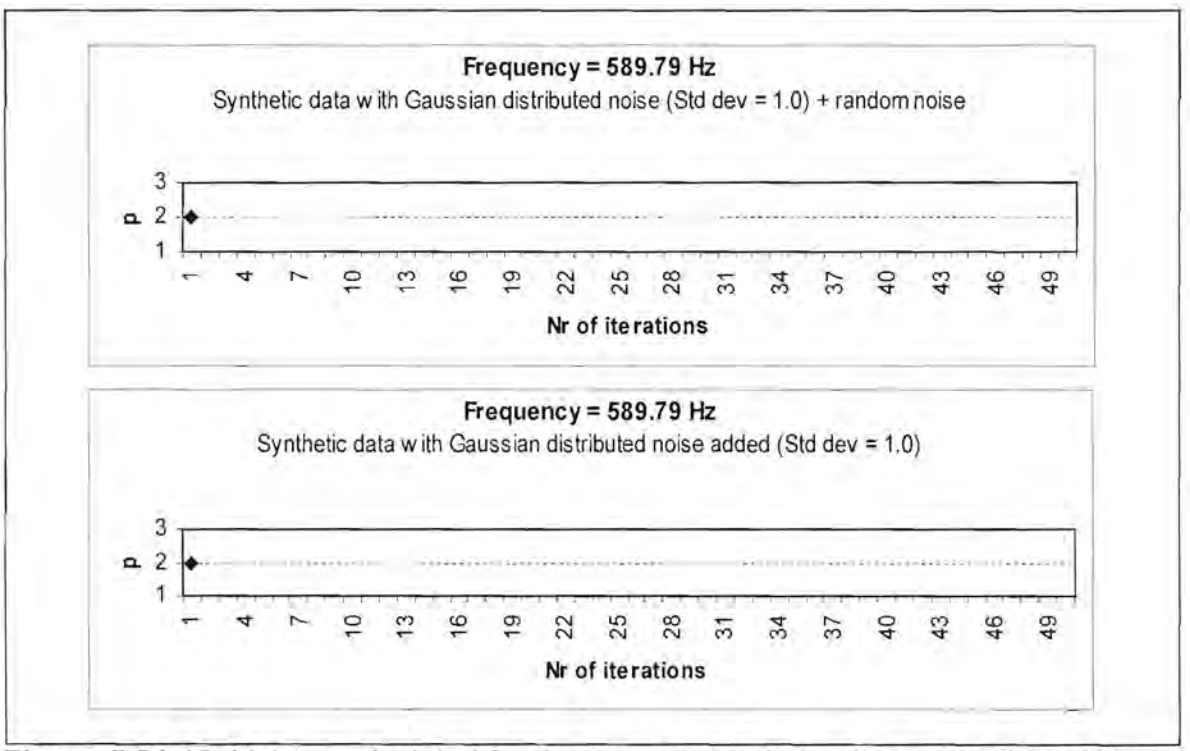

Figure 5.21.10. Values calculated for the exponent p during the estimation of the apparent resistivity values displayed in Figure 5.20 at 589.79 Hz

The Robust M estimation method yields very good results for the apparent resistivity curve at most frequencies (Figure 5.22), even though it starts with the least squares estimate of the impedance tensor as an initial estimate.

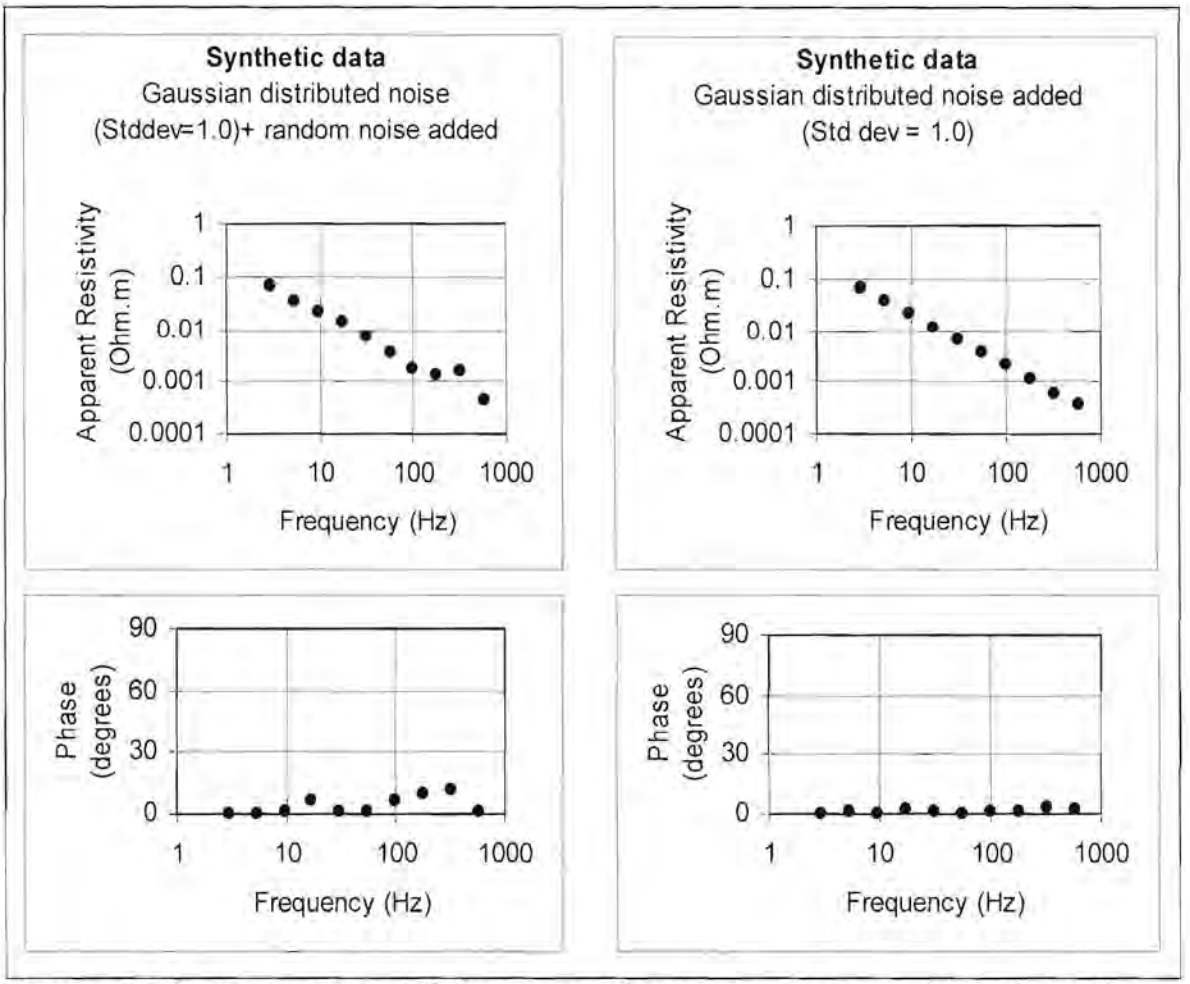

Figure 5.22. Apparent resistivity versus frequency curves produced by the Robust M estimation technique for the synthetic data displayed in Figure 5.14.

Where random noise without any specific distribution was introduced to the impedance tensor, the L_1 norm, Robust M estimation and L_p norm (using equation (5.37) to calculate p) techniques yielded satisfactory results for the apparent resistivity curves. The least squares technique and L_p norm with equation (5.38) yielded bad results. All of the estimation methods used resulted in bad fits for the phase curves.

5.5.3. Conclusions drawn from synthetic data tests

In the case where only Gaussian distributed noise are introduced to the impedance tensor, all the tested statistical reduction techniques yielded very good results. An increase in the standard deviation of the distribution of the noise causes a slight deterioration in the quality of the curve fitted to the phase data.

Completely random noise added to the impedance tensor caused a marked decrease in the success of some of the minimisation techniques. The least squares method did not produce good results at all. The same is true for the adaptive L_p technique where equation (5.38) was used to determine the value of p. Estimated values of p greater than 2 caused the adaptive process to be terminated and therefore at most frequencies L_2 minimisation occurred.

The L_1 norm, robust M estimation method and L_p norm using equation (5.37) all yielded good results, with the best fit produced by the L_1 norm. From the above examples it is concluded that the adaptive L_p-norm method is more susceptible to the starting impedance values than the robust M-estimation technique.

From the examples studied in this chapter it is clear that none of the minimisation techniques yielded perfect results. It is therefore critical that the curves obtained should be studied very carefully, keeping in mind the amount of artificial noise present near the sounding station. Additionally calculated parameters that can provide more information on the presence of noise, such as the Tipper, must be taken into account.

CHAPTER 6

CASE STUDY

A magnetotelluric (MT) survey was conducted along the road between Sishen and Keimoes in the Northern Cape Province of South Africa. It followed the route of a deep seismic reflection survey that was carried out during 1989 on behalf of the Geological Survey and the National Geophysics Programme by Geoseis (Pty) Ltd. of South Africa. The aim of the MT survey was twofold:

- Compare the results obtained by the two methods to determine whether it would be beneficial to do a magnetotelluric survey prior to a deep reflection seismic survey in order to locate areas of interest. This would be of economic interest since a deep reflection seismic survey costs considerably more than a magnetotelluric survey.
- Shed light on a number of interesting features that is visible on the reflection data.

The statistical techniques discussed in the previous chapter were applied to the data.

6.1. SURVEY LOCATION

Eleven sounding stations were positioned along the Sishen - Keimoes road at roughly 20km intervals. Figure 6.1 shows the location of the survey area in South Africa.